TORSIONAL SAFETY OF HIGHWAY TRAFFIC SIGNAL AND SIGNAGE SUPPORT

FINAL PROJECT REPORT

by

Andre R. Barbosa, Armin W. Stuedlein, and Qiang Li
Civil and Construction Engineering
Oregon State University

Sponsorship
PacTrans
Oregon Department of Transportation

for
Pacific Northwest Transportation Consortium (PacTrans)
USDOT University Transportation Center for Federal Region 10
University of Washington
More Hall 112, Box 352700
Seattle, WA 98195-2700

In cooperation with US Department of Transportation-Research and Innovative Technology Administration (RITA)

Disclaimer

The contents of this report reflect the views of the authors, who are responsible for the facts and the accuracy of the information presented herein. This document is disseminated under the sponsorship of the U.S. Department of Transportation's University Transportation Centers Program, in the interest of information exchange. The Pacific Northwest Transportation Consortium, the U.S. Government and the matching sponsor, which was the Oregon Department of Transportation, assume no liability for the contents or use thereof.

Technical Report Documentation Page

1. Report No.	2. Government Accession No.	3. Recipient's Catalog No.	
4. Title and Subtitle TORSIONAL SAFETY OF HIGHWAY TRAFFIC SIGNAL AND SIGNAGE SUPPORT		**5. Report Date** **6. Performing Organization Code**	
7. Author(s) Andre R. Barbosa, Armin W. Stuedlein, and Qiang Li		**8. Performing Organization Report No.**	
9. Performing Organization Name and Address PacTrans Pacific Northwest Transportation Consortium University Transportation Center for Region 10 University of Washington More Hall 112 Seattle, WA 98195-2700		**10. Work Unit No. (TRAIS)** **11. Contract or Grant No.**	
12. Sponsoring Organization Name and Address United States of America Department of Transportation Research and Innovative Technology Administration		**13. Type of Report and Period Covered** **14. Sponsoring Agency Code**	

15. Supplementary Notes

Report uploaded at www.pacTrans.org

16. Abstract

Deep foundations may need to resist torsional loads resulting from wind loading on traffic sign and signal pole structures, or seismic loading on curved or skewed bridges. Although methods for designing deep foundations at the ultimate limit states are readily available, and their accuracy has been quantified for selected loading test data, no significant effort to quantify the accuracy of existing load transfer-based torsion-rotation serviceability limit state methods to predict full-scale, in-service rotation performance has been reported in the literature. To facilitate the serviceability design of geometrically variable deep foundations constructed in multi-layered soils, a torsional load transfer method was developed using a finite difference model (FDM) framework. Simplified pressure- and state-dependent spring models, relating the unit torsional resistance to the magnitude of relative displacement, were developed and validated by using available interface shear tests and load transfer data from full-scale torsional loading tests. The proposed FDM methodology was validated by comparing the torsional responses of deep foundations designed with the FDM with results from previous analytical solutions and with the centrifuge and full-scale torsional loading tests. Parametric studies were conducted to illustrate the role of various design parameters and to demonstrate significant effects of nonlinear soil and structural response on the torsional behavior of deep foundations.

17. Key Words		18. Distribution Statement No restrictions.	
19. Security Classification (of this report) Unclassified.	**20. Security Classification (of this page)** Unclassified.	**21. No. of Pages**	**22. Price** NA

Form DOT F 1700.7 (8-72) **Reproduction of completed page authorized**

Table of Contents

List of Figures

List of Tables

Acknowledgments

The research team would like to extend thanks to the sponsors of this work, the Pacific Northwest Transportation Consortium and the Oregon Department of Transportation.

Executive Summary

Deep foundations may need to resist torsional loads that result from wind loading on traffic sign and signal pole structures, or seismic loading on curved or skewed bridges. Although methods for designing deep foundations at the ultimate limit states are readily available, and their accuracy has been quantified for selected loading test data, no significant effort to quantify the accuracy of existing load transfer-based torsion-rotation serviceability limit state methods to predict the full-scale, in-service rotation performance has been reported in the literature. To facilitate the serviceability design of geometrically variable deep foundations constructed in multi-layered soils, a torsional load transfer method was developed by using a finite difference model (FDM) framework. Simplified pressure- and state-dependent spring models, relating the unit torsional resistance to the magnitude of relative displacement, were developed and validated by using available interface shear tests and load transfer data from full-scale torsional loading tests. The proposed FDM methodology was validated by comparing the torsional responses of deep foundations designed with the FDM with results from previous analytical solutions and from centrifuge and full-scale torsional loading tests. Parametric studies were conducted to illustrate the roles of various design parameters and to demonstrate the significant effects of nonlinear soil and structural response on the torsional behavior of deep foundations.

Chapter 1 Introduction

1.1 Problem Statement

Drilled shafts offer an excellent alternative for transferring superstructure loads to the soil and/or rock stratigraphy present below the ground surface, and they are commonly used to support mast arm traffic sign and signal poles. The design of these drilled shafts must provide sufficient capacity to resist the maximum anticipated loads, including lateral and torsional loads, the latter of which generally result from wind gust loading or seismic loading on curved bridges.

Deep foundations must provide sufficient torsional resistance within specified performance criteria, which can range from the specification of a limiting displacement or rotation, θ, (i.e., a serviceability limit state, SLS) to life safety (e.g., ultimate limit states, ULS). Design evaluations for deep foundations that are axially and laterally loaded at the SLS and ULS are routine, and numerous methods to simulate load transfer exist (e.g., Coyle and Sulaiman 1967; Matlock 1970; Cox et al. 1974; Reese et al. 1975; Reese and Welch 1975; Vijayvergiya 1977; API 1993; Norris 1986; Ashour et al. 1996; Li and Yang 2017; Yang et al. 2017). While design methods for torsionally loaded deep foundations at the ULS are readily available, and their accuracy has been quantified for selected loading test data (e.g., Li et al. 2017), no significant effort to quantify the accuracy of existing load transfer-based torsion-rotation SLS methods to predict the full-scale, in-service rotation performance has been reported in the literature. Accordingly, the selection of a factor of safety or resistance factor suitable for limiting rotations to an acceptable, let alone known, magnitude remains a critical question for the design of torsionally loaded deep foundations.

1.2 Objectives of and Tasks of This Study

The objective of this research project was to develop a simple torsional load transfer method that could be validated against experimental interface shear data and full-scale loading tests to facilitate the serviceability design of torsionally loaded deep foundations. This work provided a modeling methodology that uses the finite difference model (FDM) framework that can be used in design.

This project consisted of the following tasks:

Task 1: Conduct a review of the relevant literature.

Task 2: Develop load transfer models, relating the unit torsional resistance to the magnitude of relative displacement.

Task 3: Develop a methodology to facilitate the serviceability and ultimate limit state design of a deep foundation subjected to torsion using a finite difference model (FDM) framework.

Task 4: Conduct parametric studies to illustrate the role of various design parameters and demonstrate significant effects of nonlinear soil and structural response on the torsional behavior of deep foundations.

1.3 Organization of This Report

Chapter 2 provides a literature review that describes previous studies on drilled shaft response in torsion. The discussion focuses on the available torsional loading tests on drilled shafts and analytical methods for estimating torsional capacity.

Chapter 3 describes this study's assumptions and governing differential equations, as well as the strategy to solve the governing differential equations.

Chapter 4 presents the simplified pressure- and state-dependent load transfer models relating the unit torsional resistance to the magnitude of relative displacement; the validation of the models by using available interface shear tests and load transfer data from full-scale torsional loading tests were also included.

Chapter 5 presents the performance of the proposed modeling methodology, which was compared with previous analytical solutions and recent full-scale loading test data to validate and evaluate its performance.

Chapter 6 presents parametric studies to illustrate the roles of various design parameters and the effects of the nonlinear structural response on the torsional behavior of deep foundations.

Finally, Chapter 7 summarizes the results and findings of the completed work and proposes areas for future study.

Chapter 2 Literature Review

2.1 Overview

This chapter presents a literature review of previous studies on the torsional response of drilled shafts. The availability of torsional loading test data was determined to be relatively limited. As described below in Section 2.2, the available torsional loading tests are categorized into three main types: (1) small-scale model piles and shafts at 1*g*, (2) small-scale, multi-*g* centrifuge shafts, and (3) full-scale shafts. Section 2.3 presents the existing analytical and numerical methods for predicting the torsional load response of deep foundations. The literature review concludes with a summary of the review, including the identification of areas where information is limited.

2.2 Torsional Loading Tests Reported in the Literature

In comparison to the axial and lateral loading tests on deep foundations, the availability of torsional loading tests is relatively limited. The available torsional loading tests on full-scale driven piles and drilled shafts, as well as scaled single- and multi-*g* piles and shafts, are described in this literature review.

2.2.1 Torsional Loading Tests on Small-Size Model Piles and Drilled Shafts

Poulos (1975) performed a series of torsional loading tests on four solid aluminum piles driven in Kaolin clay. The diameter and length of each pile were 25.4 mm and 502 mm, 25.4 mm and 254 mm, 19 mm and 527 mm, and 19 mm and 298 mm (corresponding to 1.0 in and 19.75 in, 1.0 in and 10 in, 0.75 in and 20.75 in, and 0.75 in and 11.75, respectively). All piles were driven into the soil to full embedment. The rotation of the test piles and applied torque were monitored. The relationship between the applied torque and rotation from test are shown as solid curves in figure 2.1. Although all of the piles were rotated 2° (0.035 radians), Poulos (1975)

reported test results for smaller rotations. As shown in figure 2.1, no definitive peak was observed for the torque-rotation curves.

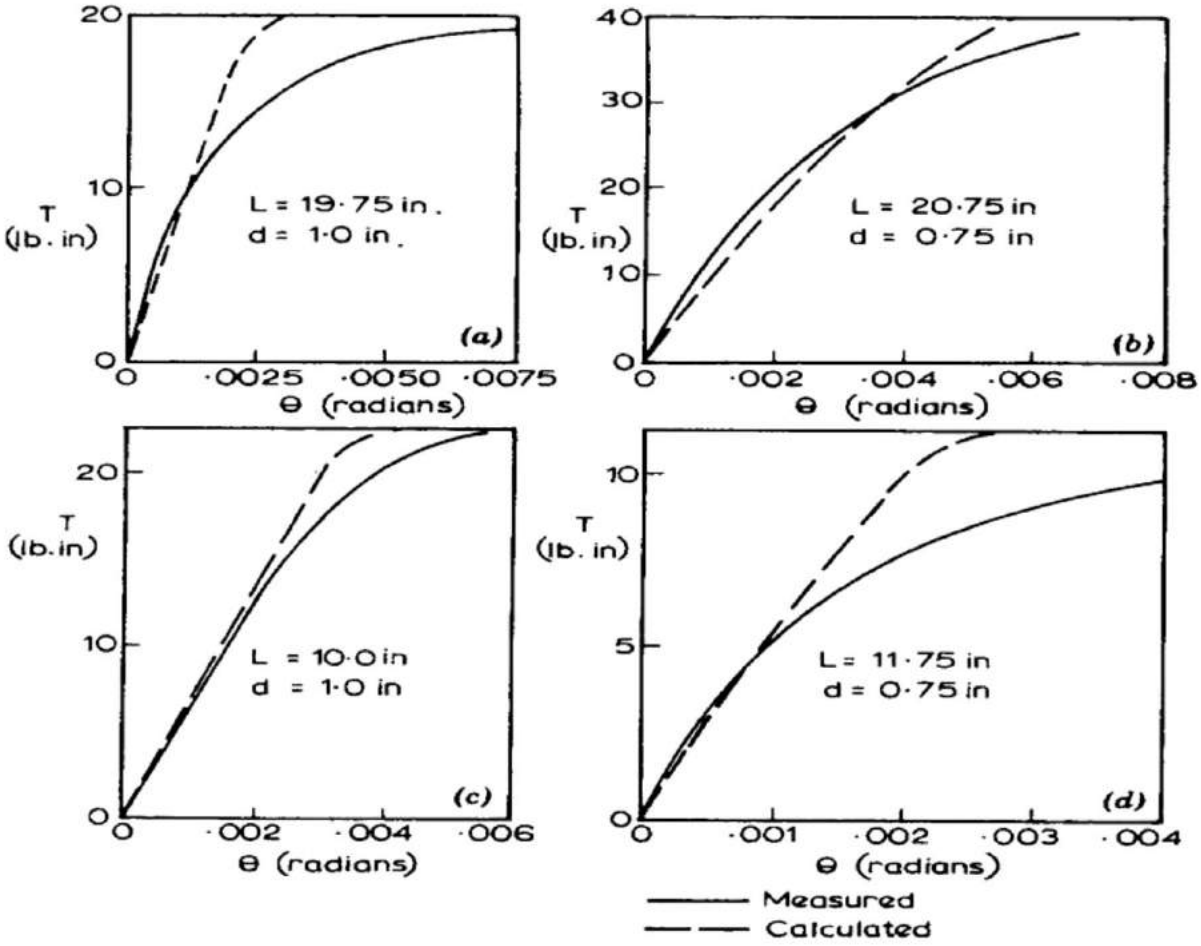

Figure 2.1 Relationship between torque and rotation (after Poulos 1975). Note: 0.005 radians equals 0.29 degrees.

Dutt (1976) and Dutt and O'Neill (1983) performed torsional loading tests using two circular aluminum piles of 48 mm (1.9 in) external diameter and 2.5 mm (0.1 in) wall thickness and two square piles of 51 mm (2.0 in) outside dimensions and 3.2 mm (0.125 in) wall thickness. The total length of each pile was 1.7 m (5.5 ft) with 0.15 m (6 in) above the ground surface, as shown in figure 2.2. Owing to the focus on drilled shafts in this report, only the results of the test on the circular pile are summarized. As shown in figure 2.3, one circular and one square pile

were installed by placing air-dried sand around the piles. Both loose and dense sand conditions were considered. After the torsional loading tests on the model piles were concluded, the same model piles were removed and then driven at the places shown in figure 2.2, and torque was applied to assess the differences in the torque-rotation response due to the construction method.

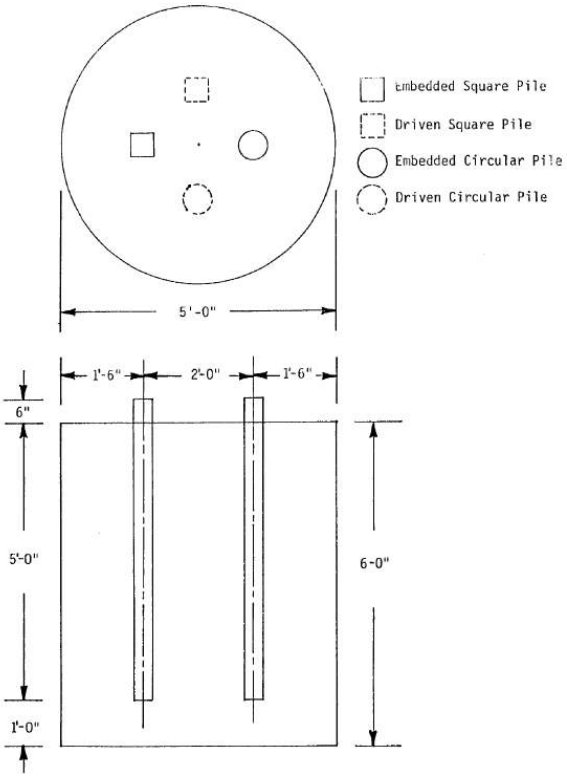

Figure 2.2 Layout of test piles (after Dutt 1976)

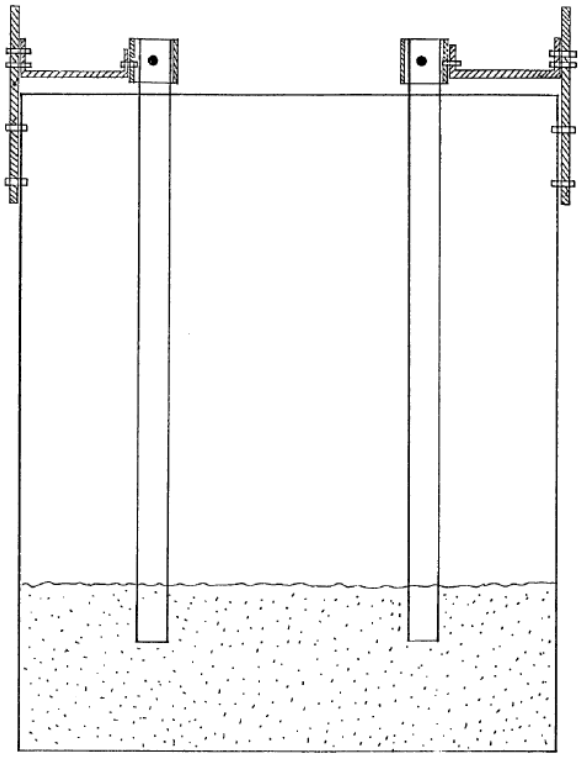

Figure 2.3 Installation of the first two piles (after Dutt 1976)

Figure 2.4 and table 2.1 summarize the physical characteristics of the sand used. Resistance strain gages were installed at four different elevations of the circular pile to measure the shear strains. However, valid data were only obtained from the pile that was embedded (as opposed to driven) in the dense sand. The relationship between torque and pile head twist (fig. 2.5) from Dutt and O'Neill (1983) indicated two things: (1) An increase of approximately four-

fold in relative density from the loose to the dense state led to a less than a two-fold increase in the apparent pile head torque for the circular pile at failure. (2) The torsional resistance for the driven pile was slightly larger than that for the embedded condition, which was due to the vibration-induced densification caused by driving. The torque distribution for the circular pile embedded in dense sand is depicted in figure 2.6. It indicates that the torsional resistance observed at a depth equal to 80 percent of its embedded length (~ 10 lb-in) was about 6 percent of the total available torsional resistance (~ 170 lb-in) at the rotation of 0.008 radians. The authors concluded that the torsional resistance offered by the base of the pile was insignificant, if not zero. The relationship between the torsion transfer and twist at different depths, as shown in figure 2.7, were computed for the circular pile embedded in dense sand. This figure shows that the apparent ultimate torque transferred to the soil increased with depth, indicating that the torque transferred to the soil was a function of the effective stresses.

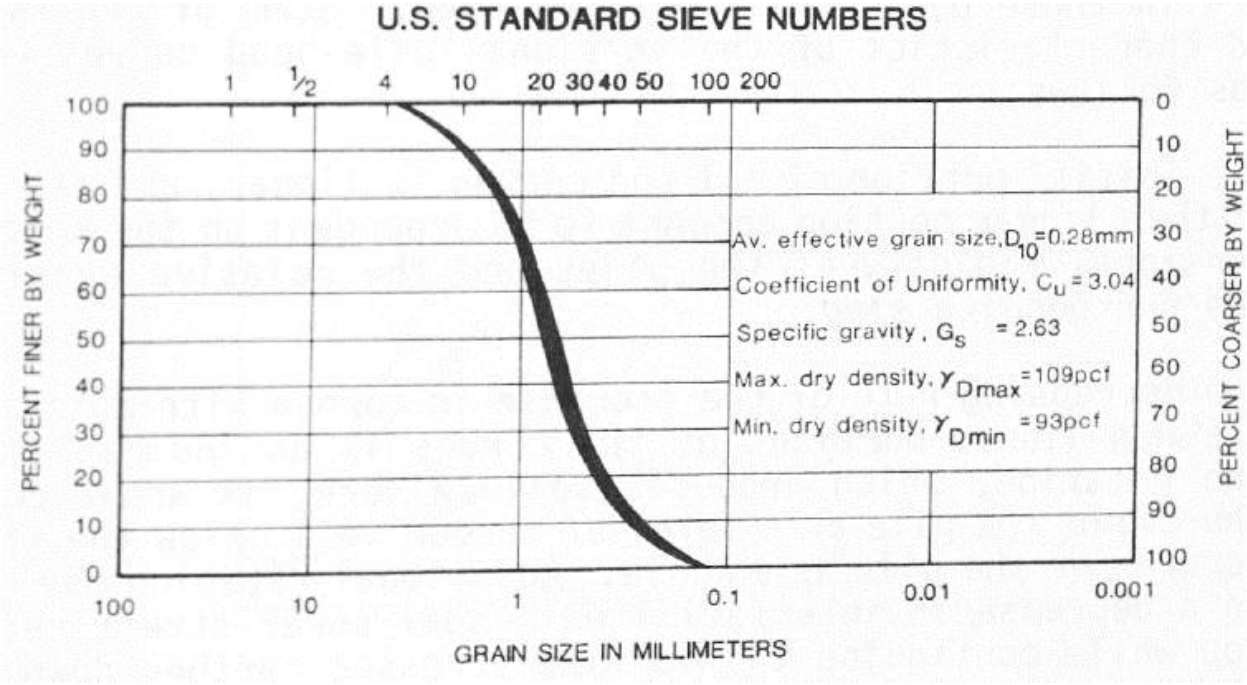

Figure 2.4 Physical properties of sands (after Dutt and O'Neill 1983)

Table 2.1 Strength properties of test sands (after Dutt and O'Neill 1983)

TRIAXIAL TEST		DIRECT SHEAR TEST (Soil-Soil)		DIRECT SHEAR TEST (Soil-Soft Aluminum)	
DRY DENSITY γ_D ,pcf	FRICTION ANGLE ϕ ,Degrees	DRY DENSITY γ_D ,pcf	FRICTION ANGLE ϕ ,Degrees	DRY DENSITY γ_D,pcf	ANGLE OF WALL FRICTION ϕ , Degrees
98.2	39.5	96.3	37.2	96.0	23.6
106.8	42.5	107.0	40.3	107.0	26.3

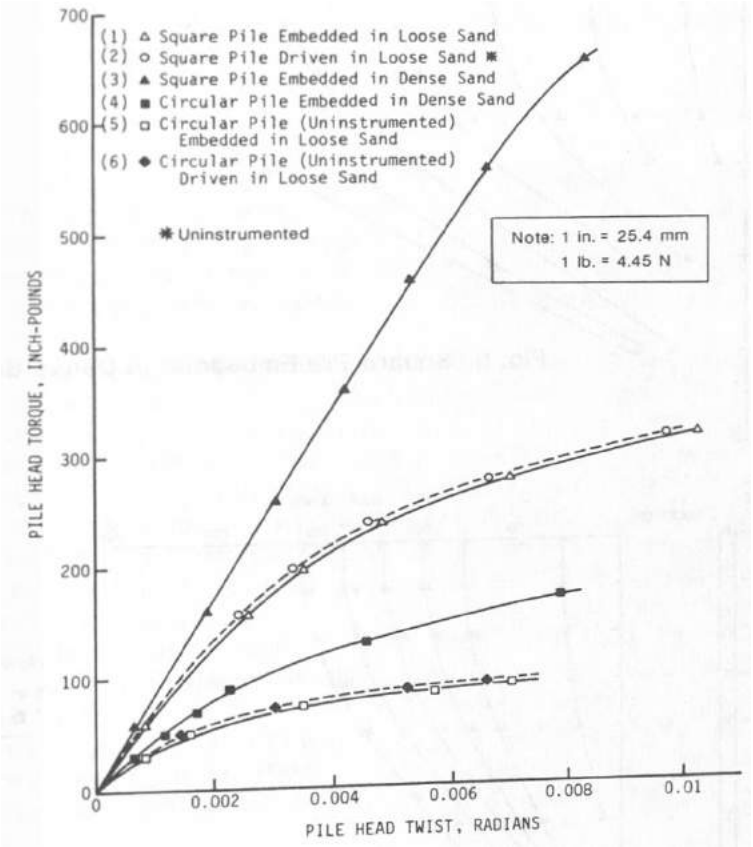

Figure 2.5 Pile-head torque-twist curves (after Dutt and O'Neill 1983)

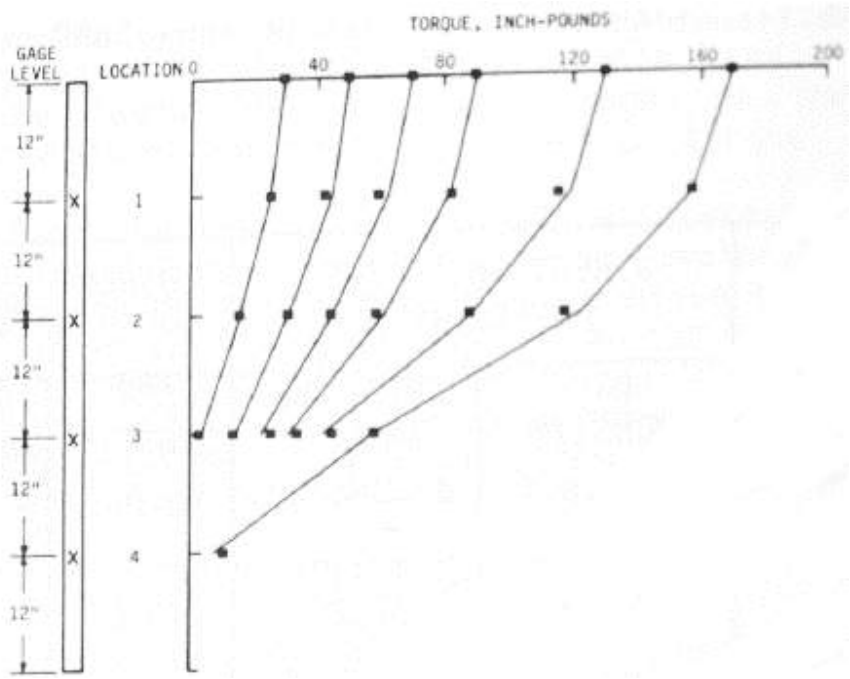

Figure 2.6 Torque distribution for circular pile embedded in dense sands (after Dutt and O'Neill 1983)

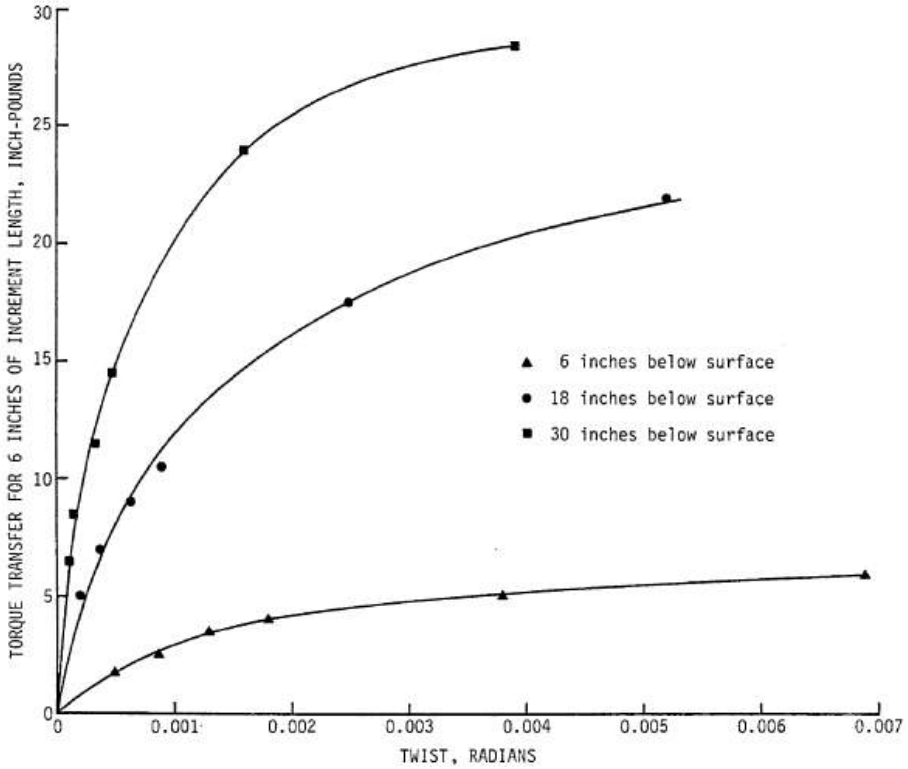

Figure 2.7 Shear stress-strain curves at different depths for the circular pile embedded in dense sands (after Dutt and O'Neill 1983)

Randolph (1983) described torsional loading tests on a steel pile of 10.6 mm (0.42 in) diameter and a polypropylene pile of 11.2 mm (0.44 in) diameter jacked 300 mm (11.8 in) into normally consolidated Kaolin clay to study the effect of the flexibility of a pile on its performance under monotonic and cyclic loading. The shear modulus of the polypropylene pile was between 0.30 and 0.44 GPa (44 to 64 ksi), whereas the shear modulus of the steel pile was about 77 GPa (11×10^3 ksi). To achieve a consistent surface texture for the different piles, both piles were coated with a thin layer of araldite (an adhesive) and fine sand. Monotonic loading was applied on the piles followed by cyclic loading. Cyclic loading tests were performed between 2 percent and 50 percent (point A in fig. 2.8a) and between 2 and 63 percent (point B in fig. 2.8a) of the peak capacity for the steel pile. For the polypropylene pile, the cyclic loading tests were conducted between 3 and 53 percent (point A in fig. 2.8b), 3 and 73 percent (point B in fig. 2.8b), and 3 and 93 percent (point C in fig. 2.8b) of the peak capacity.

The torque-twist relationships for both test piles are shown in figure 2.8. The steel pile, which had higher stiffness, reached its peak at the rotation of about 0.05 radians (3°). However, the torsional response was softer for the polypropylene pile, which achieved its peak value at a rotation of about 1.05 radians (60°). A reduction in torsional resistance was observed beyond the peak capacity. During the cyclic loading, no obvious degradation of torsional resistance was observed for the steel pile. For the polypropylene pile, the initial stiffness seemed constant during the cyclic loading, and permanent rotation was developed during every loading cycle.

Tawfiq (2000) used a 1.2-m (4-ft) diameter and 1.5-m (5-ft) deep steel chamber, as shown in figure 2.9, to perform torsion tests for a small-scale shaft model in sand. The shaft, which was made of plain concrete, was 508 mm (20 in) long with a diameter of 102 mm (4 in). The torque was applied by using a loading wheel and two 20-gallon buckets that were filled with

water at a constant flow rate to achieve a constant rate of loading. Two sets of loading tests were conducted: the first consisted of a set of tests that allowed the development of both toe and shaft resistance, whereas the second set of tests was conducted to evaluate base and shaft resistance separately. The toe resistance was eliminated by placing two greased metal plates at the shaft bottom; and the side friction was eliminated by enlarging the borehole so that the shaft surface was separated from the surrounding soil. As shown in figure 2.10, the tests by Tawfiq (2000) indicated that the shaft resistance comprised about 91 percent of the total available torsional resistance (~27 ft-lbs or 0.04 kN-m) at approximately two radians (approximately 115 degrees). On the other hand, the toe resistance was not observed to be larger than 5 ft-lbs (0.007 kN-m) when evaluated alone, and about 2.5 to 3 ft-lbs (0.0034 to 0.004 kN-m) when evaluated with shaft resistance.

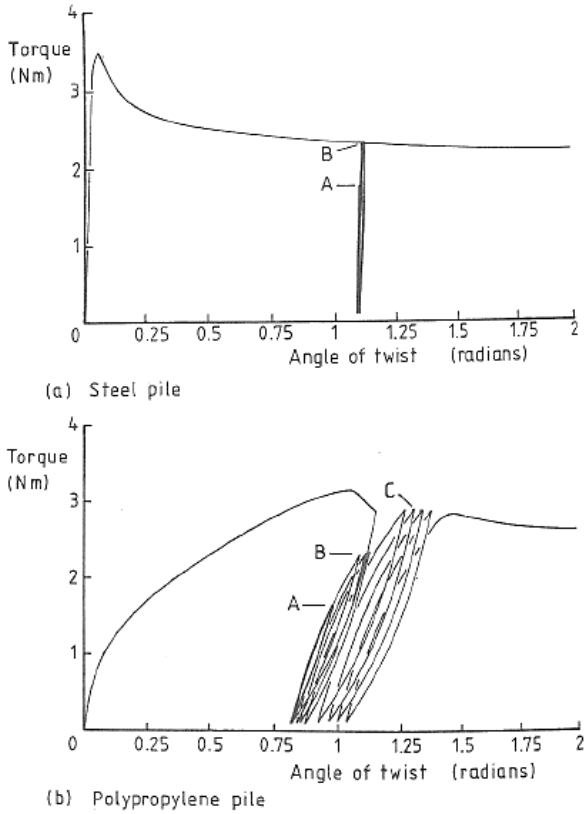

Figure 2.8 Torque-twist relationships for (a) steel pile and (b) polypropylene pile (after Randolph 1983)

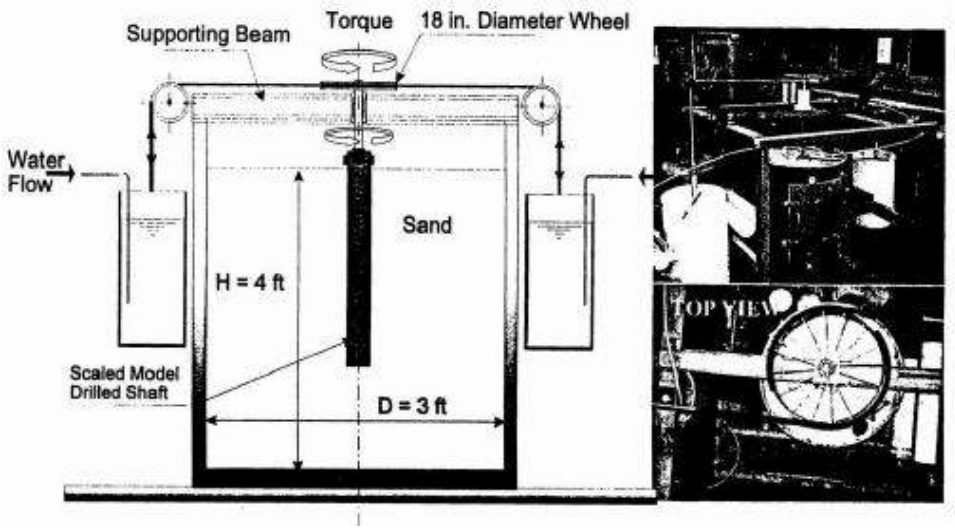

Figure 2.9 Scaled model torsional testing apparatus (after Tawfiq 2000)

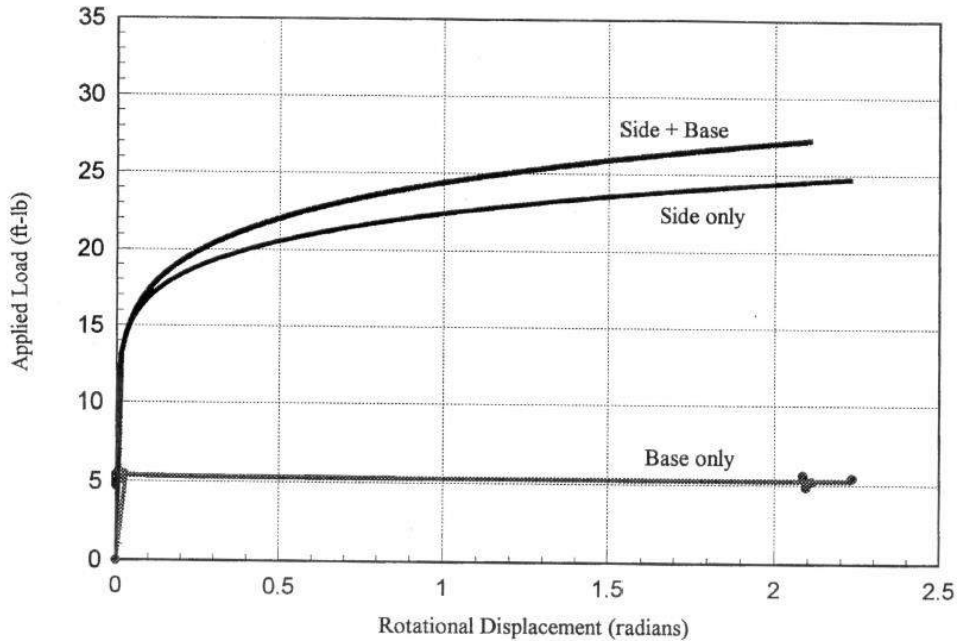

Figure 2.10 Relationship between torque and rotation (after Tawfiq 2000)

2.2.2 Torsional Loading Tests on Centrifuge Model Piles and Shafts

Bizaliele (1992) conducted static and cyclic torsion tests on aluminum model piles of 21 mm (0.83 in) diameter, 1 mm (0.04 in) wall thickness, and 340 mm (13.4 in) embedded length in sands. The total length of the model pile was 380 mm (15 in). With the chosen acceleration level of 50*g*, the model piles simulated prototype piles of 1.05 m (41 in) diameter and 17.0 m (56 ft)

embedded length. Strain gages were mounted at 45° to the axis of the pile at five levels. The applied load and resulting rotation were measured by using a load cell and a linear variable displacement transducer, respectively. The sand used in this test was uniformly graded, with an effective grain size D_{10} of 0.12 mm and an angle of internal friction of 38°. The maximum and minimum dry density were 1.69 and 1.42 g/cm^3, respectively. Figure 2.11 shows the centrifuge model set-up. The static pile head torque-twist behavior is depicted in figure 2.12. A linear response was observed for applied torque up to 8 N-m (6 lb-ft); the response transitioned to nonlinear for greater torsion. The maximum torque was approximately 28 N-m (24 lb-ft) at approximately 0.07 radians of pile head twist, followed by softening. The shaft resistance at each level was calculated by using the measured shear strain. Figure 2.13 shows the magnitude of torsional shaft resistance at different depths (*n.b.*, L = depth and r = shaft radius) as a function of the number of cycles. Results indicated that a small change in shaft resistance was observed for the first 10 cycles. After that, little variation of the shaft resistance with additional cycling was observed.

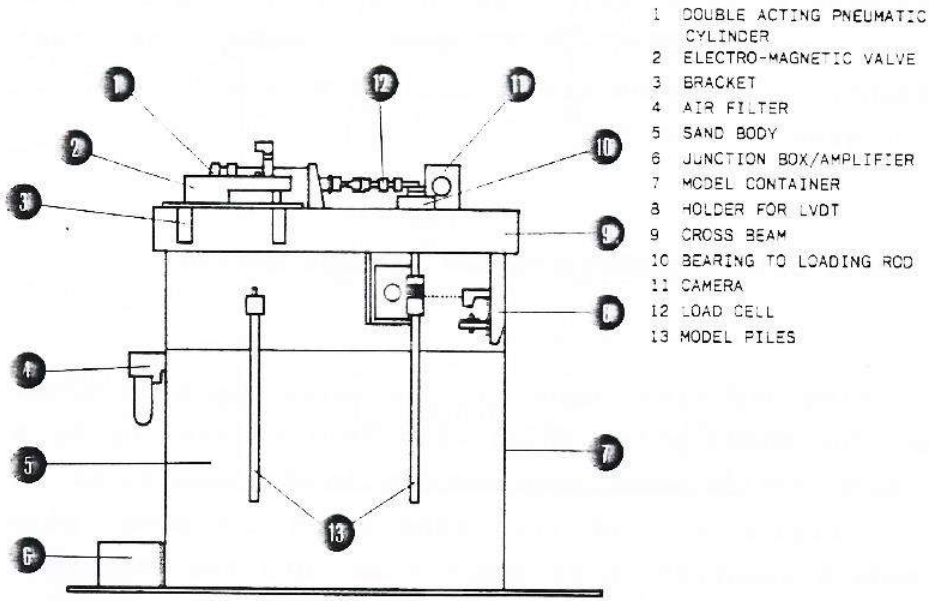

Figure 2.11 Centrifuge model set-up (after Bizaliele 1992)

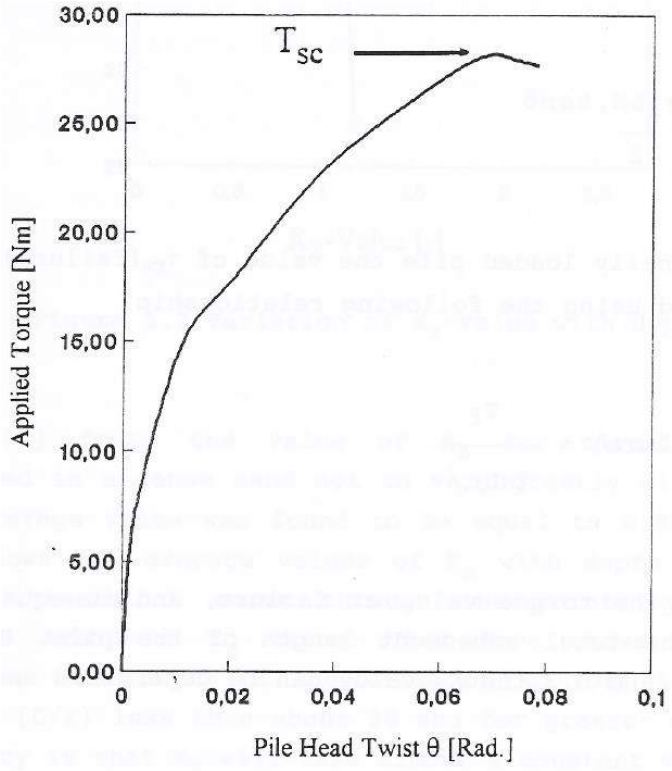

Figure 2.12 Static pile head torque-twist behavior in model scale (after Bizaliele 1992)

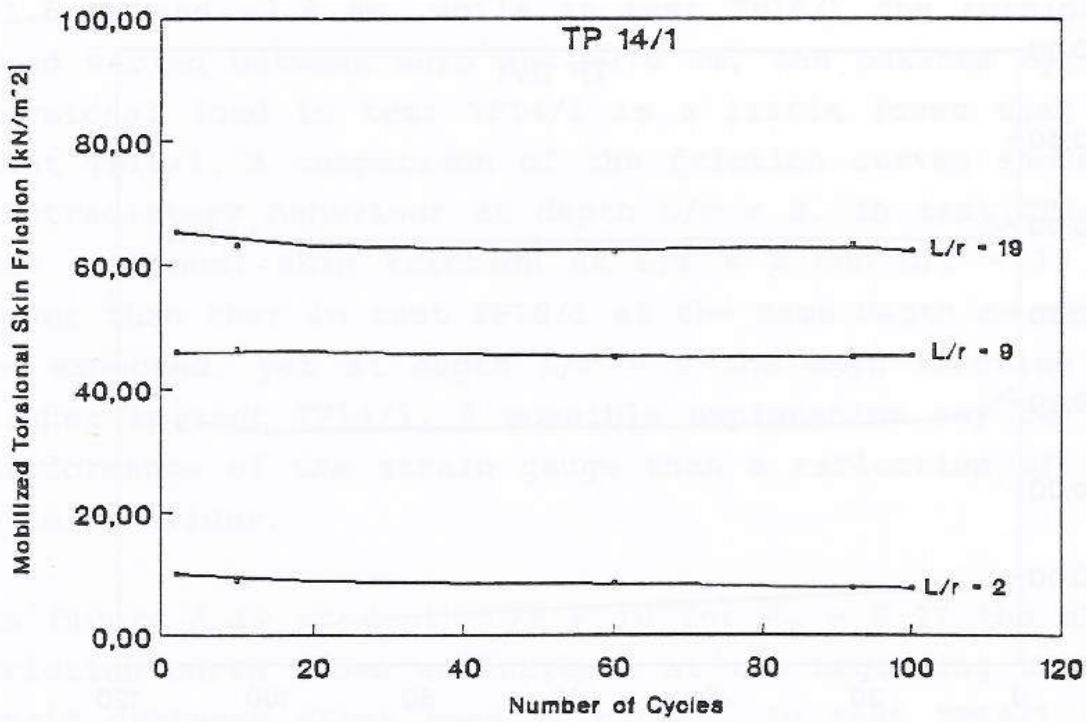

Figure 2.13 A typical distribution of torsional shaft resistance at different depths as a function of the number of cycles (after Bizaliele 1992)

Laue and Sonntag (1998) performed torsion tests on hollow aluminum model piles with a diameter of 15 mm (0.6 in) and a length of 170 mm (6.7 in) in sand. The acceleration level was 100*g*, and the model piles represented prototype piles of 1.5 m (5 ft) diameter and 17.0 m (56 ft) length. Two types of sand in a dense state were used: Normsand (angle of internal friction = 38°) and fine Fontainebleau sand (angle of internal friction = 37°). The gradation of the test sands is shown in figure 2.14.

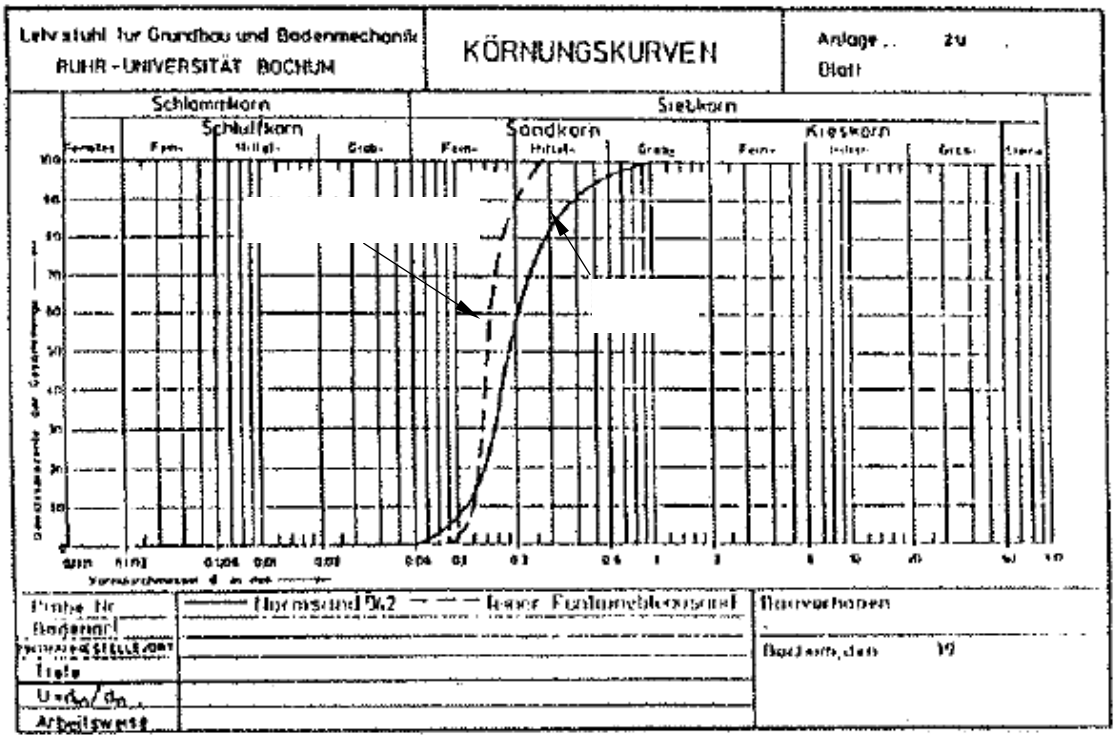

Figure 2.14 Gradation of the Normsand and fine Fontainebleau sand (after Laue and Sonntag 1998)

Figure 2.15 shows the torque-rotation response under different soil-shaft interface and soil conditions, as summarized in table 2.2. The torque-rotation response of smooth-shaft TP 2.1 was consistent with a hyperbolic relationship, whereas the rough-shaft TP 3.2 exhibited a near-linear perfectly plastic response; neither pile exhibited post-peak softening. The torque-rotation

response of the smooth-shaft pile TP 6.1 was also consistent with a hyperbolic curve, requiring significant rotation to achieve the peak resistance. However, the rough-shaft TP 6.2 achieved a peak torsional load at approximately 1° of rotation, as a result of the rough interface being modeled. The results showed that the relative value of roughness and gradation influenced the torsional resistance of pile. Tests with combined axial and torsional loads were performed and the results are depicted in figure 2.16. It shows that the applied torque increased without any rotation of piles at the beginning of the test. Because of the limitations of the loading system, the maximum torsional resistance was not obtained for the rough pile in Normsand under 500 N axial loading. The existing axial loads increased the torsional capacity for the smooth pile in Normsand from about 1.8 N-m (1.3 lb-ft) to 2.8 N-m (2.1 lb-ft). A cyclic loading test was also performed. Figure 2.17 shows the results of the first four cycles; the initial stiffness and post-yield slope for each loading cycle were quite similar.

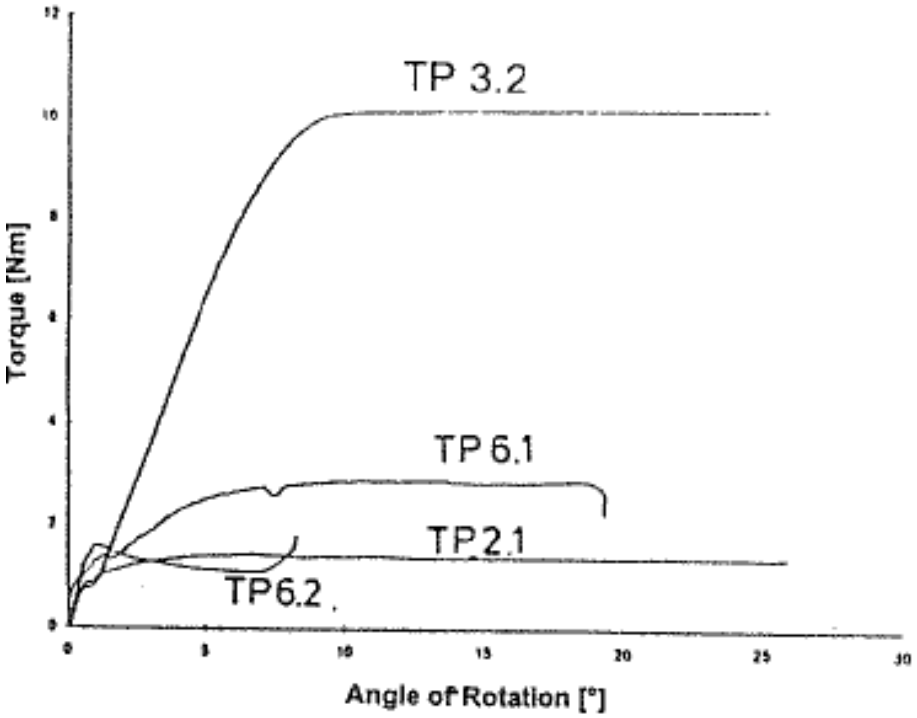

Figure 2.15 Comparison of the torque-rotation response (after Laue and Sonntag 1998)

Table 2.2 Summary of test conditions evaluated by Laue and Sonntag (1998)

Test Designation	Shaft Interface Condition	Soil Evaluated
TP 2.1	Smooth	Normsand
TP 3.2	Rough	Normsand
TP 6.1	Smooth	Fine Fontainebleau sand
TP 6.2	Rough	Fine Fontainebleau sand

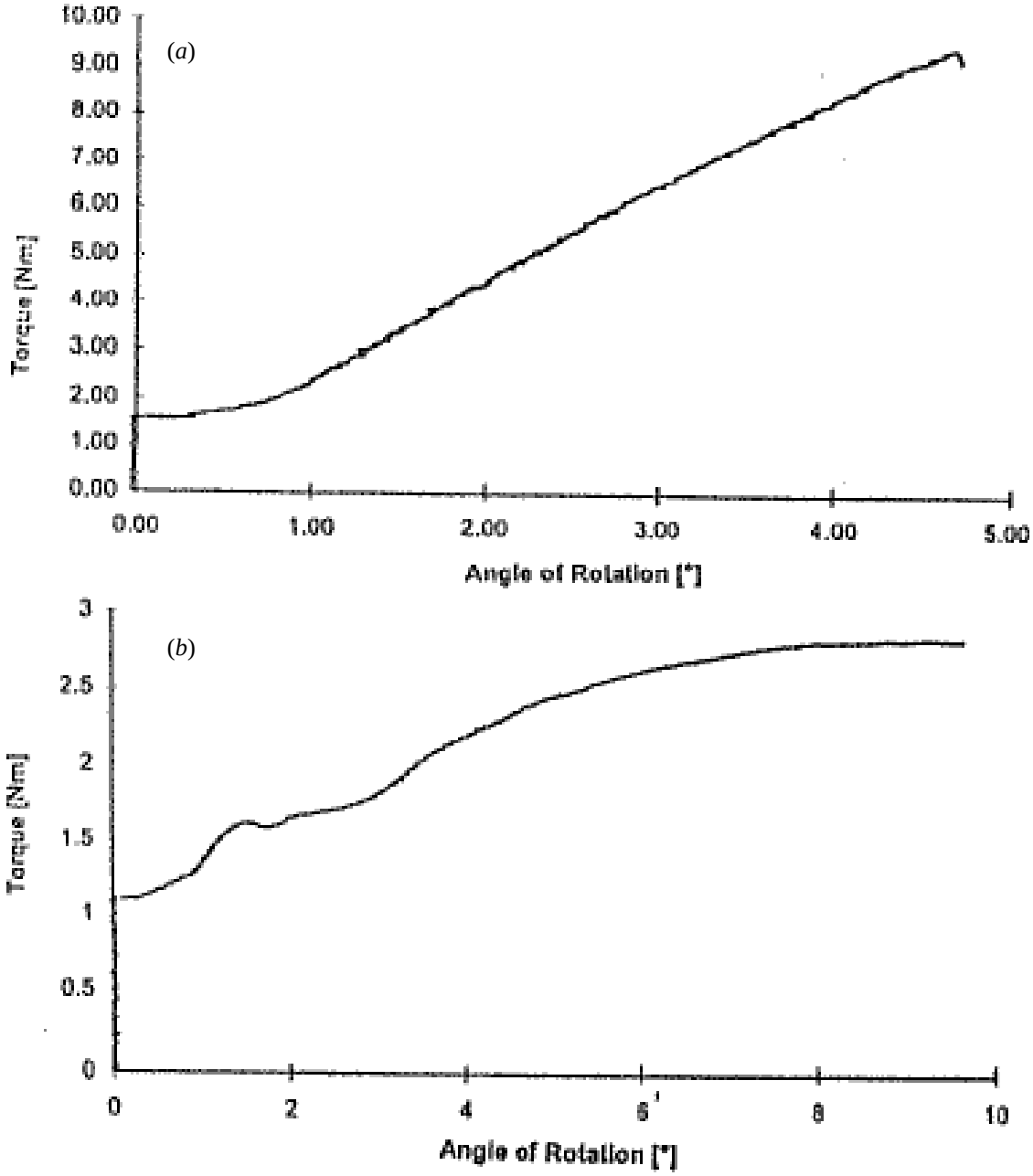

Figure 2.16 Torque vs. rotation response of (a) rough pile in Normsand with an axial load of 500 N and (b) smooth pile in Normsand with an axial load of 100 N (after Laue and Sonntag 1998)

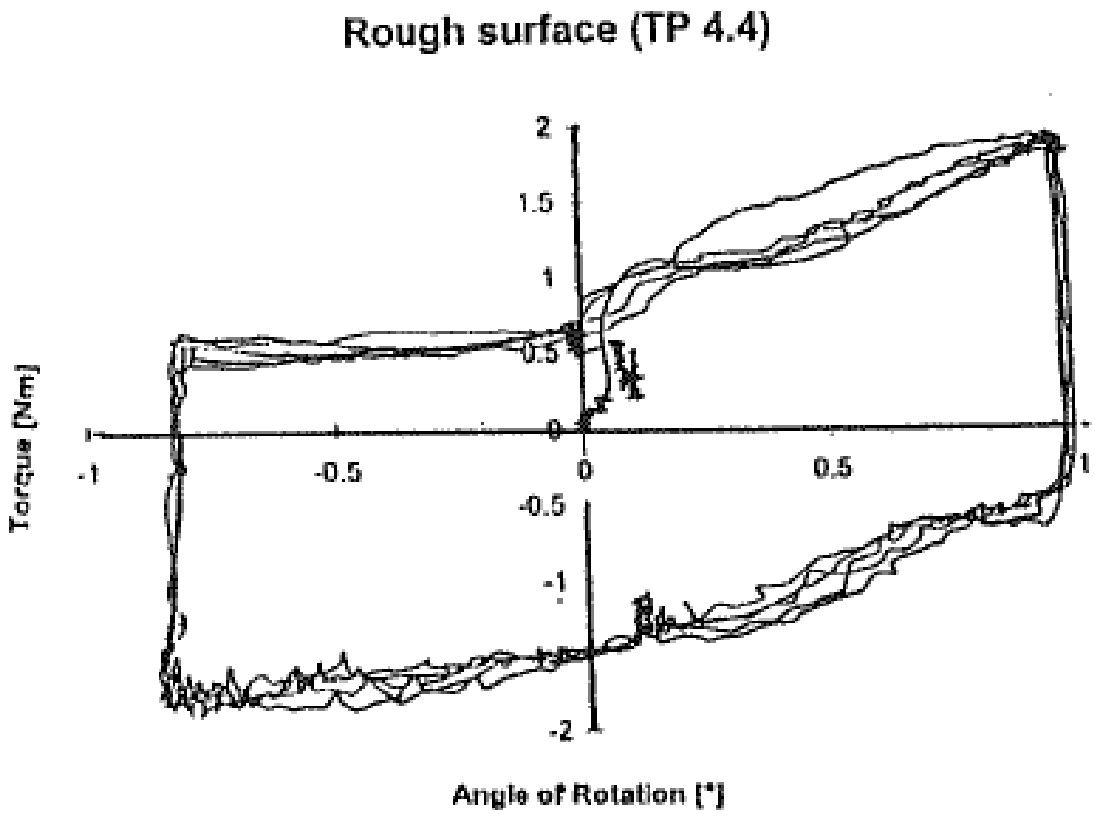

Figure 2.17 Pile under cyclic torsional loading (after Laue and Sonntag 1998)

A number of centrifuge tests on high mast sign/signal structures (mast arm, pole, and drilled shaft) were conducted in University of Florida to determine the optimum depth of drilled shafts subjected to combined torsion and lateral loads (McVay et al. 1989, McVay and Hu 2003, and Hu 2003). The prototype shaft diameter was 1.5 m (5 ft), and the prototype embedment length ranged from 4.6 m (15 ft) to 10.7 m (35 ft). The shafts were constructed in dry and saturated silica-quartz sand from Edgar, Florida, compacted to loose, medium dense, and dense conditions. To investigate the effects of various construction methods, steel casings and wet methods, using bentonite slurry and KB polymer slurry produced by KB Technologies Ltd. (http://www.kbtech.com), were evaluated. Table 2.3 summarizes the centrifuge tests, whereas figure 2.18 shows the centrifuge test set-up.

Table 2.3 Summary of the centrifuge tests conducted at the University of Florida

	McVay et al. (2003)	McVay and Hu (2003)	Hu (2003)
Construction Method	Steel casings and wet methods using bentonite slurry	Wet methods using polymer slurry	Wet methods using bentonite and polymer slurry
Soil state with relative density	Loose (29%), medium dense (51%) and dense (64%)	Loose (34%) and dense (69%)	Loose (34%) and dense (69%)
Prototype embedment length m (ft)	4.6, 7.6, and 10.7 (15, 25, and 35)	7.6 and 10.7 (25 and 35)	7.6 and 10.7 (25 and 35)

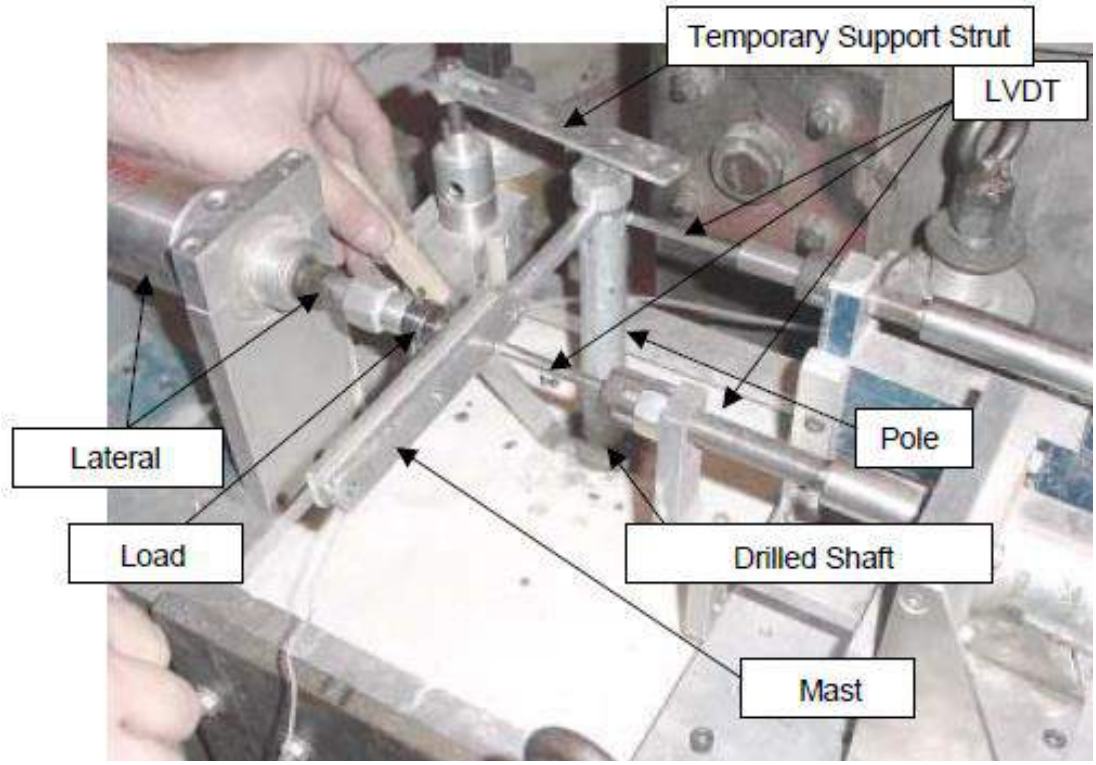

Figure 2.18 Centrifuge test set-up (after McVay et al. 2003)

Torque was applied with a lateral load applied on the middle and tip of the mast arm. Some typical test results of the relationship between torque and shaft rotation from Hu (2003) are shown in figure 2.19. No definitive peak was observed for the shafts constructed with both types of slurries. Summaries of the torsional capacity of the shafts constructed with bentonite and KB polymer slurry are listed in

Table 2.4 and 2.5, respectively. For both cases, the loading point did not have significant effects on the torsional capacity. For the shafts constructed with bentonite slurry, the results from the shaft constructed in loose sand were not significantly different than those from the shaft constructed in dense sand. The torsional capacities increased with an increasing embedment length. The average torsional capacity of a drilled shaft constructed with bentonite slurry and a 7.6-m (25-ft) embedment length was 1216 kN-m (897 kip-ft) and with a 10.7-m (35-ft) embedment length was 1979 kN-m (1460 kip-ft).

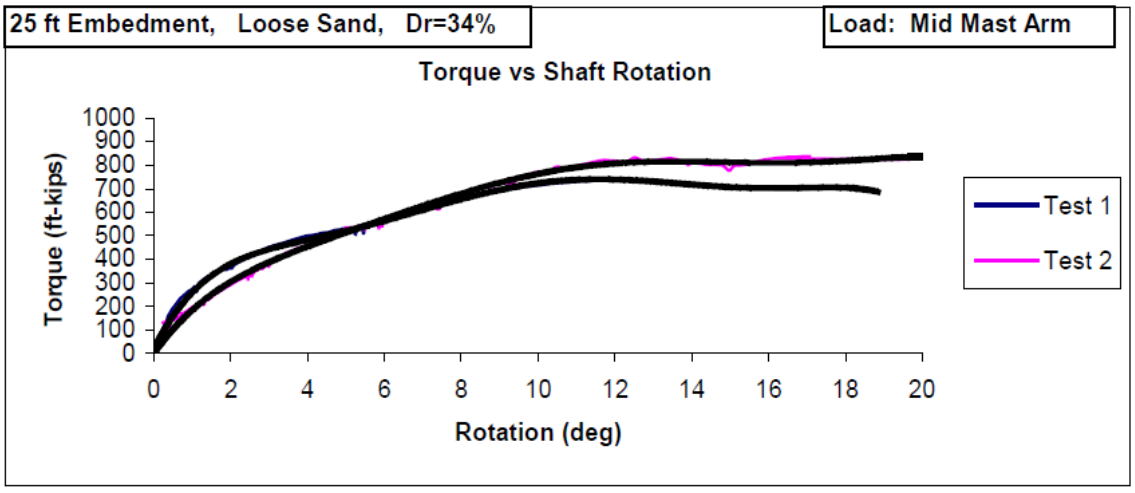

(a)

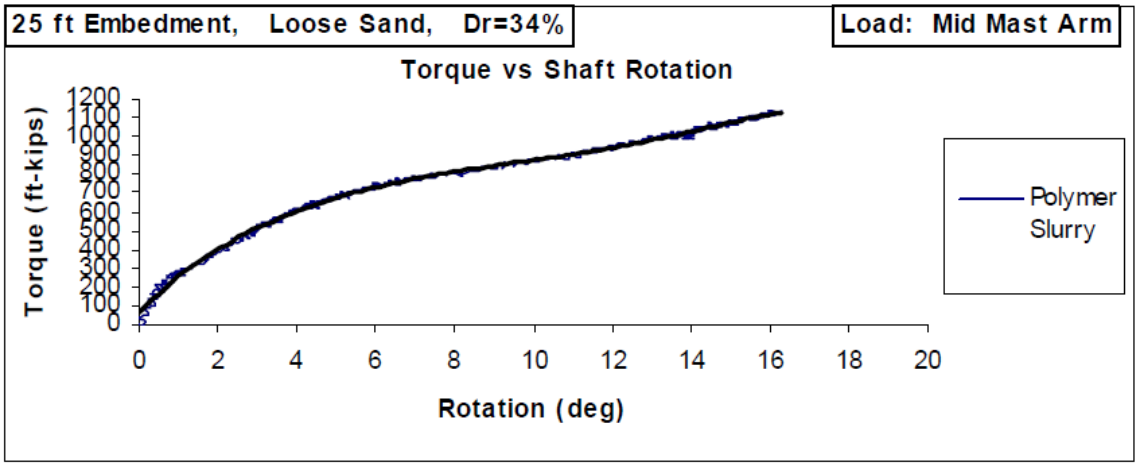

(b)

Figure 2.19 Torque-shaft head rotation response for shafts constructed with (a) bentonite and (b) polymer slurry with a 25-ft embedment length in loose sand (after Hu (2003))

For the drilled shafts constructed with KB polymer slurry, a significant increase in torsional capacity was observed for the shafts in dense sand in comparison to the shafts in loose sand. For drilled shafts of 7.6 m (25 ft), the average torsional capacities in dense and loose sand were 1510 and 2222 kN-m (1114 and 1639 kip-ft), respectively; for drilled shafts of 10.7 m (35 ft) the average torsional capacities in dense and loose sand were 2080 and 3043 kN-m (1534 and 2244 kip-ft), respectively. This may have been due to the efficiency of the polymer strands in a dense pore network, with smaller void spaces to span, as opposed to a loose pore network. Other test results from University of Florida can be found in McVay et al. (2003), McVay and Hu (2003), Hu (2003).

Table 2.4 Summary of the torsional capacity of the shafts constructed using bentonite slurry (based on the data provided by Hu (2003))

Point of load application	Soil State	Shaft Embedment Length, m (ft)	Applied Torque kN-m (kip-ft)
Mid mast arm	Dense	7.6 (25)	1207 (890)
	Dense		1464 (1080)
	Loose		1003 (740)
	Loose		1112 (820)
Arm tip	Dense	7.6 (25)	1288 (950)
	Dense		1003 (740)
	Loose		1308 (965)
	Loose		1342 (990)
Mid mast arm	Dense	10.7 (35)	1952 (1440)
	Dense		2291 (1690)
	Loose		1993 (1470)
	Loose		2156 (1590)
Arm tip	Dense	10.7 (35)	1817 (1340)
	Dense		1817 (1340)
	Loose		1898 (1400)
	Loose		1912 (1410)

Table 2.5 Summary of the torsional capacity of the shafts constructed using KB polymer slurry (based on the data provided by Hu (2003))

Point of load application	Soil State	Shaft Embedment Length, m (ft)	Applied Torque kN-m (kip-ft)
Mid mast arm	Dense	7.6 (25)	2420 (1785)
	Loose		1467 (1082)
Arm tip	Dense	7.6 (25)	2024 (1493)
	Loose		1552 (1145)
Mid mast arm	Dense	10.7 (35)	3277 (2417)
	Dense		3097 (2284)
	Loose		2122 (1565)
Arm tip	Dense	10.7 (35)	2755 (2032)
	Loose		2050 (1512)
	Loose		2069 (1526)

Zhang and Kong (2006) studied torsional load transfer by using aluminum tubes that were 300 mm (1 ft) in length, 15.7 mm (0.6 in) in outside diameter, and 0.9 mm (0.035 in) in wall thickness under 40*g* acceleration. For this level of acceleration, the prototype length was equal to 12 m (39 ft), the outside diameter was 628 mm (24 in), and wall thickness was 36 mm (1.4 in). A quartz-based uniform sand with D_{50} = 0.14 mm and grain size distribution, shown in figure 2.20, was used. The relative densities evaluated were 32 percent for the loose condition and 75 percent for the dense condition. Figure 2.21a shows the layout of the typical centrifuge test. The test piles were instrumented with strain gages along the length of model piles, as shown in figure 2.21b. The test piles were pushed into the sand bed after the centrifuge was spun to 40 *g* and the ground settlement ceased to develop. The embedded length of the prototype pile was 10.8 m (35 ft). Six tests were performed with various loading rates (i.e., 1, 3, and 8 degree/s) for each of the two relative densities, for a total of 12 tests. The torque-twist curves, shown in figure

2.22, indicate an approximately hyperbolic relationship. With a rotation of 1°, the applied torque was about 75 percent of the torsional capacity in the loose sand and 57 percent in dense sand. The torsional resistance was almost fully mobilized at approximately 4° for all of the cases. As expected, the relative density of the sand had a significant influence on the torsional resistance.

Figure 2.23 displays the torque distribution along the pile shaft at the loading rate of 1.0 degree/second. For this case, the toe resistance contributed 23 percent of the total torsional resistance in the loose sand and 40 percent in dense sands. However, this finding was not consistent with the results from Tawfiq (2000) and Dutt and O'Neill (1983), in which the contribution of toe resistance was less than 10 percent. The manifestation of the toe resistance in the centrifuge test could be a result of the downward acceleration of the sand deposit, which possibly imparted a drag load due to downward movement relative to the shaft.

To study the effect of loading rate, a semi-log plot, as shown in figure 2.24, was used to fit a trend line to the test data, given by:

$$T_u(\dot{\theta}) = T_u(\dot{\theta}_{ref})\left[1+\alpha \log\left(\frac{\dot{\theta}}{\dot{\theta}_{ref}}\right)\right] \tag{2.1}$$

where $T_u(\dot{\theta})$ and $T_u(\dot{\theta}_{ref})$ = torsional capacities at loading rates $\dot{\theta}$ and $\dot{\theta}_{ref}$, respectively, and α = a coefficient, which is 0.04 for the loose sand and close to zero for the dense sand.

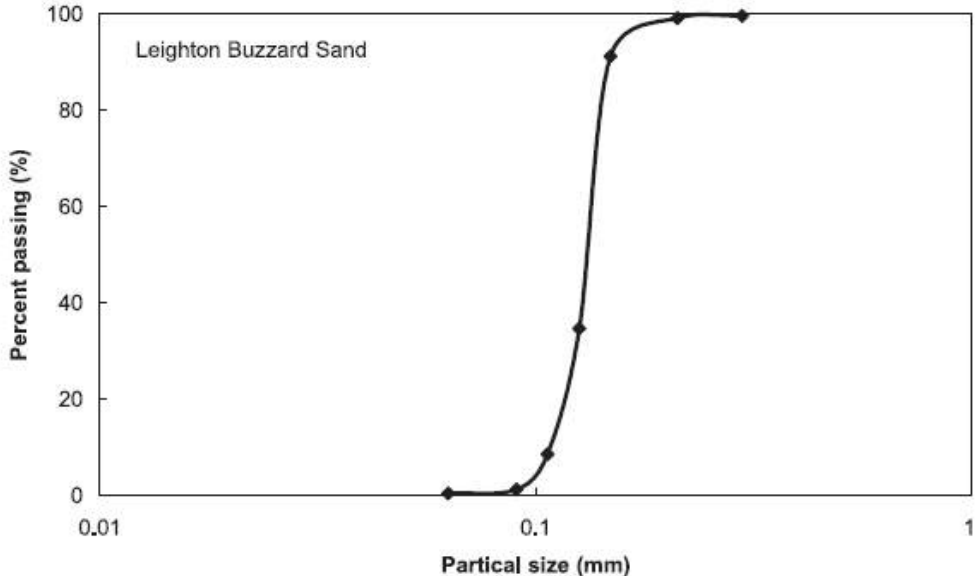

Figure 2.20 Grain size distribution of the test sand (after Zhang and Kong 2006)

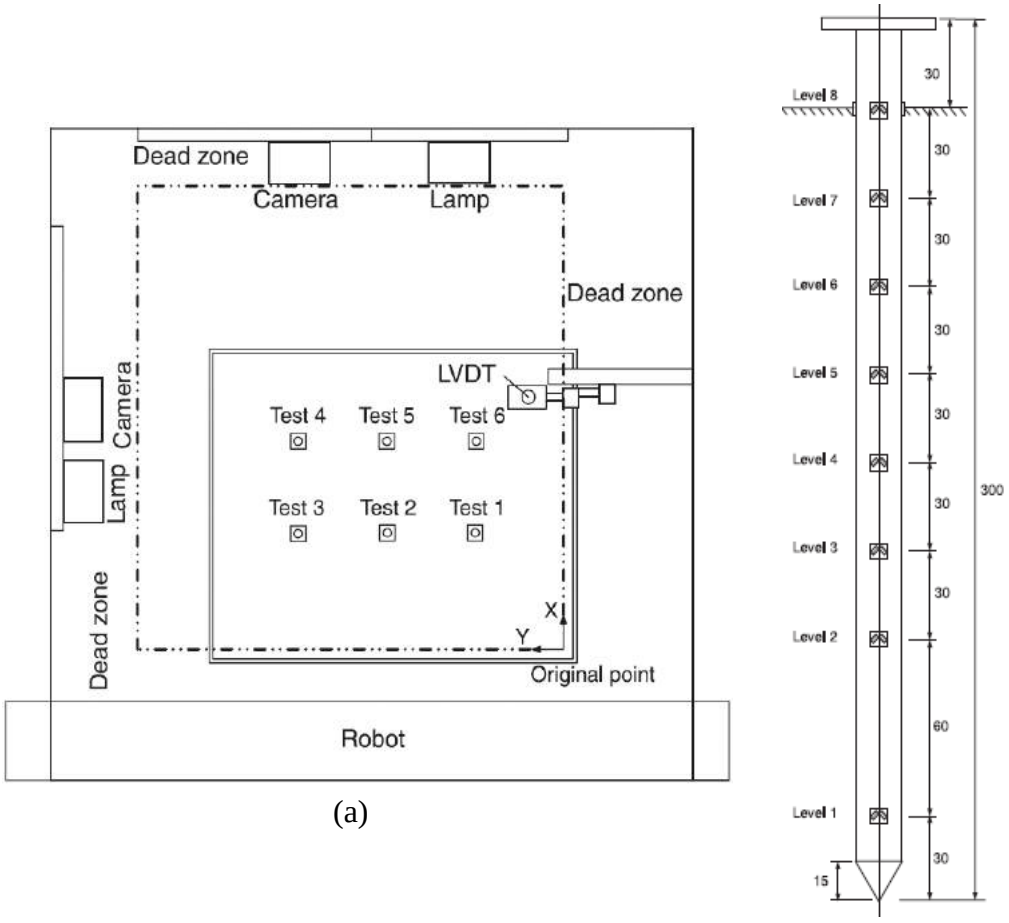

(a)

Figure 2.21 (a) Test layout, and (b) instrumentation showing dimensions in mm (after Zhang and Kong 2006)

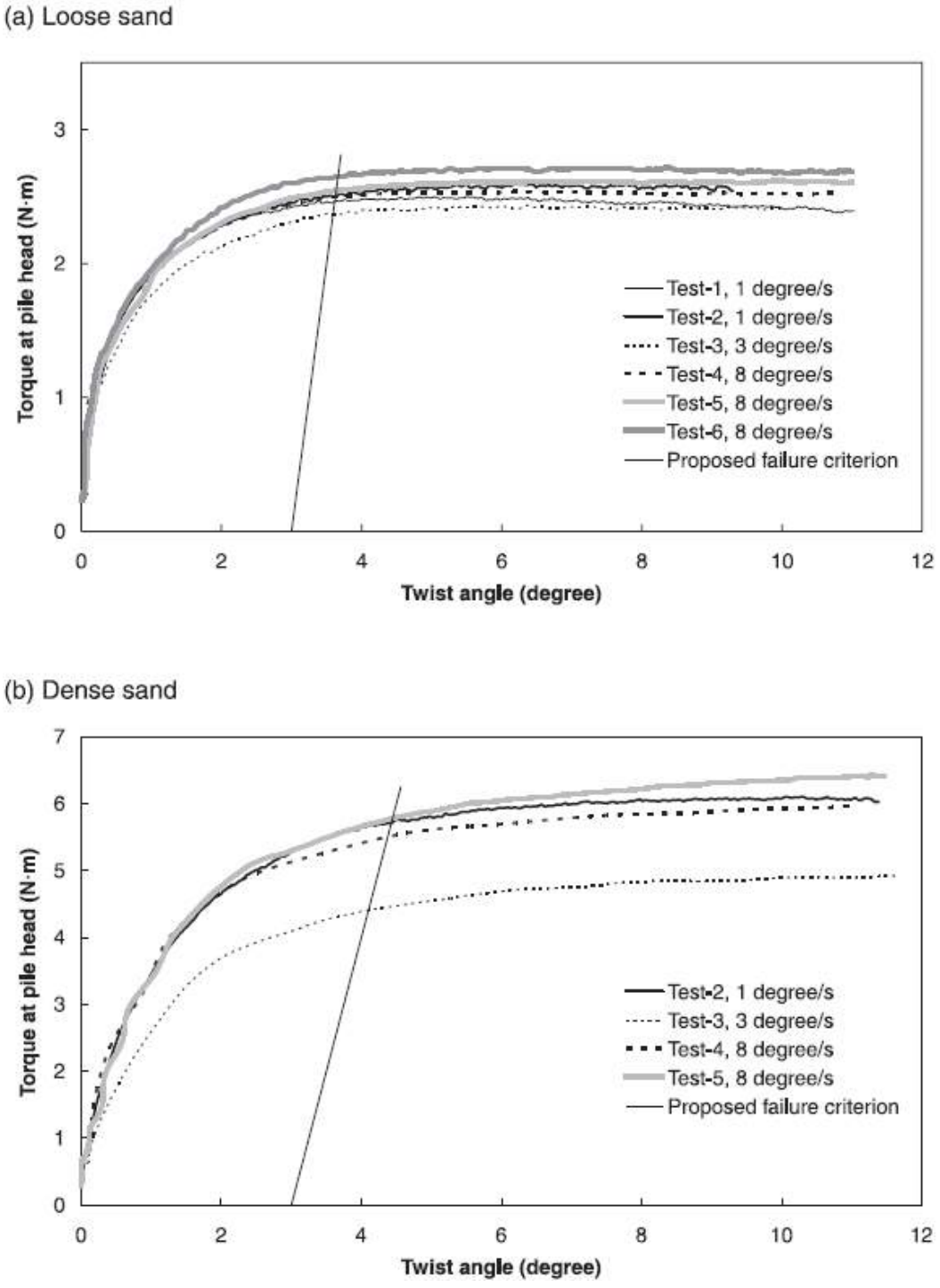

Figure 2.22 Torque-twist curves (after Zhang and Kong 2006)

(a) Loose sand

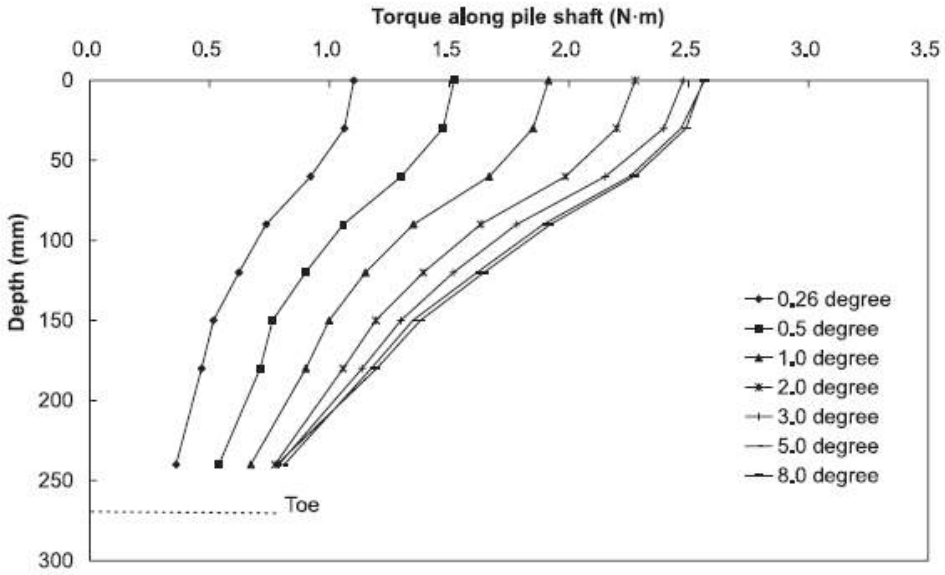

(b) Dense sand

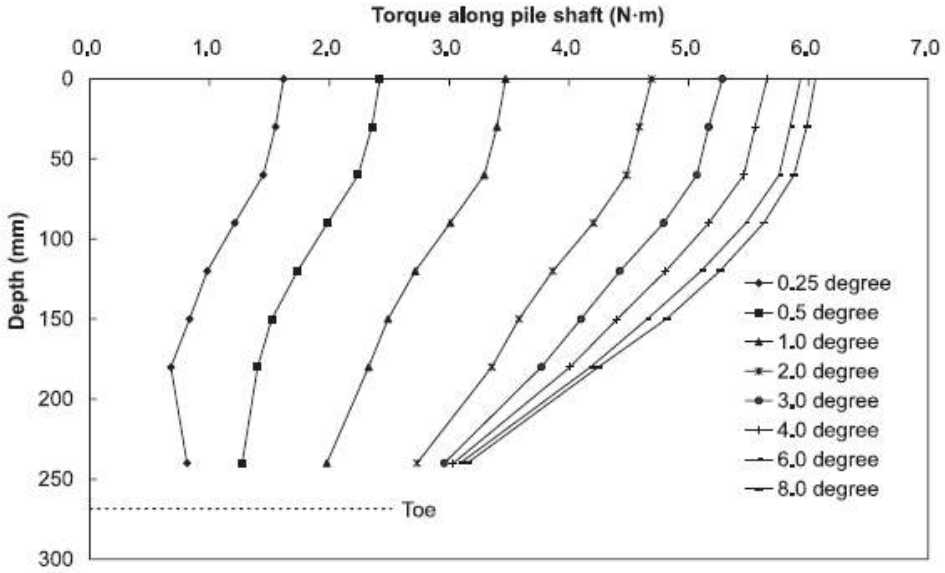

Figure 2.23 Torque distribution along pile shaft at a loading rate of 1.0°/s (after Zhang and Kong 2006)

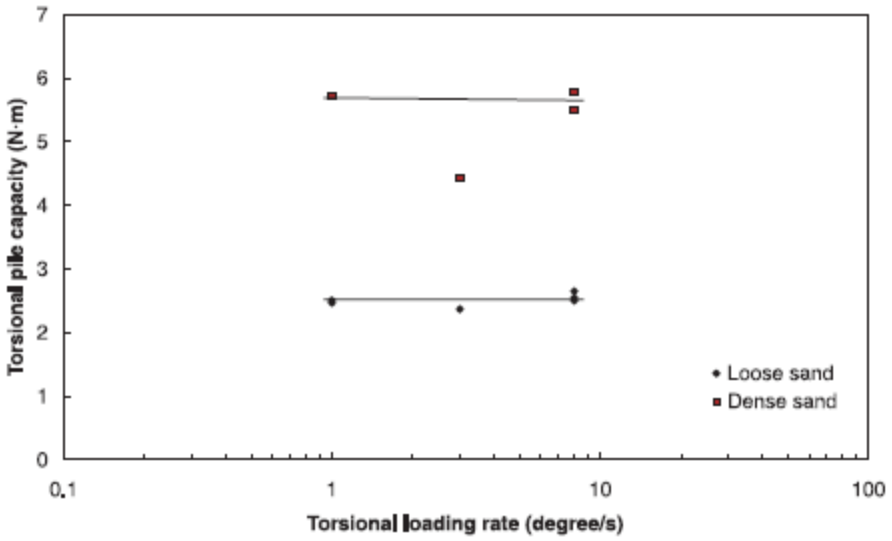

Figure 2.24 Effect of loading rate on torsional pile capacity (after Zhang and Kong 2006)

2.2.3 Torsion Tests on Full-scale Driven Piles and Drilled Shafts

In what may be the first reported test of torsional capacity, Stoll (1972) applied torque to two driven steel pipe piles filled with concrete, designated Pile A-3 and Pile V-4. The steel piles were 0.27 m (10.75 in) external diameter and had a 6.3-mm (0.25-in) wall thickness.

Figure 2.25 shows the set-up of the loading test. The soil profiles and driving logs for each test pile are shown in figure 2.26 and indicate the piles were driven in heterogeneous soil conditions. The test piles were driven to a final penetration resistance of 50 to 60 blows/foot. The resulting embedded length of Pile A-3 was 17.4 m (57 ft) and of Pile V-4 was 20.7 m (68 ft). On the basis of figure 2.26, the lengths of the pile above-ground surface for Pile A-3 was 1.0 m (3 ft) and of Pile V-4 was 0.7 m (2 ft). The rotation at the top of each test pile and applied torque were monitored and are shown in figure 2.27. The torsional resistance of both piles increased with the increase of pile rotation until failure at approximately 0.055 radians (3.2°). No definitive peak was observed for either of the test piles.

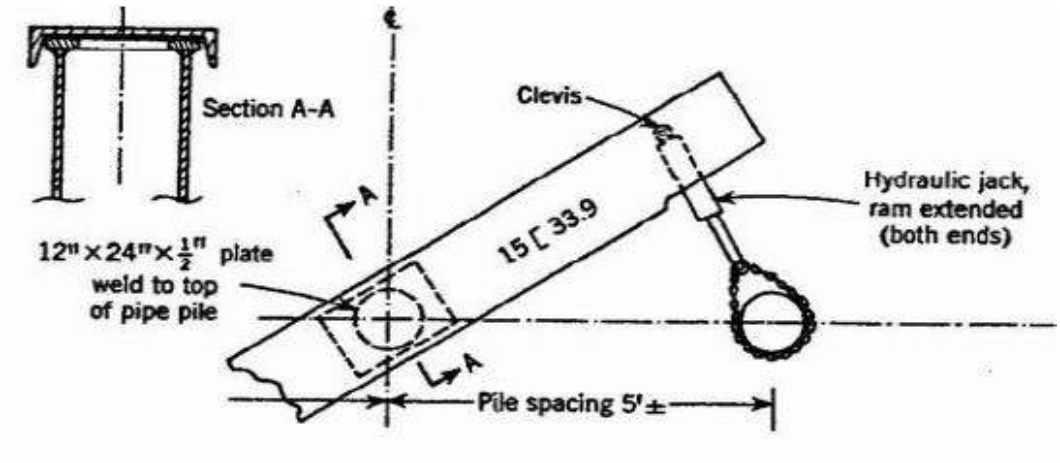

Figure 2.25 Pile torque shear test set-up (after Stoll 1972)

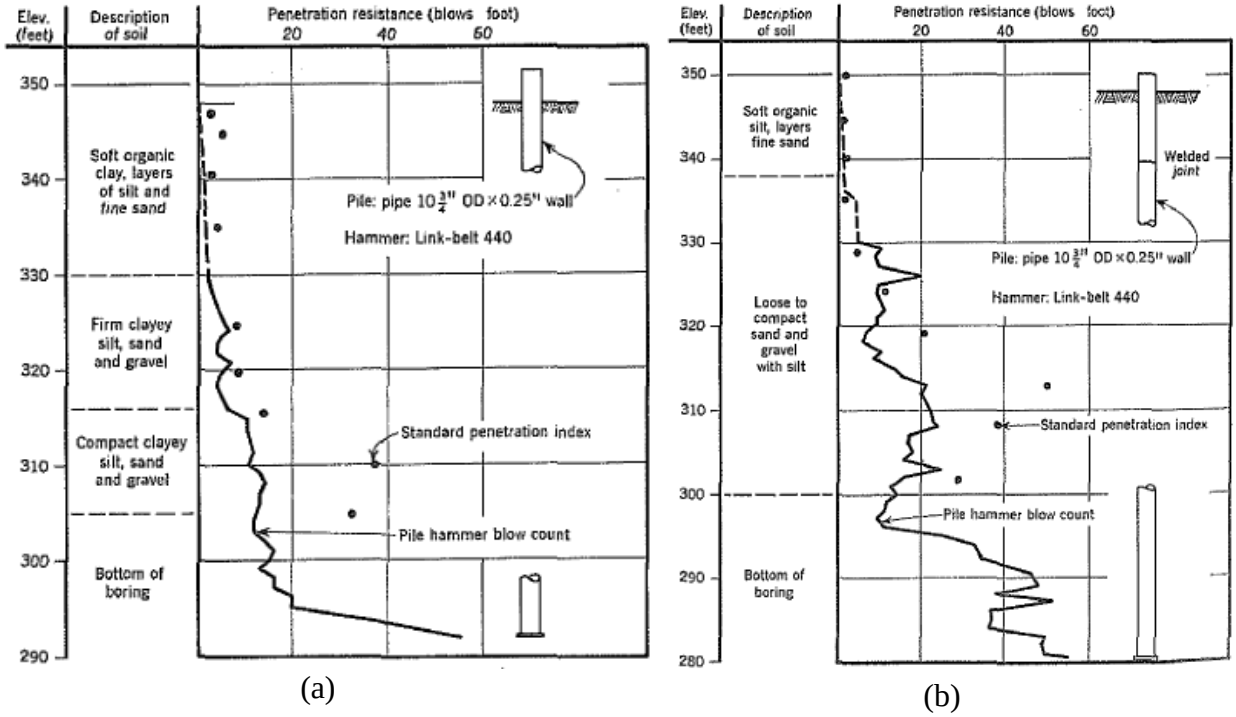

Figure 2.26 Soil profile and driving log for (a) Pile A-3 (b) Pile V-4 (after Stoll 1972)

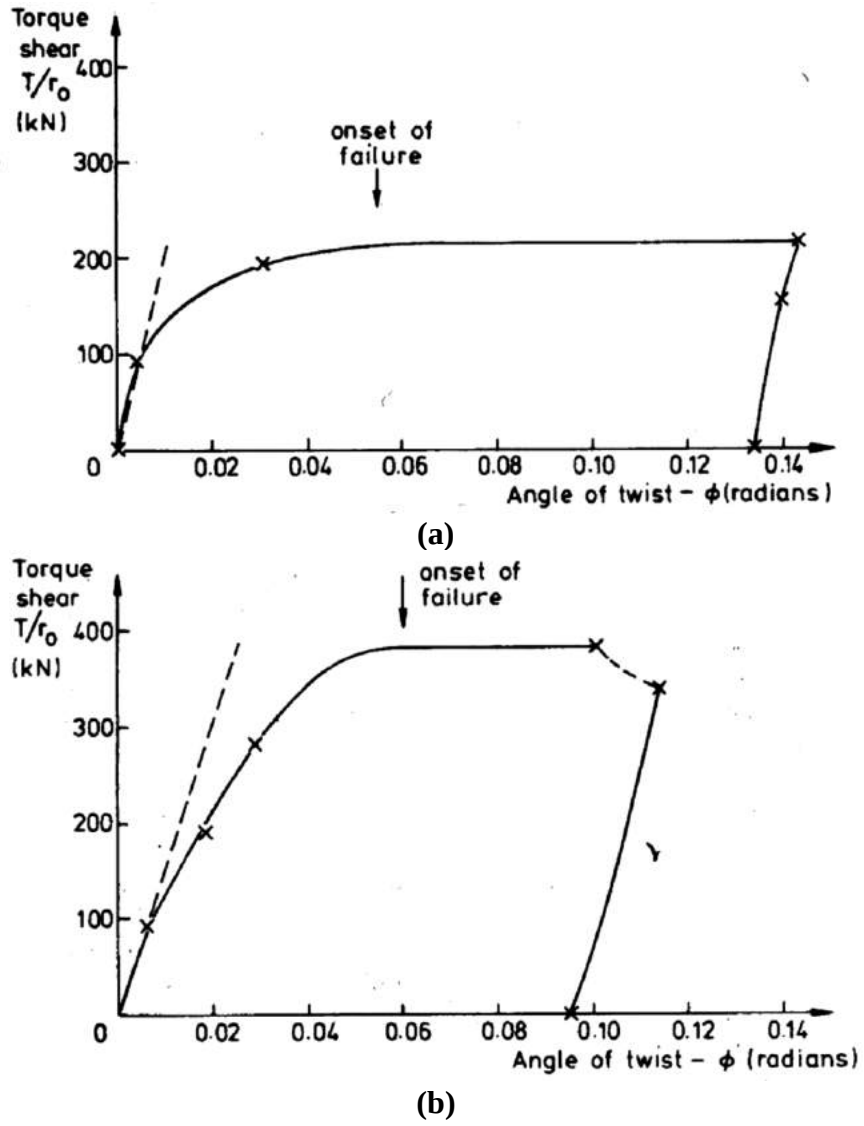

Figure 2.27 Results from torsional load tests: (a) Pile A-3 (b) Pile V-4 (after Randolph 1981, originally from Stoll 1972). Note: 0.1 radians = 5.7 degrees.

In addition to the model tests, Tawfiq (2000) performed full-scale field tests on three 1.2-m (4-ft) diameter by 6.1-m (20-ft) deep drilled shafts constructed in Tallahassee Florida. As shown in figure 2.28, load was applied with a 3.1-m (10-ft) steel cantilever beam. One shaft was constructed with the dry method (no slurry). The other two shafts were constructed with the wet method, with one supporting the drill cavity with a bentonite slurry and the other with a polymer slurry. Soil borings, as shown in figure 2.29, were drilled at the proposed locations of the drilled

shaft to investigate soil conditions. The soil profiles are shown in figure 2.30. Generally, a layer of silty sand was encountered from the ground surface to a depth of 0.3 m (1 ft), underlain by a layer of clayey sand or sandy clay to a depth ranging from 2.7 to 5.0 m (9 to 16 ft). Below this layer is a stratum of clayey, silty, fine sand underlain by a layer of sand with silt for the dry shaft (TH1) or sandy clay for the shaft using polymer slurry (TH2). The groundwater table was below the depth of the base of the foundation (over 20 ft).

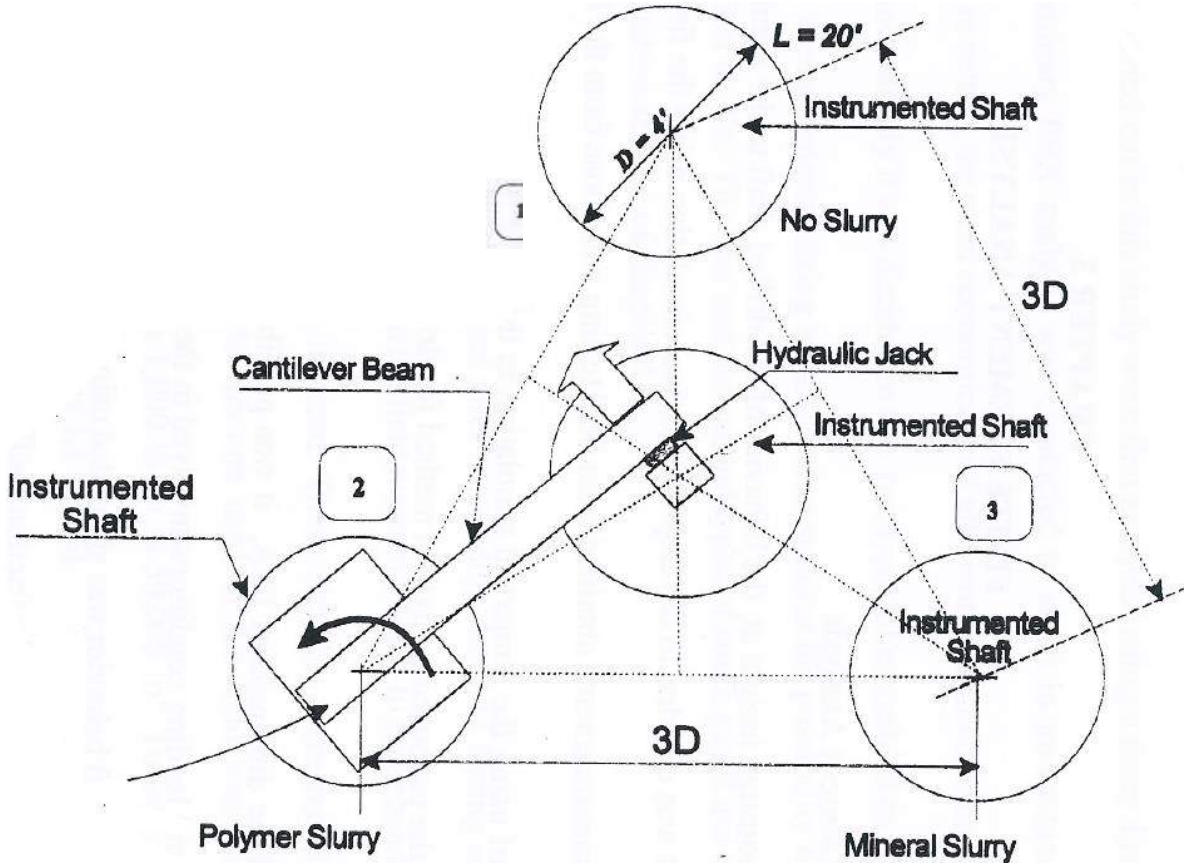

Figure 2.28 Full-scale test set-up (after Tawfiq 2000)

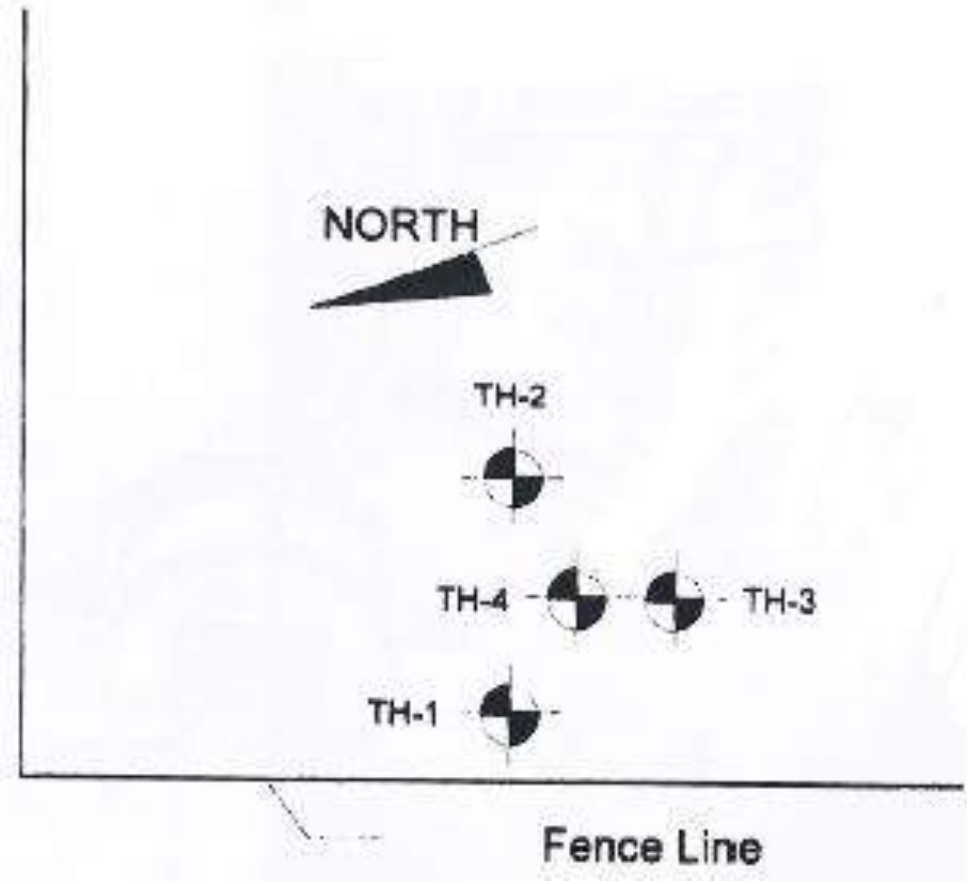

Figure 2.29 Locations of test shafts and borings (after Tawfiq 2000)

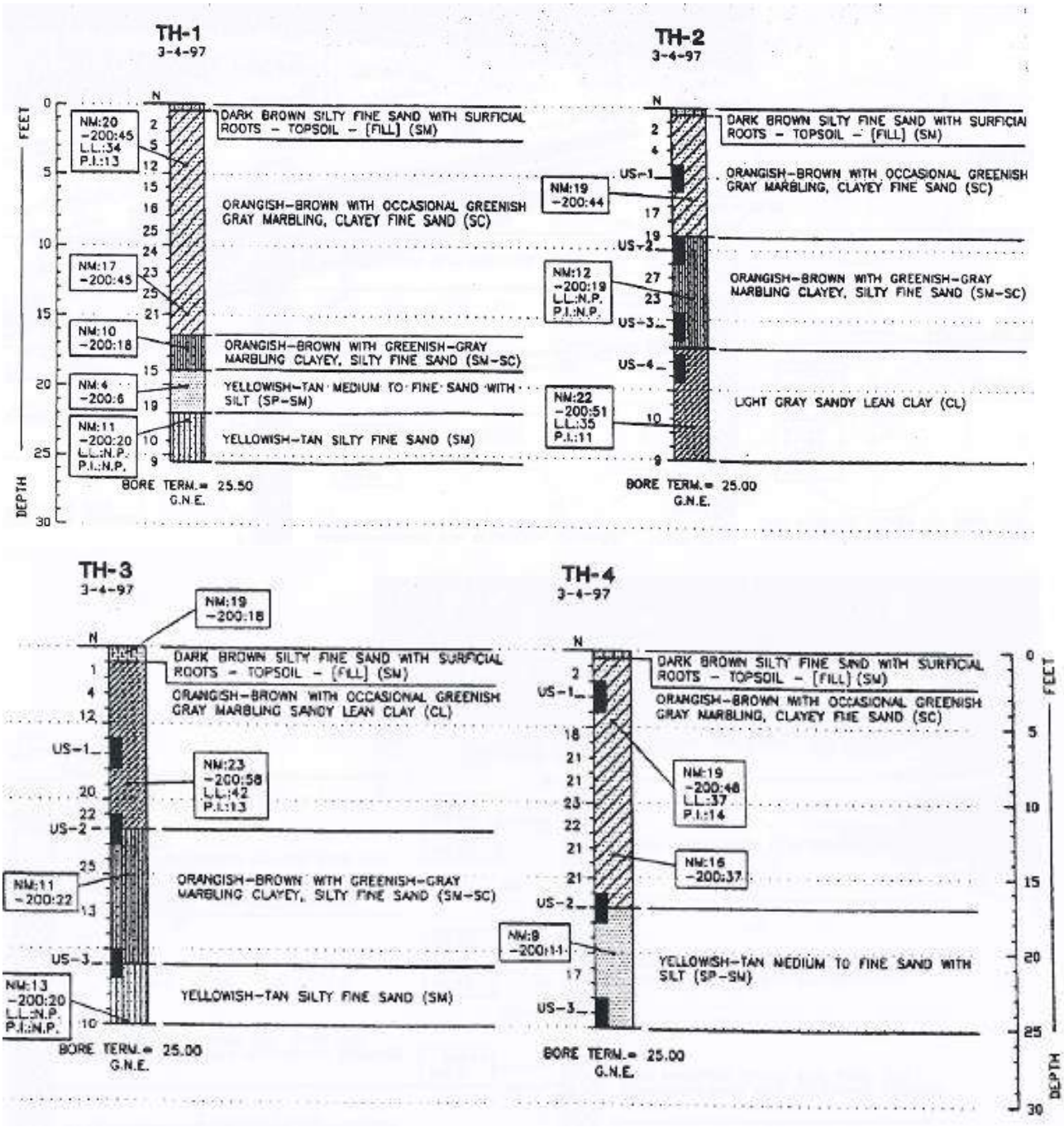

Figure 2.30 Soil profile at the test site (after Tawfiq 2000)

The test results for the shafts constructed with the (a) dry method and (b) bentonite slurry are shown in figure 2.31. The load-rotation response for the shaft constructed with polymer slurry was not provided by the author. Note that the applied torque could be calculated by

multiplying the applied load by the length of loading arm, which was 3.1 m (10 ft). The induced rotation of the dry shaft was limited to 0.45°, with a corresponding maximum torque of 664 kN-m (490 kip-ft), as the shaft experienced structural failure.

The maximum applied torque for the shaft constructed with bentonite slurry was 380 kN-m (280 kip-ft), which was 43 percent less than the maximum applied torque of the dry shaft, as shown in figure 2.31b. For the torsional loading test on the shaft constructed with polymer slurry, Tawfiq (2000) reported that the performance of the shaft was similar to that of the dry shaft at a torque of 380 kN-m (280 kip-ft). Because of the experience with the dry shaft, the upper 1.5 m (5 ft) of soil around the polymer slurry-constructed shaft was removed during loading to avoid structural failure. The maximum applied torque for the shaft constructed with polymer slurry was 569 kN-m (420 kip-ft). Given that the final embedded length for the shaft constructed with polymer slurry was 4.6 m (15 ft), the torsional capacity for this shaft with same embedded length may have been larger than that of the dry shaft. Note that there was a concern regarding the set-up of the test: the center-to-center distance from the reaction shaft to each test shaft was only about 2.1 m (7 ft), and the clear span between shafts was only 0.9 m (3 ft). Therefore, the effect of shaft-to-shaft interaction should have been investigated. Since the torsional load transfer was not studied in this test, the effect of interaction between the shafts could not be explored.

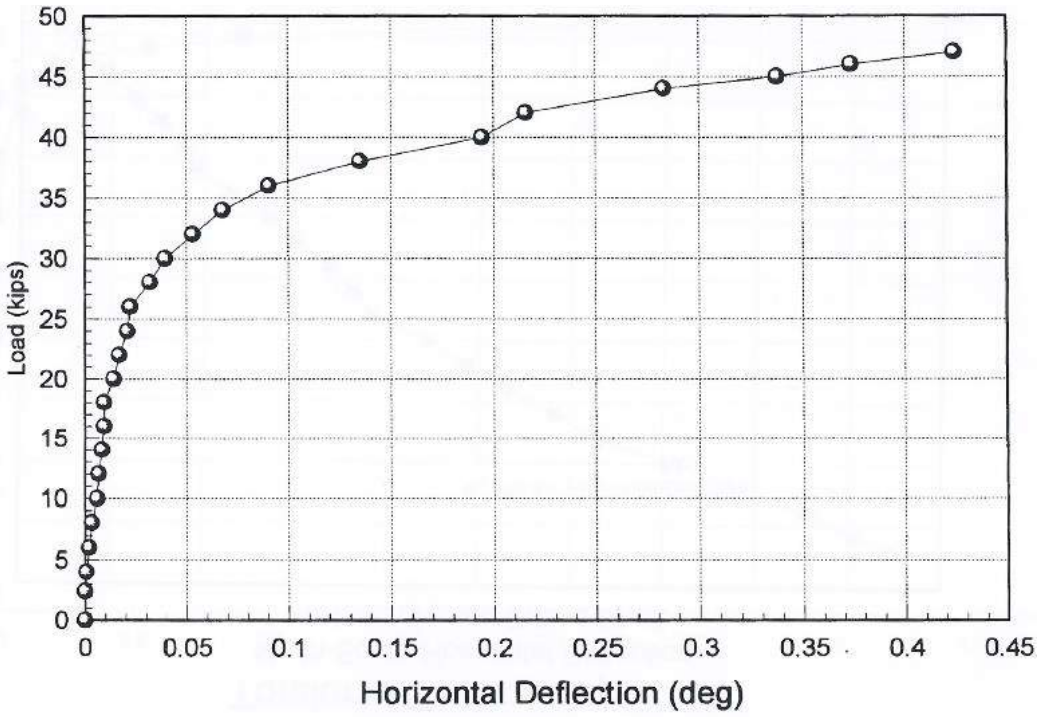

(a)

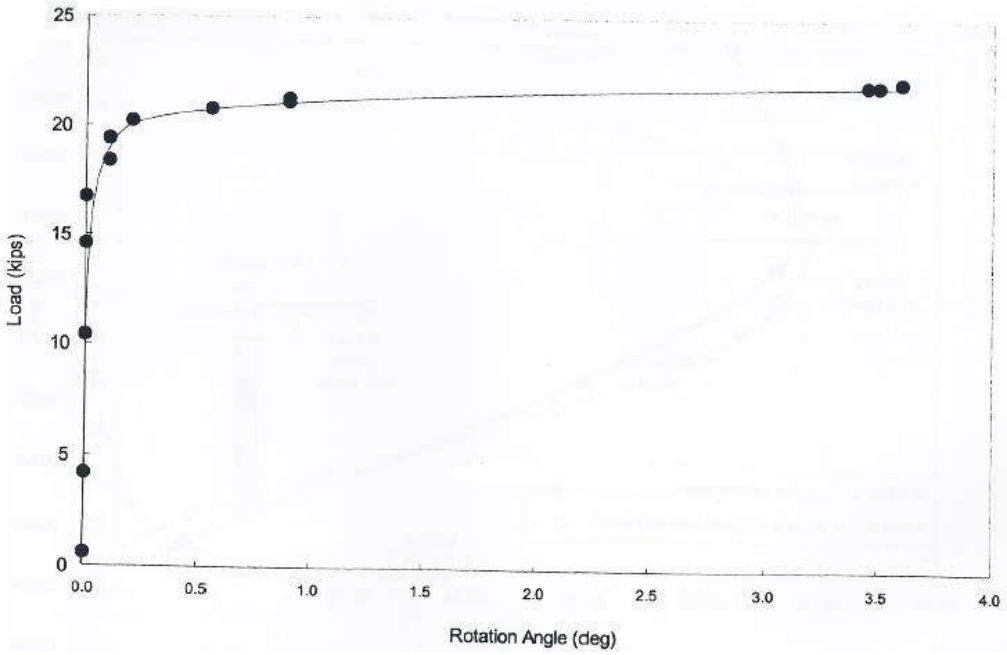

(b)

Figure 2.31 Test results of shafts constructed with (a) the dry method and (b) bentonite slurry (after Tawfiq 2000)

McVay et al. (2014) performed a series of full-scale torsional loading tests on three drilled shafts in Keystone Heights, Florida. The drilled shafts included one with a 1.2-m (4 -ft) diameter and 3.7-m (12-ft) embedded length (designated TS1), and the other two shafts were constructed with a 1.2-m (4-ft) diameter and 5.5-m (18-ft) embedded length (designated TS2 and TS3). All of the shaft heads were 0.46 m (1.5 ft) above ground surface. The soil profile for each test shaft is shown in figure 2.32. No temporary casing was used during excavation of the test shafts. The shaft cavities were drilled by using the dry method to a depth of about 1.8 m (6 ft), and then bentonite slurry was used to support the cavity for the remainder of the shaft excavation. After installation of the test shafts, mast arm-pole assemblies were attached to the test shafts. The lengths of the pole and arm were 6.7 m and 12.2 m (22 and 40 ft), respectively. Lateral loading was applied with increments of 0.5 kips on the mast arm at an offset distance of 10.7 m (35 ft), as shown in figure 2.33, to supply the torque to the test shaft. A load cell was installed between the mast arm and a crane-mounted winch cable to measure the load associated with the applied load. Upon the observation of failure for shafts TS2 and TS3, the shafts were unloaded. Three types of instrumentation were used to measure the rotation of the test shafts, including two total stations and survey monitoring, two sets of string potentiometers (four potentiometers in each set), and a set of four dial gauges. The water table was about 3 m (10 ft) below ground surface.

Figure 2.34 displays the relationships between applied torque and rotation for each test shaft. The torsional resistances were fully mobilized at 95 kN-m (70 kip-ft) for TS1,, 285 kN-m (210 kip-ft) for TS2, and 232 kN-m (171 kip-ft) for TS3,. The difference in torsional capacity

between TS2 and TS3 can be attributed to the difference in soil profile. TS2 was constructed with a greater length in the sand layer, which provided more torsional resistance.

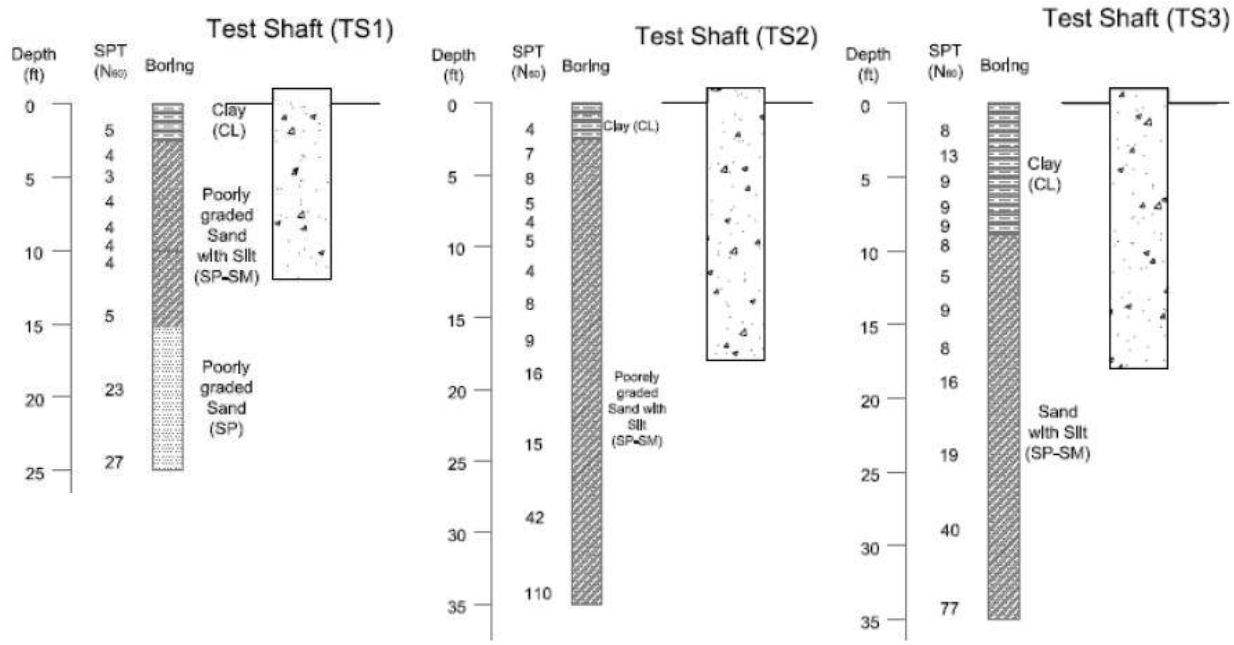

Figure 2.32 Soil profile at the location test drilled shafts (after McVay et al. 2014)

Figure 2.33 Combined torsion and lateral loading (after McVay et al. 2014)

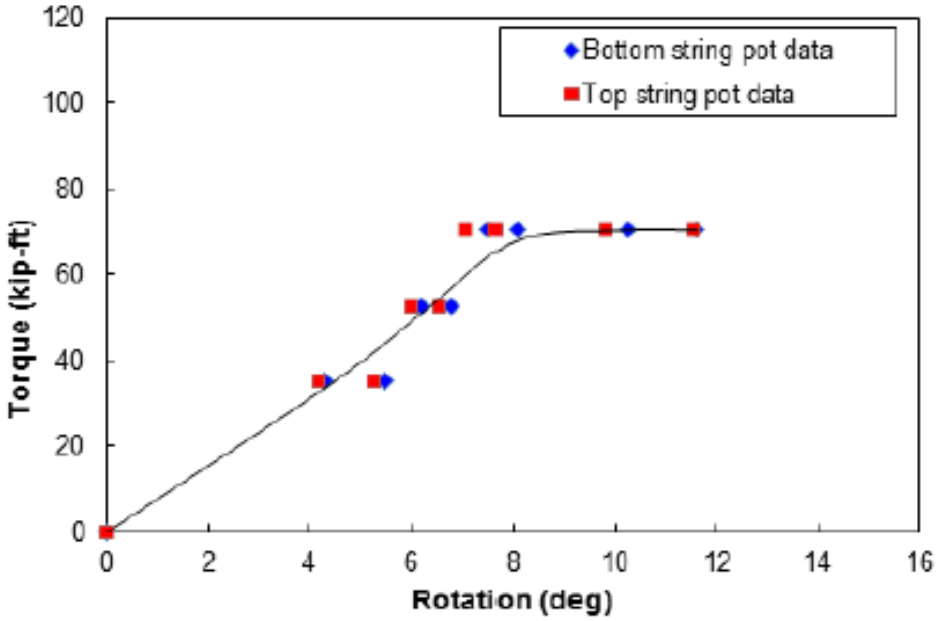

(a)

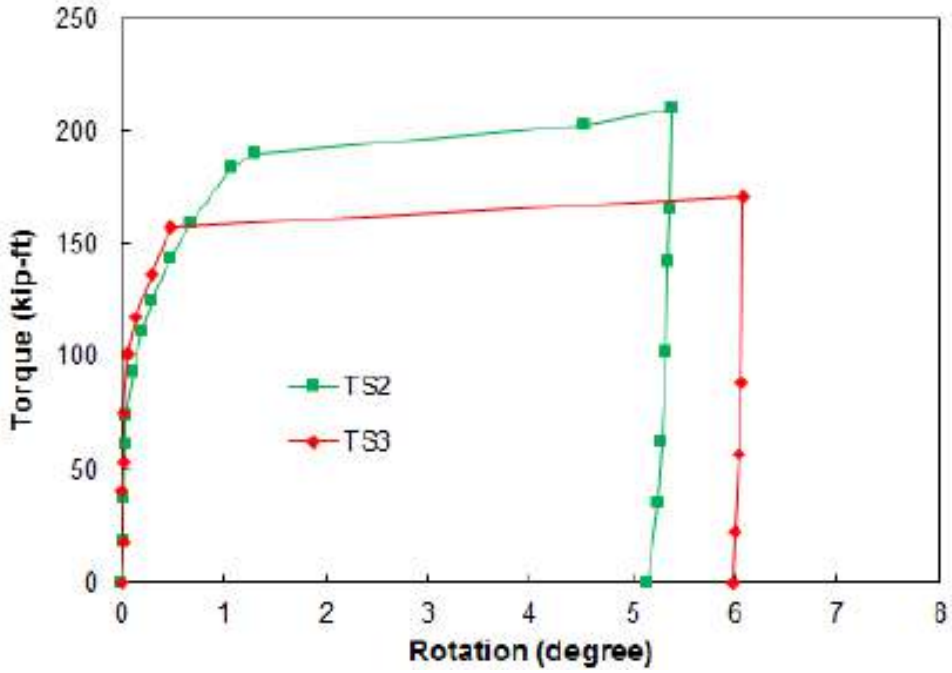

Figure 2.34 Torque vs. rotation response of (a) TS1 and (b) TS2 and TS3 (after McVay et al. 2014)

Li et al. (2017) conducted full-scale torsional loading tests on two drilled shafts with diameter of 0.9 m (36 in) and am embedded length of approximately 4.0 m (13 ft) at the geotechnical field research site on the Oregon State University (OSU) campus in Corvallis,

Oregon, as shown in figure 2.35. One test shaft was designated as the test drilled shaft with production base (TDS; constructed by using normal methods), and the other one was designated as the test drilled shaft with a frictionless base (TDSFB). Both of the test shafts were instrumented to observe torsional shear and flexural strains, displacements and rotations, and loads (to compute the applied torque). As shown in figure 2.36, the subsurface consisted of over-consolidated silty clay to clayey silt to an approximately 5.2-m (17-ft) depth, underlain by a layer of sand to silty sand. The near-surface soils were desiccated to a depth of 0.9 m (3 ft) and formed a very stiff to hard crust (when dry), as indicated by the high q_t and SPT N conducted during a period of extended low groundwater levels, as is typical for the test site in general. From a depth of 0.9 m to approximately 5.2 m, the silty clay to clayey silt was of medium stiff to very stiff consistency, and is associated with overconsolidation ratios ranging from 5 to 10. A 1.1-m (3.6-ft) thick layer of dense silty sand with gravel (SM) was encountered in CPT-2, in B-2014-1, and in the excavated spoils of the test shaft installed at this location. The groundwater table varied between 0.6 to 2.5 m deep over a typical year and was located at 1.9 m deep during the loading tests, as shown in figure 2.36.

Quasi-static loading was conducted. At the end of the loading, the TDSFB rotated approximately 13°, whereas the TDS only rotated 0.14° because of the layer of dense silty sand. The relationship between torque and applied rotation for the test shafts under quasi-static loading is shown figure 2.37. Since the measured torque-rotation response of shaft TDSFB was consistent with a hyperbolic relationship, the same was used to estimate the torque-rotation response of shaft TDS at larger rotations. On the basis of the measured torque-rotation response, the torsional resistance of shaft TDSFB was fully mobilized at 185 kN-m (136 kip-ft) and a rotation of the shaft head of about 1.0°. The extrapolated torsional capacity of shaft TDS was 250

kN-m (184 kip-ft). The torsional load transfer along the test shafts was evaluated in consideration of the angle of twist and the relationship between unit torsional shaft resistance and rotation to develop the relationship between unit torsional shaft resistance and rotation, known as a τ–θ curve, for each tributary area, as shown in figure 2.38. The hyperbolic model was used to extrapolate τ–θ curves for the TDS.

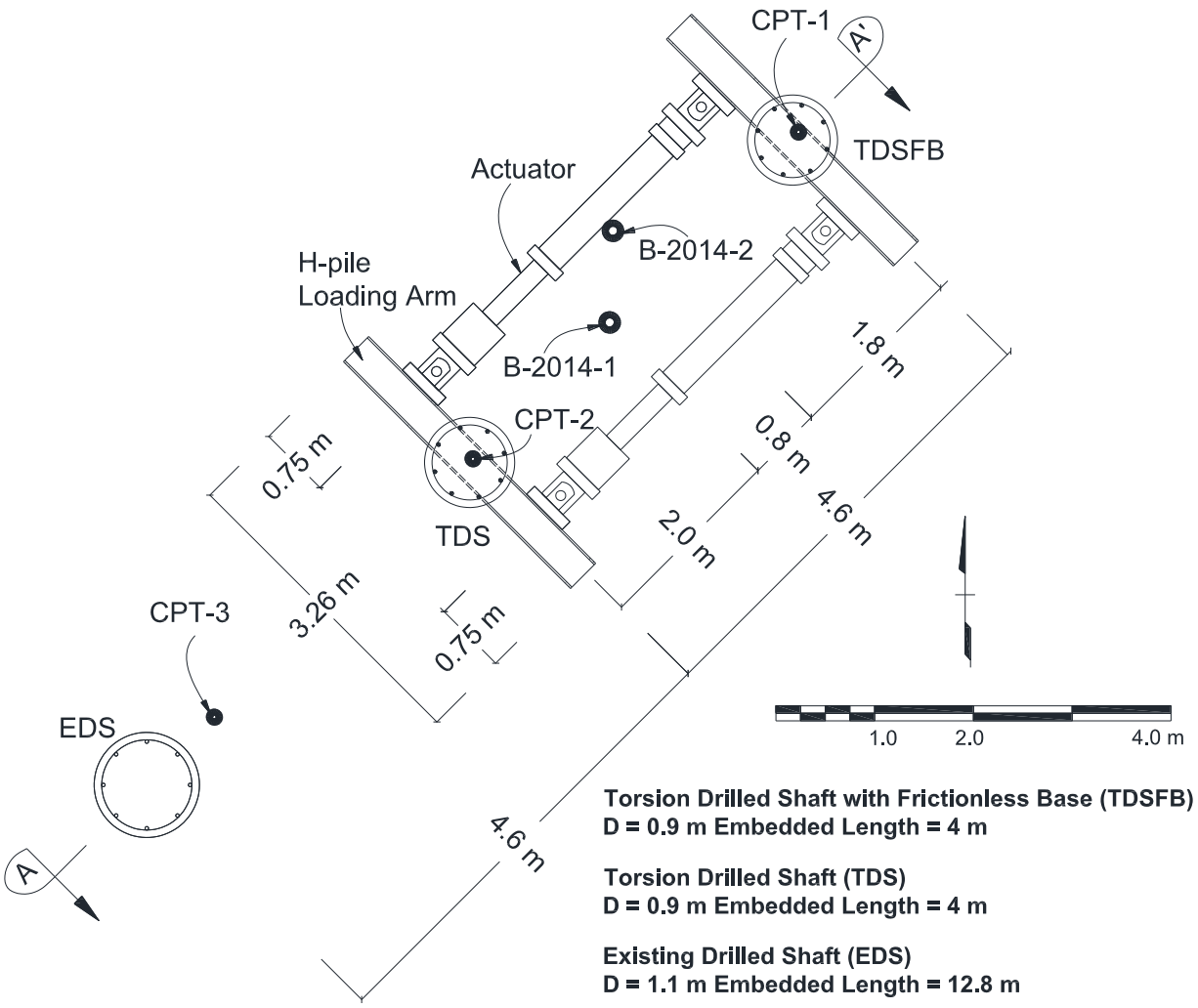

Figure 2.35 Test site layout, including the torsion drilled shaft with frictionless base (TDSFB), torsion drilled shaft (TDS), an existing drilled shaft (EDS), and exploration plan.

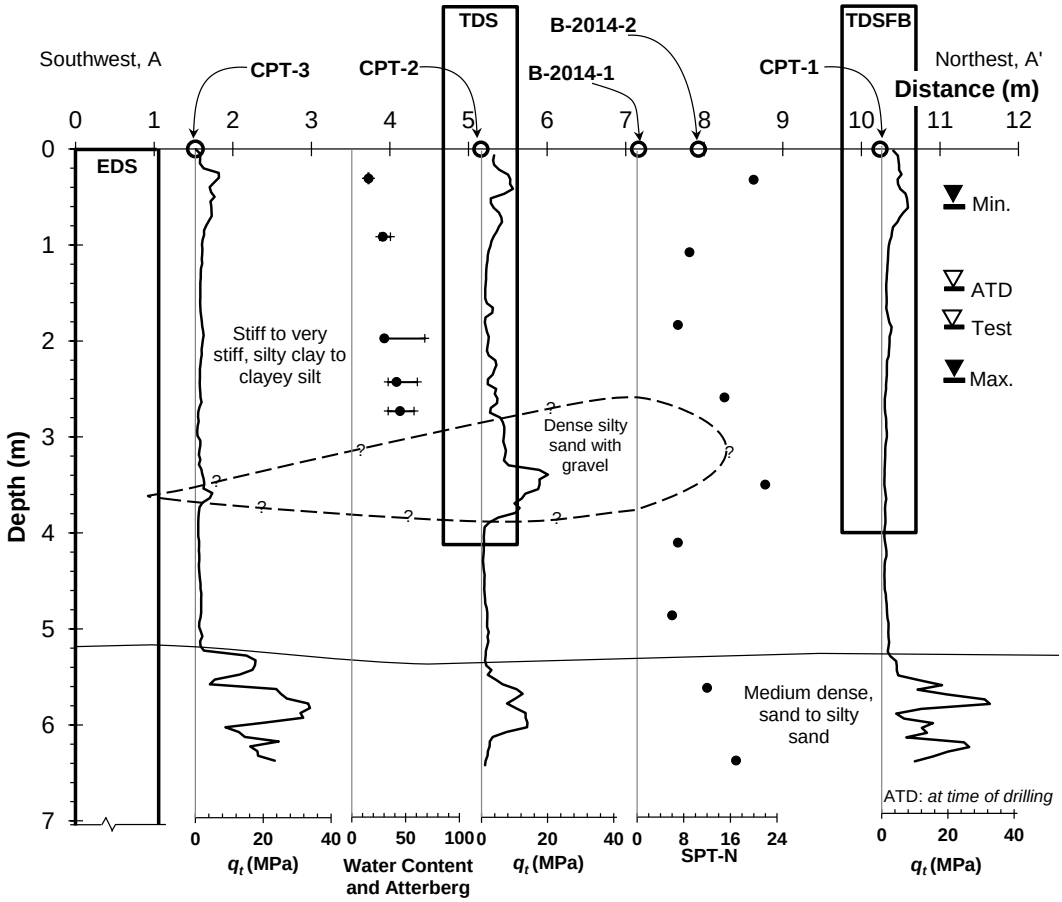

Figure 2.36 Subsurface profile at the test site indicating the locations of the test shafts (after Li et al. (2017)).

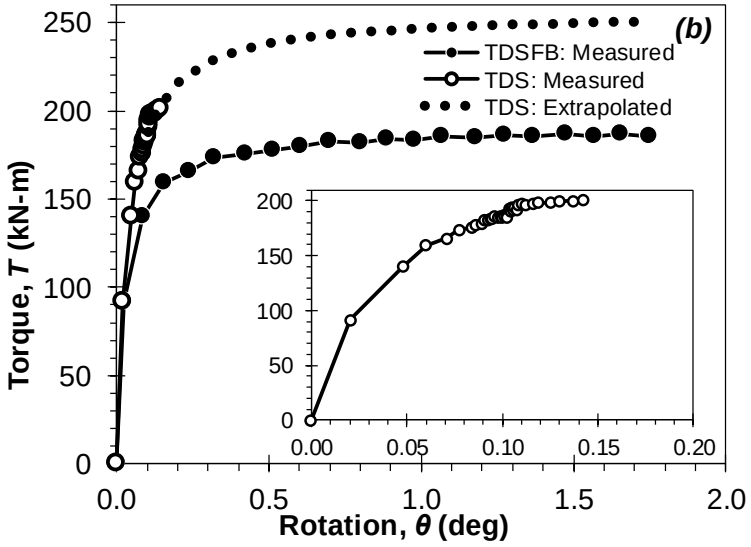

Figure 2.37 Relationship between torque and applied rotation for the test shafts under quasi-static loading with inset showing the small rotation response of TDS (after Li et al. (2017)).

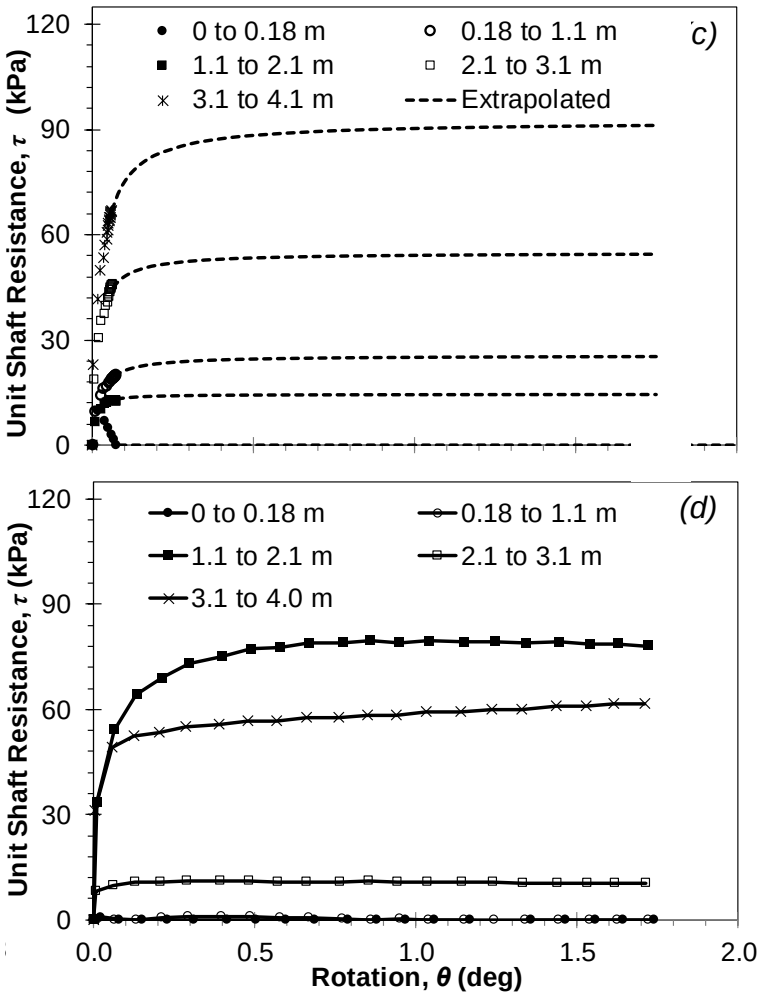

Figure 2.38 τ–θ curves for the instrumented test shafts: (a) comparison of selected τ–θ data in hyperbolic space for shaft TDS; (b) comparison of fitted hyperbolic models and back-calculated τ–θ data corresponding to (a), (c) back-calculated and extrapolated τ–θ curves for shaft TDS, and (d) back-calculated τ–θ curves for shaft TDSFB (after Li et al. (2017)).

2.3 Design Methods for Torsionally Loaded Deep Foundations

In general, the torsional capacity or ultimate torsional resistance of drilled shafts, defined as the maximum torsional resistance possible independent of the magnitude of rotation, consists of the sum of the ultimate shaft and toe resistance, given by:

$$T = T_s + T_t \tag{2.2}$$

where T_s = shaft resistance, and T_t = toe resistance.

Design methods available to estimate the torsional capacity of drilled shaft foundations include the Florida Structural Design Office method, the District 5 method, and District 7 method developed by Florida Department of Transportation (e.g., Tawfiq 2000 and Hu 2003) and the Colorado Department of Transportation (CDOT) design method (Nusairat et al. 2004).

For estimating the torsional shaft resistance, the Florida Structural Design Office method considers the deep foundation to be a rigid body and that the soil behaves as a rigid plastic material. The District 5 method employs the β method (O'Neill and Reese 1999) for a drilled shaft in granular soils. The District 7 method combines the β method for granular soils and the α method (Brown et al. 2010) for plastic, fine-grained soils in a single equation so that it can be used in both cohesive and cohesionless soils. For the CDOT method, the unit shaft resistance for drilled shafts in plastic, fine-grained soils is assumed equal to the undrained shear strength, which may cause over-predicted torsional shaft resistance. The CDOT method proposed a function for lateral earth pressure coefficient for granular soil without physical basis provided.

For torsional toe resistance, the Florida District 7 method assumes that the mobilized unit torsional toe resistance distributes linearly with distance away from the center of the toe, whereas the Florida Structural Design Office and CDOT methods assume it is uniformly distributed. In granular soils, the Florida District 7 method assumes that the normal force giving rise to the frictional toe resistance is the sum of shaft weight and axial dead load applied to the drilled shaft, whereas the CDOT design method assumes the normal force is equal to shaft weight. However, the normal force at the toe should actually equal the sum of the shaft weight, and axial dead load applied to the drilled shaft, minus the mobilized axial shaft resistance.

Analytical and numerical methods to model the torsional response of deep foundations have been proposed assuming variously that the shear modulus of the soil is constant or varies with depth. Linear elastic or linear elastic-perfectly plastic solutions for torsionally loaded deep foundations have been developed by O'Neill (1964), Poulos (1975), Randolph (1981) Chow (1985), Hache and Valsangkar (1988), Guo and Randolph (1996), Guo et al. (2007), and Zhang (2010). O'Neill (1964) developed closed-form differential equations for piles in a homogenous soil. Poulos (1975) and Randolph (1981) developed boundary element solution and closed form solution, respectively, for piles in a homogeneous or linearly varying soil. Chow (1985) proposed discrete element approach for piles with varying sections in nonhomogeneous soil. Hache and Valsangkar (1988) provided non-dimensional charts for piles in layered soils. Guo and Randolph (1996) proposed analytical and numerical solutions for piles in a layer of nonhomogeneous soils with a stiffness profile following a simple power law with depth. Zhang (2010) developed an analytical method for piles in a two-layer soil profile assuming that the shear modulus of soil of each layer varies linearly. Guo et al. (2007) established closed-form solutions for a pile in a two-layer nonhomogeneous soil deposits, assuming that the stiffness profile for each layer increases as a simple power law of depth. These methods can only produce reasonable results for small rotations and cannot account for the reality of nonlinear soil response.

Load transfer models have been proposed for the study of torsionally loaded deep foundations that use nonlinear springs to model the soil-structure interaction (SSI). Georgiadis (1987) and Georgiadis and Saflekou (1990) used elasto-plastic and exponential torsional springs, respectively, along the shaft with the relationship of pile rotation, θ, and torsional shaft resistance, T, to study the influence of torque on axial pile response. However, the torsional toe resistance was not considered in these models. In addition, the model from Georgiadis and

Saflekou (1990) was only validated on the axial response, in terms of axial load and pile head settlement relationship, with model tests; and no validation was performed on predicting the torsional behavior of deep foundations. Guo et al. (2007) presented a logarithmic relationship between pile rotation, θ, and unit torsional shaft resistance, τ_s for the torsional springs. Again, no torsional toe resistance was explicitly considered; nonetheless the results of the analyses compared well with those from continuum-based numerical approaches and finite element models for elastic soil response. However, none of the load transfer methodologies described above were validated with empirically derived load transfer data.

2.4 Summary

This chapter reviewed the literature on torsionally loaded deep foundations, torsional load transfer investigated with some scale model and centrifuge loading tests by measuring the shear strains along the test shafts. However, only three full-scale torsional loading tests were found in literature. Only one was a full-scale test on drilled shafts instrumented to measure load transfer in torsion.

To evaluate ultimate torsional resistance, design methods have been proposed by FDOT and CDOT. Analytical and numerical methods have been developed that assume that the shear modulus of soil follows a certain type of variation with depth. The load transfer method has been used for deep foundations loaded in torsion with load transfer models that are both limited (i.e., purely elastic, or elastic-perfectly plastic) and unproven at full-scale. None of these approaches has been validated in the literature. Therefore, a methodology for and implementation of load transfer models that have been validated with measured torsional load transfer would be helpful to improve our understanding of the torsional response of deep foundations.

Chapter 3 Finite Difference Model

3.1 Overview

This chapter presents the finite difference model (FDM) framework. Section 3.2 describes the assumptions associated with this FDM approach and governing differential equations. The approach used to solve the governing differential equations is presented in Section 3.3

3.2 Assumptions and Governing Differential Equations

The well-known FDM approach was used herein within a one-dimensional framework to solve the governing differential equations for a circular, torsionally loaded deep foundation. The following was assumed:

- The deep foundation (fig 3.1a) could be treated as a beam (fig 3.1b) with m elements and $2m+1$ nodes, including a node at the toe.
- The base of the deep foundation (fig 3.1c) could be divided into n cylindrical elements with equal radial increments.
- The foundation properties, in terms of the diameter and the torsional rigidity, would remain constant within each element; however, these properties might vary between elements along the foundation, and that the nonlinear torsional rigidity might decrease with increasing internal twist.
- The nonlinear relationship between the soil and structure would be constant for a given element.
- The complicated SSI was simplified as a beam interacting with discrete nonlinear torsional springs along the shaft and base elements.

- For each spring, the unit interface shear stress, τ, was a function of the relative circumferential displacement, Δ.

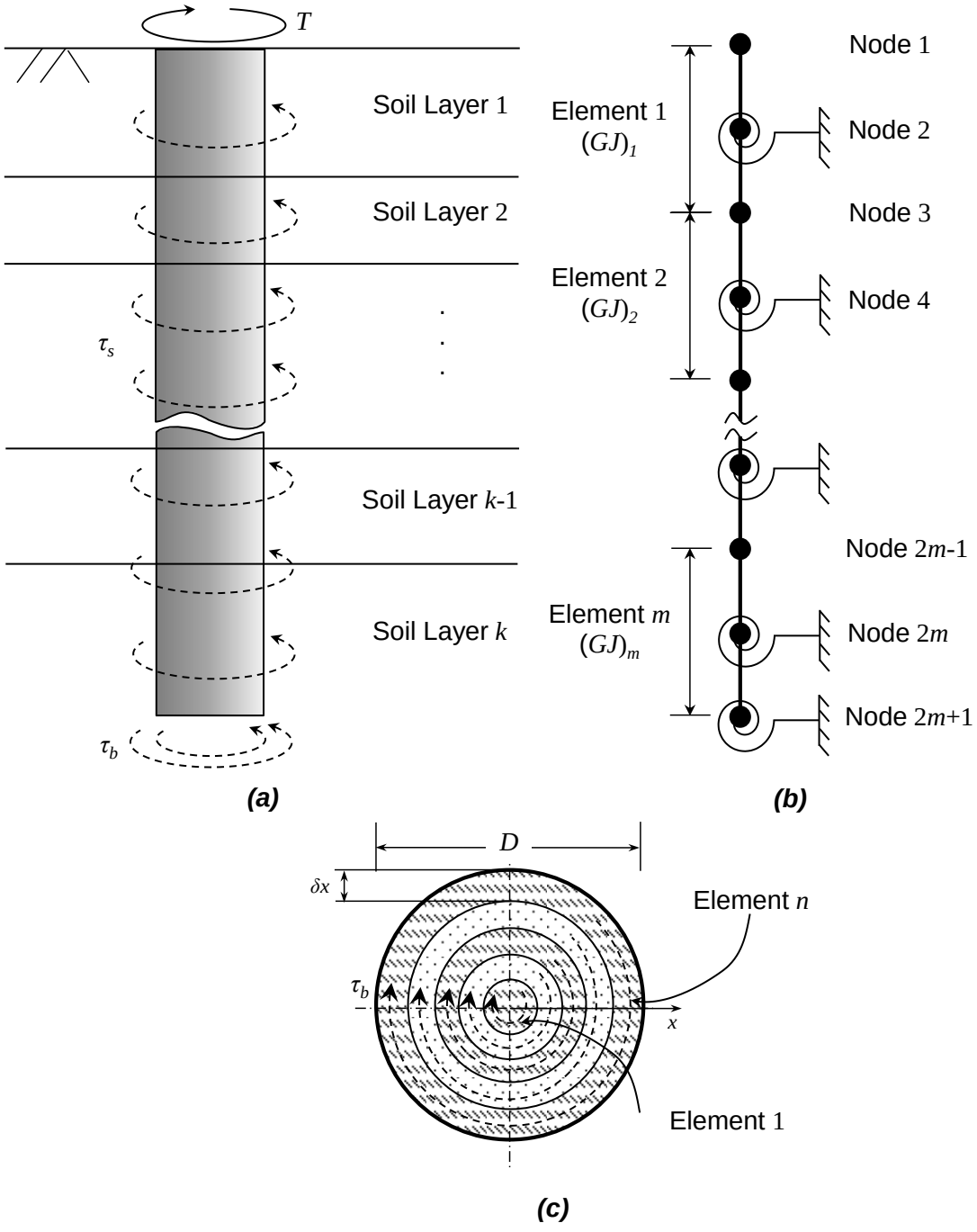

Figure 3.1 Schematic illustration of (a) torsionally loaded deep foundation, (b) finite difference model with discrete springs along the shaft and base, and (c) discretization of the base of the deep foundation with n cylindrical elements; n = number of soil layers, and m = number of the shaft elements.

The differential equation for a shaft element with a length of *dz* along the deep foundation and subjected to torsional loading, as shown in figure 3.2a, is given by:

$$\frac{dT(z)}{dz} = 0.5\pi\tau_s(z)\cdot D(z)^2 \tag{3.1}$$

where $T(z)$ = torque in the shaft at depth z, $D(z)$ = shaft diameter at depth z, and $\tau_s(z)$ = unit torsional shaft resistance provided by the soil at depth z. The internal change in rotation with depth, $d\theta(z)/dz$, as shown in figure 3.1b, can be expressed by (Gere and Timoshenko 1997):

$$\frac{d\theta(z)}{dz} = \frac{T(z)}{GJ(z)} \tag{3.2}$$

where $GJ(z)$ = torsional rigidity of the shaft at depth z, G = shear modulus of the shaft, and J = polar moment of inertia. The nonlinear torsional springs along the shaft are represented by τ_s-Δ_s curves, where τ_s is the unit torsional shaft or interface shear resistance and Δ_s is the relative circumferential displacement. The rotation of the shaft, $\theta(z)$ at depth z, can be determined by:

$$\theta(z) = \frac{2\Delta_s(z)}{D(z)} \tag{3.3}$$

The torsional springs at the base of the deep foundation are represented by τ_b-Δ_b curve, where τ_b and Δ_b are the unit torsional base or base interface shear resistance and the relative displacement, respectively. The torsional toe resistance, T_b, at a given rotation can be calculated by evaluating an arbitrary cylindrical element of very small width *dx*, as shown in figure 3.1c. The distance from the center of foundation to the mid-point of the annulus is *x*. The differential area of the element is:

$$dA = \pi(x + \frac{dx}{2})^2 - \pi(x - \frac{dx}{2})^2 = 2\pi x \cdot dx \tag{3.4}$$

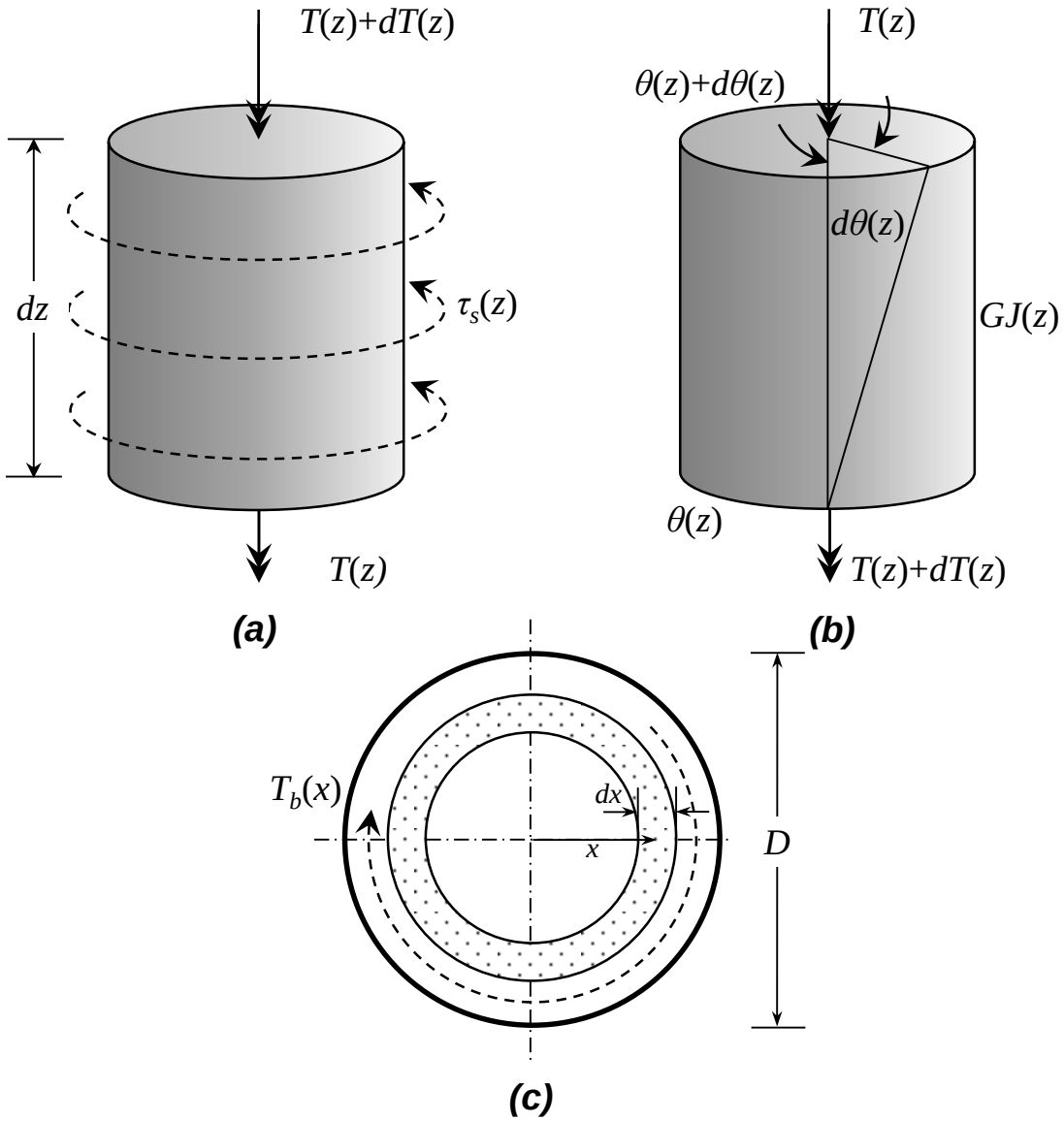

Figure 3.2 Schematic illustration of (a) an element of the torsionally loaded shaft, (b) the internal twist of a shaft element under torsion, and (c) an element at the foundation base.

With a certain rotation at base, θ_b, the whole element undergoes the same relative displacement, $\Delta_b(x) = \theta_b \cdot x$, so that the corresponding torsional toe resistance, $\tau_b(x)$, is the same within the

differential annulus. This implies that the outermost differential area will achieve a maximum or peak resistance prior to any other interior ring at a given rotation, and that the interface shear mechanism is necessarily progressive in nature. The torsional toe resistance for any given differential cylindrical element is:

$$dT_b(x) = x \cdot \tau_b(x) dA = 2\pi\tau_b(x) \cdot x^2 dx \tag{3.5}$$

which may be integrated over the radius to determine the total mobilized toe resistance, T_b:

$$T_b = 2\pi \int_0^{D/2} \tau_b(x) \cdot x^2 dx \tag{3.6}$$

3.3 Solution of Governing Differential Equations

The central difference scheme was adopted to approximate the continuous derivatives in the GDEs (e.g., Desai and Zaman 2014). For an arbitrary element *j*, where $j = 1, 2, \ldots, m$, with a length of $2h$, as shown in figure 3.3, the change of rotation with depth at node $2j$ can be estimated by using:

$$\left(\frac{d\theta}{dz}\right)_{2j} \cong \left(\theta_{2j-1} - \theta_{2j+1}\right)\frac{1}{2h} = \frac{T(2j)}{(GJ)_j} \tag{3.7}$$

where $T(2j)$ = the average torque in the element *j*, which assumes to be $(T_{2j-1} + T_{2j+1})/2$. For the shaft element *j*, equation 1.1 can be expressed as:

$$T_{2j-1} - T_{2j+1} = \pi D_j^{\,2} \cdot h \cdot \tau_j \tag{3.8}$$

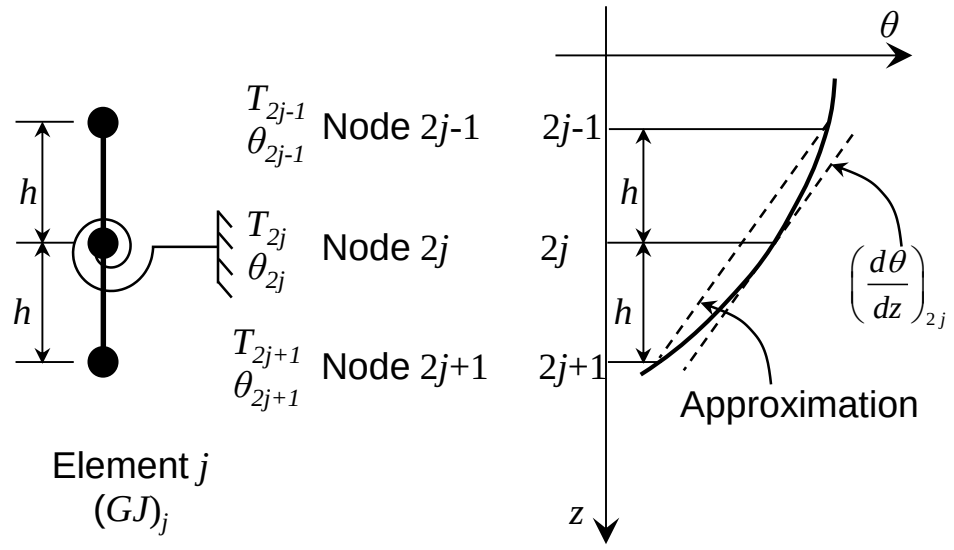

Figure 3.3 An arbitrary element *j* along the deep foundation and central difference approximation.

The torsional toe resistance can be determined directly with the summation of the torsional resistance from each base element. With *n* base elements, the radial increment is:

$$\delta_x = \frac{D}{2n} \tag{3.9}$$

For an arbitrary base element *i*, where $i = 1, 2,\ldots,n$, the area, $A(i)$, and the distance from the center of base to the mid-point of the element, $r_b(i)$, are:

$$A(i) = \pi\left\{(i\cdot\delta_x)^2 - \left[(i-1)\delta_x\right]^2\right\} = (2i-1)\pi(\delta_x)^2 \tag{3.10}$$

$$r_b(i) = (i-0.5)\delta_x \tag{3.11}$$

Then, the torsional resistance from the element *i* is:

$$T_b(i) = \tau_b(i)\cdot A(i)\cdot r_b(i) \tag{3.12}$$

τ_b is a function of Δ_b and can be determined from the proposed τ-Δ models as described subsequently. Therefore, the total torsional toe resistance, T_b, can be determined by:

$$T_b = \sum_{i=1}^{n} T_b(i) \tag{3.13}$$

The determination of the load transfer for the torsionally loaded deep foundation using the FDM followed a similar procedure that was proposed by Coyle and Reese (1966) for axially loaded piles. First, an arbitrarily small base rotation is applied. Then, the equilibrium of torque and compatibility of rotation for each element is achieved by using an iterative solution scheme with equations 3.7 and 3.8. Therefore, this method is not applicable for a deep foundation with a fully fixed base.

Chapter 4 Proposed Torsional Load Transfer Curves

4.1 Relevant Soil-Interface Mechanics

Torsional resistance is derived from interface shear between the surface of the deep foundation and the interacting soil. Accordingly, interface shear tests provide the best laboratory-based analog to actual in-situ interaction. A review of soil-structure interface tests on granular soils reported in the literature (e.g., Clough and Duncan 1971; Gómez et al. 2000a, 2000b; and Iscimen 2004) suggested that two simplified unit torsional resistance-relative displacement relationships, known as τ-Δ curves, are sufficient to describe the interface shear behavior. These include hyperbolic-type displacement-hardening and -softening models, which are proposed and implemented in the FDM for torsional load transfer. In general, granular soil-structure interfaces can be categorized as nondilatant (i.e., contractive) or dilatant (Lings and Dietz 2005; Dove and Jarrett 2002). The tendency for dilation depends on the interface properties, including surface topography and the hardness of the interface and the granular soil properties (e.g., relative density, angularity, and gradation), as observed in previous studies on soil-structure interfaces (e.g., Kulhawy and Peterson 1979; Uesugi and Kishida 1986; Paikowsky et al. 1995; DeJong and Frost 2002; Dove and Jarrett 2002; Frost et al. 2002; Iscimen 2004; and Lings and Dietz 2005). Since the effects of hardness are not significant for the structure of engineering materials such as steel and concrete (Dove and Frost 1999 and DeJong and Frost 2002), hardness was not considered herein. The structure surface topography is commonly quantified by using the average roughness, R_a, and maximum roughness, R_{max}. The one-dimensional average roughness of structure, R_a, is defined by:

$$R_a = \frac{1}{L_s}\int_0^L \left|z(\mathrm{x})\right| dx \tag{4.1}$$

where L_s = sample length, and $|z(x)|$ = the absolute height of the profile from the mean (Ward 1982; and DeJong and Frost 2002). The maximum roughness is the maximum absolute vertical relief along the surface profile over a sample length $L_s = d_{50}$. The granular soil-structure interface roughness is generally evaluated by using normalized roughness, $R_n = R_{max}/d_{50}$, as introduced by Uesugi and Kishida (1986) and relative roughness, $R_r = R_a/d_{50}$, as introduced by Subba Rao et al. (1998).

On the basis of a series of sand-steel interface tests with normal effective stress σ'_n = 25 kPa, Lings and Dietz (2005) categorized the interfaces into three categories: (1) smooth interfaces with $R_r \leq 0.003$ or $R_n \leq 0.02$, (2) rough interfaces with $R_r \geq 0.008$ or $R_n \geq 0.5$, and intermediate interfaces for $0.003 < R_r < 0.008$ or $0.02 < R_n < 0.5$. Lings and Dietz (2005) found that contractive behavior occurred for smooth interfaces and dilatant behavior was observed for intermediate and rough interfaces for the interface tests using fine, medium, and coarse sand with d_{50} of 0.09, 0.34, and 0.64 mm, respectively, and for relative densities, D_r, ranging from 20 to 99 percent. Not surprisingly, these tests showed that D_r contributed to the tendency for dilation along the interface. By extrapolating the interface test data, Lings and Dietz (2005) found zero dilation occurred at D_r = 16 percent with σ'_n = 25 kPa, similar to the calculated relative density at critical state, $D_{r,cs}$ = 15 percent using (Bolton 1986, Boulanger 2003):

$$D_{r,cs} = \frac{R}{Q - \ln \frac{100\sigma'_n}{P_a}} \tag{4.2}$$

where R = empirical constant, which is approximately equal to 1.0, Q = empirical constant equal to 10 for quartz and feldspar, 8 for limestone, 7 for anthracite, and 5.5 for chalk (Bolton 1986), and P_a = atmospheric pressure.

Owing to the need to capture ultimate and serviceability limit state performance, the τ-Δ curve selected for a given soil deposit should be accurate across the range of rotations implied by the interface displacements. An appropriate model should capture the hardening (i.e., contractive) or softening (dilatant) response, depending on the in-situ state of the granular soil deposit relative to the critical state and the interface characteristics. The approach incorporated into the proposed FDM consists of determining the tendency for dilation by using the relative roughness; smooth interfaces are considered contractive. Equation 4.2 may then be used to calculate the normal stress-dependent D_r at the critical state. If the in-situ $D_r < D_{r,cs}$, then the interface is contractive and modeled as a hardening material (described below). If the in-situ $D_r > D_{r,cs}$, then the interface is dilatant and should exhibit softening at large relative displacements. Regardless of the in-situ state, the soil-structure interface response can be sufficiently modeled by using a hyperbolic model at small relative displacements prior to the manifestation of softening (Gómez et al. 2000a, 2000b). The details of the selected τ-Δ models are described below. The proposed τ-Δ models can be used for the springs along the shaft as well the springs at the base.

4.2 Displacement-Hardening Model

The stress-strain and load transfer response of contractive granular soil has been simulated by using the hyperbolic model for a variety of applications (e.g., Kondner 1963; Duncan and Chang 1970; and Huffman et al. 2015) and extensively for soil-deep foundation interface analyses (e.g., Chin 1970, 1971; Clemence and Brumund 1975; Wong and Teh 1995; Kim et al. 1999; Cao et al. 2014; Stuedlein and Reddy 2014). Clough and Duncan (1971) extended the hyperbolic model to soil-structure interfaces by incorporating the relative displacement, Δ, as given by:

$$\tau = \frac{\Delta}{\frac{1}{K_{si}} + \frac{\Delta}{\tau_{ult}}} \tag{4.3}$$

where τ_{ult} = asymptotic interface shear stress of the hyperbola, K_{si} = initial interface stiffness. The initial interface stiffness is pressure-dependent, and given by:

$$K_{si} = K_I \cdot \gamma_w \cdot \left(\frac{\sigma'_n}{P_a} \right)^{n_j} \tag{4.4}$$

where K_I = dimensionless stiffness number, γ_w = unit weight of water, n_j = dimensionless stiffness exponent. The dimensionless K_I and n_j are determined by using the results of interface shear tests. The hyperbolic model is well suited for application to the torsional response of deep foundations, since it has relatively few physically justified model parameters, and a large catalogue of hyperbolic interface shear model parameters are available in the literature.

Figure 4.1 shows the characteristic shape of the hyperbolic model, whereas the determination of the hyperbolic parameters from interface tests is shown in figure 4.2 for medium-dense Density sand against plywood-formed concrete reported by Gómez et al. (2000a). This test series used σ'_n = 35, 104, and 276 kPa to evaluate pressure dependence. Figures 4.2a and 4.2b compare the observed and fitted hyperbolic models, and present the test data to 4 mm only to illustrate the process of estimating the hyperbolic parameters for contractive soils. In the hyperbolic space (Δ_s/τ_s versus Δ_s), the intercept and slope of the fitted line are reciprocal of K_{si} and τ_{ult}, respectively, as shown in Figure 4.2b. After obtaining K_{si} and τ_{ult} for each normal stress, K_I and n_j, can be estimated by fitting K_{si}/γ_w and σ'_n/P_a with a power law, as shown in Figure 4.2c.

The coefficient K_I in equation 4.4 is equal to K_{si}/γ_w at $\sigma'_n = P_a$; and the slope of the straight line in Figure 4.2c is the power law exponent, n_j.

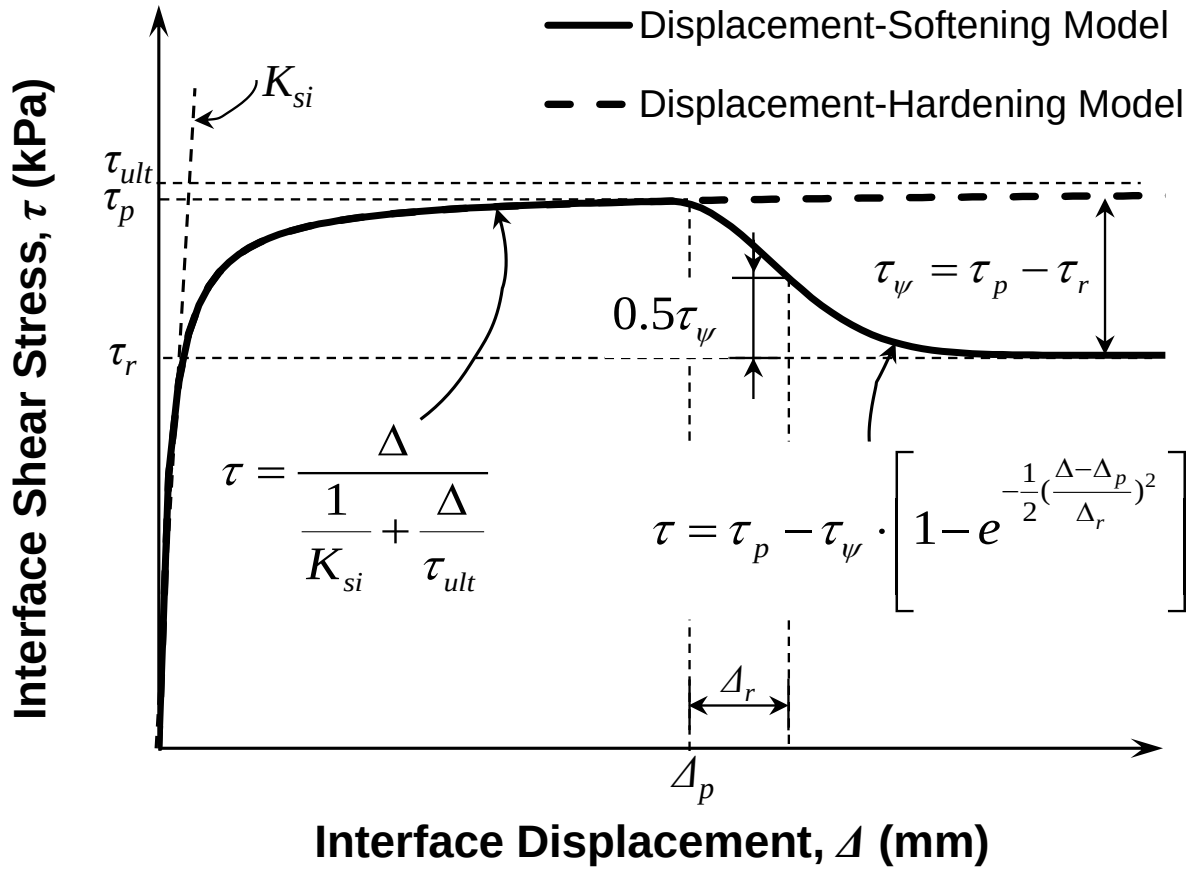

Figure 4.1 The characteristic shapes of the hyperbolic displacement-hardening and displacement-softening models.

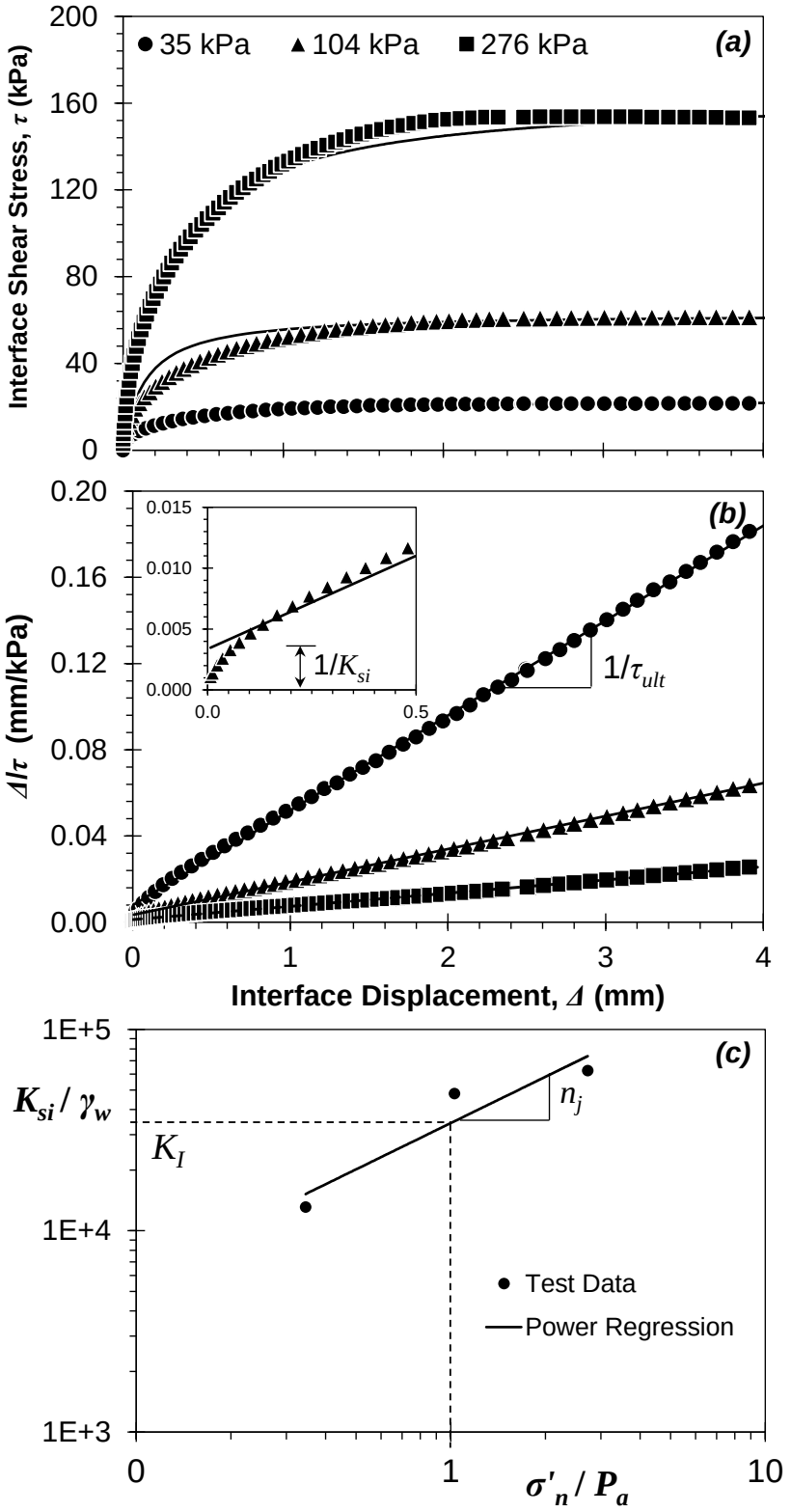

Figure 4.2 Determination of hyperbolic parameters with (a) test data for medium-dense Density sand against concrete under different normal stresses, σ_n = 35, 104, and 276 kPa, from Gómez et al. (2000a) and comparison with fitted hyperbolic model, (b) evaluation of K_{si} and τ_{ult}, and (c) evaluation of K_I and n_j.

The parameters derived from available interface test data, summarized in table 4.1, can be used to model granular soils in the absence of soil-interface-specific test data. The hyperbolic model parameters in table 4.1 represent those reported in the literature without consideration for softening, which is addressed subsequently. With the given parameters in table 4.1, the asymptotic or ultimate interface shear stress is given by:

$$\tau_{ult} = \frac{\tau_f}{R_f} = \frac{\sigma_n' \cdot \tan\delta}{R_f} \tag{4.5}$$

where δ = interface friction angle, τ_f = the interface shear stress at failure, and R_f = failure ratio. For drilled shafts in granular soils, the asymptotic interface shear stress of the hyperbola, τ_{ult}, can also be determined by using the β method:

$$\tau_{ult} = \beta \cdot \sigma_{v0}' \tag{4.6}$$

where σ'_{v0} = vertical effective stress at the mid-point of the layer of interest and β = shaft resistance coefficient. O'Neill and Reese (1999) proposed the estimation of β on the basis of the depth, z, and the energy-corrected SPT blow count, N_{60}; alternatively, Brown et al. (2010) correlated the coefficient with overconsolidation ratio, OCR, internal friction angle, ϕ', and SPT blow count, N_{60}. These approaches were summarized and compared to full-scale loading test performance by Li et al. (2017).

For the springs along the shaft (i.e., τ_s-Δ_s curves), an alternative method can also be used to determine the initial shear stiffness K_{si} of the hyperbolic model on the basis of the following equation derived by Randolph (1981) for a torsionally loaded pile in elastic soil:

$$\frac{\Delta_s}{r} = \frac{\tau_s}{2G_s} \tag{4.7}$$

where r = shaft radius and G_s = soil shear modulus. Although not specified by Randolph (1981), the maximum shear modulus, G_{max}, is recommended for use herein, and the initial shear stiffness, K_{si}, can be estimated by rearranging equation 4.7:

$$K_{si} = \frac{\tau_s}{\Delta_s} = \frac{2G_{max}}{r} \tag{4.8}$$

Table 4.1 Summary of hyperbolic parameters for the concrete-sand interface from the literature.

Soil					Concrete Surface & σ'_n (kPa)	K_I	n_j	R_f	δ (deg)
Type	Particle shape	D_r (%)	C_u	d_{50} (mm)					
Uniform sand Clough and Duncan (1971)	Subrounded subangular	Dense[a]	1.7	-	Smooth (45-224)	75,000	1.0	0.87	33.0
Chattahoochee River Sand Clemence (1973)	Subangular	65	2.5	0.37	Smooth (10-23)	51,000	0.67	0.86	30.4
		65			Rough (10-23)	46,800	0.70	0.86	38.2
		75			Rough (9-27)	54,600	0.66	0.88	42.9
Chattahoochee River Sand Holloway et al. (1975)	Subangular	50	2.5	0.37	Mortar	29,400	0.77	0.82	32.3
		75			Mortar (45-224)	36,200	0.77	0.76	33.6
		100			Mortar	46,200	0.77	0.78	33.3
Arkansas River Lock and Dam No. 4 Sand Holloway et al. (1975)	-	0	-	-	Mortar	21,600	1.15	0.87	29.9
		57				27,700	1.15	0.94	31.3
		100				55,700	1.15	0.95	34.6
Jonesville Lock and Dam Sand Holloway et al. (1975)	-	60	-	-	Mortar	51,000	0.81	0.83	34.5
		80			Mortar (96-960)	62,400	0.83	0.80	36.9
		100			Mortar	76,900	0.84	0.72	37.9

[a]The relative density, D_r, was not quantified by the authors

Table 4.1 (continued).

Soil					Concrete Surface& σ'_n, (kPa)	K_I	n_j	R_f	δ (deg)
Type	Particle shape	D_r (%)	C_u	d_{50} (mm)					
Uniform sand Peterson (1976)	Subrounded to Well rounded	33	1.7	0.30	Smooth (96-479)	10,200	0.87	0.71	30.0
		62				12,700	0.84	0.62	28.7
		77				8,400	1.17	0.40	31.2
		33	1.7	0.30	Inter-mediate (96-479)	11,000	0.79	0.82	26.9
		62				16,600	0.42	0.71	30.8
		77				8,900	0.85	0.30	33.8
		33	1.7	0.30	Rough (96-479)	10,000	0.83	0.85	31.6
		62				11,900	0.71	0.78	29.8
		77				10,400	0.70	0.41	32.9
Graded Sand Peterson (1976)	Subrounded to rounded	13	4.6	0.84	Smooth (96-479)	12,000	0.83	0.89	30.4
		40				9,200	0.94	0.69	30.7
		73				10,500	1.11	0.75	31.4
		13	4.6	0.84	Inter-mediate (96-479)	9,200	0.66	0.78	32.1
		40				9,200	0.74	0.76	33.6
		73				13,800	0.49	0.60	36.3
		13	4.6	0.84	Rough (96-479)	7,700	0.70	0.78	34.8
		40				13,100	0.67	0.69	32.9
		73				14,800	0.51	0.74	37.0

Table 4.1 (continued).

Soil					Concrete Surface & σ'_n, (kPa)	K_I	n_j	R_f	δ (deg)
Type	Particle shape	D_r (%)	C_u	d_{50} (mm)					
Ottawa sand 50-60 (Lee et al. 1989)	Subrounded	Dense[a]	-	-	Smooth (34-207)	19,470	0.35	0.89	26.3
		Dense[a]			Rough (34-207)	19,240	0.82	0.95	30.4
Blacksburg Sand (Gómez et al. 2000b)	Subangular	80	3.0	0.70	Cast against Plywood (38–292)	23,000	0.80	0.76	31.6
Density sand (Gómez et al. 2000a)	Subrounded to rounded	49	1.8	0.51	Cast against Plywood (35-276)	26,600	0.83	0.85	31.0
		75			Cast against Plywood (15-274)	21,800	0.71	0.88	29.3
Light Castle Sand (Gómez et al. 2000a)	Subangular to angular	80	1.8	0.40	Cast against Plywood (15-276)	20,700	0.79	0.79	33.7
Ottawa Sand 20/30 (Iscimen 2004)	Subrounded	80	1.46	0.64	Wet-cast Concrete R_a = 25 μm (40–120)	15,090	0.66	0.68	33.2
					Packerhead Concrete R_a = 55 μm (40–120)	19,750	0.68	0.87	37.1

[a]The relative density, D_r, was not quantified by the authors

4.3 Displacement-Softening Model

In order to account for softening at dilatant interfaces and the consequences thereof, a displacement softening model, as shown in figure 4.1, is proposed herein by extending the existing hyperbolic model. The hyperbolic model is used to model small relative displacements prior to the manifestation of softening. The relative displacement associated with the onset of softening, Δ_p, corresponds to the peak interface shear stress, τ_p. For a given interface test, the hyperbolic model can be constructed by using equations 4.3 thru 4.5 with the procedure shown in figure 4.2. However, K_{si} and τ_{ult} should be determined by fitting to data where $\tau_s \leq \tau_p$. Therefore,

a new set of the hyperbolic parameters was derived for the cases that exhibited displacement-softening behavior and is summarized in table 4.2.

The post-peak portion of the displacement-softening model is defined by an exponential function to represent the softening behavior, for $\Delta > \Delta_p$, given by:

$$\tau = \tau_p - \tau_\psi \cdot \left[1 - e^{-\frac{1}{2}\left(\frac{\Delta - \Delta_p}{\Delta_r}\right)^2} \right] \tag{4.9}$$

where τ_ψ = difference between the peak and residual (or constant volume) interface shear stress, defined as:

$$\tau_\psi = \tau_p - \tau_r = \sigma_n' \cdot (\tan\delta_p - \tan\delta_r) \tag{4.10}$$

where τ_r = residual interface shear stress, δ_r = residual interface friction angle, and Δ_r = relative interface displacement that corresponds to one-half of τ_ψ. On the basis of interface tests reported by Holloway et al. (1975), Gómez et al. (2000a, 2000b) and Iscimen (2004), the average value of Δ_r is approximately 1.0 mm. The displacement-softening model appears to sufficiently capture various rates of softening, as shown in figure 4.3 for dense Density sand-concrete (DDSC) interfaces reported by Gómez (2000a) and for the Ottawa sand-packerhead concrete (OSPC) interface reported by Iscimen (2004).

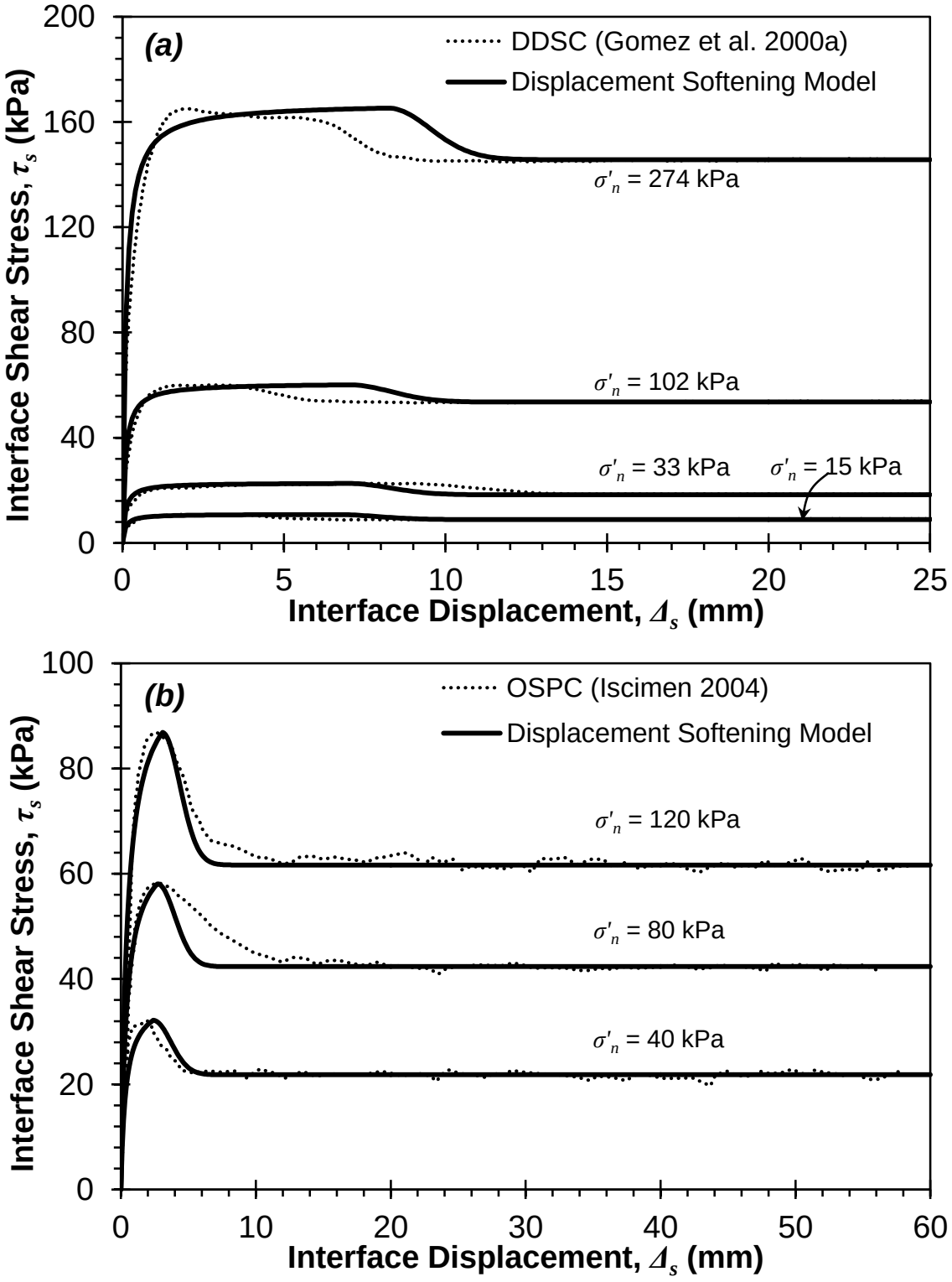

Figure 4.3 Examples of comparison between the displacement softening model and the test data (a) from Gomez et al. (2000) for the dense density sand-concrete (DDSC) interface and (b) from Iscimen (2004) for the Ottawa sand-packerhead concrete (OSPC) interface.

Table 4.2 Summary of hyperbolic parameters for the dilatant interfaces from the literature.

Soil					Concrete Surface & σ'_n (kPa)	K_I	n_j	R_f
Type	Particle Shape	D_r (%)	C_u	d_{50} (mm)				
Jonesville Lock and Dam Sand Holloway et al. (1975)	-	80	-	-	Mortar (96-960)	73,420	0.71	0.81
Blacksburg Sand (Gómez et al. 2000b)	Subangular	80	3.0	0.70	Cast against Plywood (38–292)	31,630	0.86	0.84
Density sand (Gómez et al. 2000a)	Subrounded to rounded	49	1.8	0.51	Cast against Plywood (35-276)	34280	0.76	0.98
		75			Cast against Plywood (15-274)	72,290	0.86	0.99
Light Castle Sand (Gómez et al. 2000a)	Subangular to angular	80	1.8	0.40	Cast against Plywood (15–276)	54,220	1.22	0.98
Ottawa Sand 20/30 (Iscimen 2004)	Subrounded	80	1.5	0.64	Wet-cast Concrete R_a = 25 μm (40–120)	15,090	0.66	0.68
					Packerhead Concrete R_a = 55 μm (40–120)	19,750	0.68	0.87

4.4 Proposed Torsional Load Transfer Curves for Plastic, Fine-Grained Soils

The hyperbolic model (equation 4.3) can also be used to study the interaction between deep foundations and plastic, fine-grained soils. The hyperbolic parameters K_{si} and τ_{ult} can be determined with the procedure shown in figure 4.2b if interface test data are available. It is assumed that the parameters K_{si} and τ_{ult} for plastic, fine-grained soils are to be used in transient loading cases (i.e., undrained) and therefore not pressure-dependent. In the absence of interface shear test data, the initial shear stiffness K_{si} can be calculated by using equation 4.8 and the measured or estimated shear wave velocity to compute G_{max}. The asymptotic interface shear

stress of the hyperbola, τ_{ult}, can be obtained by using the α method, proposed for drilled shafts under axial loading:

$$\tau_{ult} = \alpha \cdot s_u \tag{4.11}$$

where s_u = average undrained shear strength over the depth of interest, and α = an adhesion factor. The methodology described by O'Neill and Reese (1999) may be used to estimate, α, on the basis of the average s_u for the stratum of interest; see Li et al. (2017) for a discussion regarding its use in torsion. For deep foundations in plastic, fine-grained soils, the shaft resistance from the ground surface to a depth of 1.5 m, or to the depth of seasonal moisture change, should be neglected (Li et al. 2017).

The torsional load transfer derived from full-scale loading tests described by Li et al. (2017) was used to validate the hyperbolic model for plastic, fine-grained soils. The torsional load transfer data from a drilled shaft designated TDSFB were used. TDSFB was embedded full-depth in an overconsolidated silty clay and clayey silt. The soil properties, including undrained shear strength, s_u, maximum shear modulus, G_{max}, measured maximum unit torsional resistance, τ_m, and the average shaft radius, r, at each layer are summarized in table 4.3. Since the torsional shaft resistance on TDSFB was negligible from the ground surface to the depth of 1.1 m, only the portion from the depth of 1.1 m to the bottom of the shaft (4.0 m) was studied, which was divided into three layers according to the location of instrumentations along the shaft. The maximum shear modulus for each layer was estimated by using the average soil shear wave velocity, V_s, measured less than 5 m away using:

$$G_{\max} = \rho \cdot V_s^{\,2} \tag{4.12}$$

where ρ = soil density. The shear wave velocity profile at the location of TDS as well as the soil profiles at the locations of both shafts are shown in figure 4.4. The weighted average of V_s was used for depths of 1.1 to 2.1 m. The shear wave velocity, V_s = 267 m/s, for the silty clay to clayey silt at depths of 1.8 to 3.0 m for the TDS was used for the TDSFB at depths of 2.1 to 4.0 m. The hyperbolic parameter K_{si} for each layer was calculated by using equation 4.8 and is summarized in table 4.3. Then, the hyperbolic model was constructed with the hyperbolic parameter K_{si} and τ_m by using equation 4.3. The hyperbolic model using the measured V_s and τ_m accurately reproduced the load transfer observed for each layer.

Table 4.3 Soil and drilled shaft properties and hyperbolic parameters for TDSFB from the torsional loading tests conducted by (Li et al. 2017).

Depth (m)	Shaft	Soil						
	r (m)	ρ (kg/m3)	s_u (kPa)	V_s (m/s)	G_{max} (MPa)	τ_c (kPa)	τ_m (kPa)	K_{si} (kPa/mm)
1.1 to 2.1	0.461	1837	104	189	66	57.2	78.9	285
2.1 to 3.1	0.464	1837	76	267	131	41.5	10.5	564
3.1 to 4.0	0.494	1837	55	267	131	30.0	60.9	530

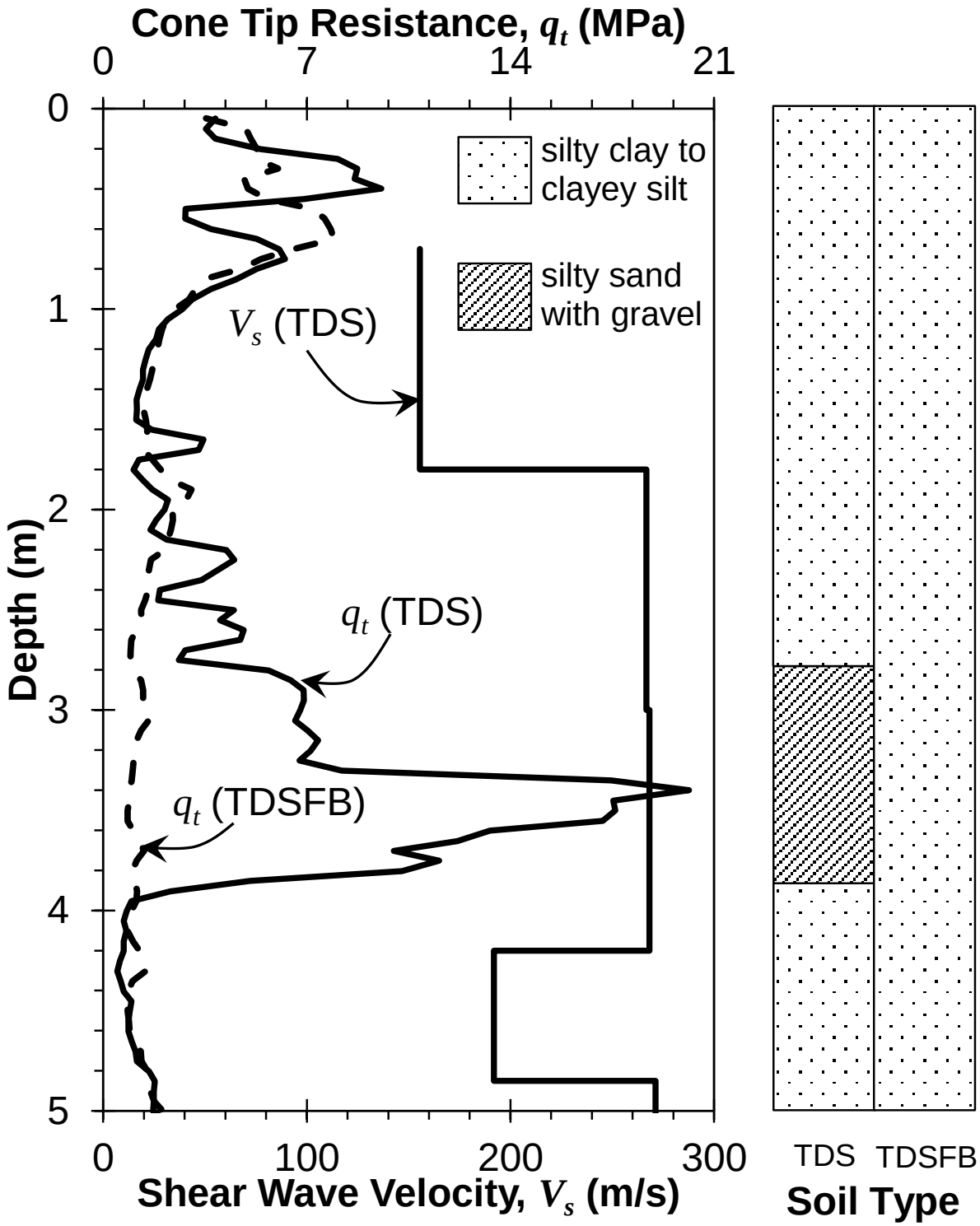

Figure 4.4 Shear wave velocity, V_s, profile at the location of TDS, and corrected cone tip resistance, q_t, profile at the locations of both shafts, and the soil profiles at the locations of both shafts.

Chapter 5 Validation and Evaluation of the FDM

To validate the proposed FDM, the FDM results were compared to the previous analytical solutions (Poulos 1975; Hache and Valsangkar 1988; Guo and Randolph 1996; Guo et al. 2007; and Zhang 2010) and two sets of torsional loading tests, including the centrifuge torsional loading tests conducted by Zhang and Kong (2006) and the full-scale loading tests conducted by Li et al. (2017). The accuracy of the proposed τ_s-Δ_s curves constructed from the torsional resistance calculated with equations 4.6 and 4.11 was evaluated by comparing the FDM results with the test data from Li et al. (2017).

5.1 Comparison of the FDM with Previous Analytical Solutions

In a first effort at model validation, the torsional responses of deep foundations found with the FDM were compared with previously reported analytical solutions. In the validation trials, the variation of the maximum soil shear modulus of the surrounding soil with depth was assumed equal to (e.g., Guo and Randolph 1996; Guo et al. 2007):

$$G_{\max}(z) = A_g \cdot z^{n_g} \tag{5.1}$$

where A_g = a modulus constant, n_g = depth exponent termed the nonhomogeneity factor. The value of n_g ranges from 0, corresponding to uniform shear modulus, to 1.0, corresponding to a linearly increasing shear modulus with depth. The shear modulus follows a power law when n_g lies between 0 to 1.0. Three values of n_g are selected to consider three general types of variations of soil shear modulus with depth (i.e., 0.0, 0.5, and 1.0). For a deep foundation with constant torsional rigidity, GJ, the relationship between the torque at the head of the deep foundation, T_h, and the corresponding rotation, θ_h, can be expressed as (e.g. Poulos 1975, Hache and Valsangkar 1988, and Guo and Randolph 1996):

$$\theta_h = \frac{I_\theta}{F_\theta}\frac{L}{GJ}T_h \tag{5.2}$$

where L = length of the deep foundation, I_θ = elastic torsional influence factor, F_θ = correction factor for the effect of soil yielding, equal to 1.0 for linear elastic soil. A dimensionless, relative torsional foundation-soil stiffness ratio, π_t, introduced by Guo and Randolph (1996), was used herein to generalize the validation:

$$\pi_t = \left[\frac{\pi D^2 \cdot A_g}{GJ}\right]^{\frac{1}{2+n_g}} \cdot L^2 \tag{5.3}$$

Figure 5.1 compares the linear elastic torsional responses produced with the FDM and the analytical solutions for a deep foundation in a single layer soil in terms of I_θ and π_t. Base resistance was not considered here to facilitate a one-to-one comparison with previous work. Figure 5.1 shows that the FDM reproduced the solutions by Poulos (1975), Hache and Valsangkar (1988), Guo and Randolph (1996), and Zhang (2010). To extend the range of validation for the FDM, the linear elastic response of a deep foundation in a two-layer soil profile with an upper layer thickness of 0.25L was compared to the analytical solutions from Guo et al. (2007), shown in figure 5.2. The relative stiffness ratio of the upper and lower layer is π_{t1} and π_{t2}, respectively. Figure 5.2a shows the relationship between I_ϕ and π_{t1} with π_{t2} = 0.4, 1, 5, and 50; whereas figure 5.2b shows the relationship between I_ϕ and π_{t2} with π_{t1} = 0.4, 1, 5, and 15. Good agreement between the FDM and previous solutions was observed.

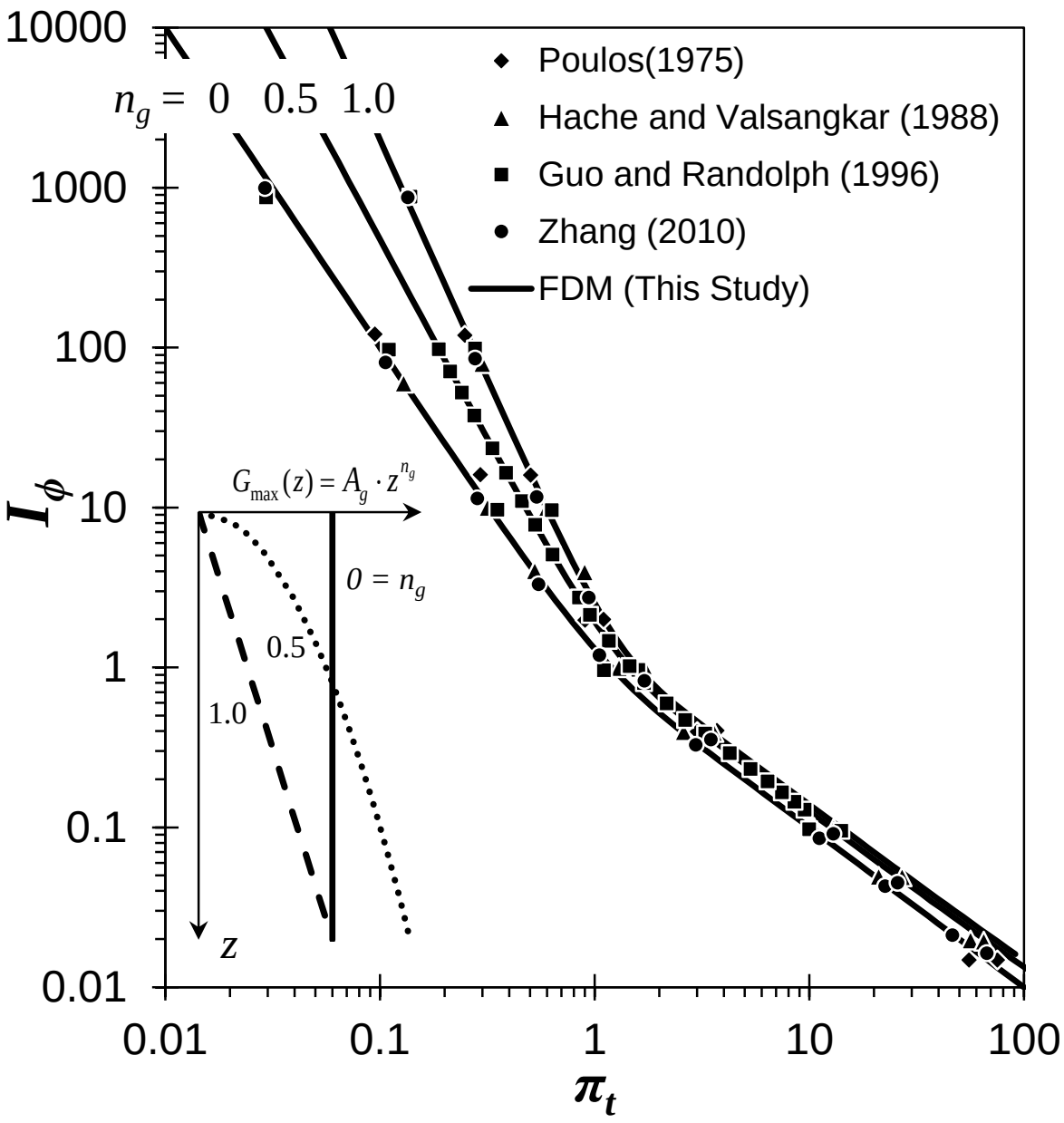

Figure 5.1 Validation of the FDM for linear elastic deep foundations and a single soil layer. Inset shows three variations of the maximum soil shear modulus, G_{max}, with depth, z; A_g = a modulus constant, n_g = depth exponent.

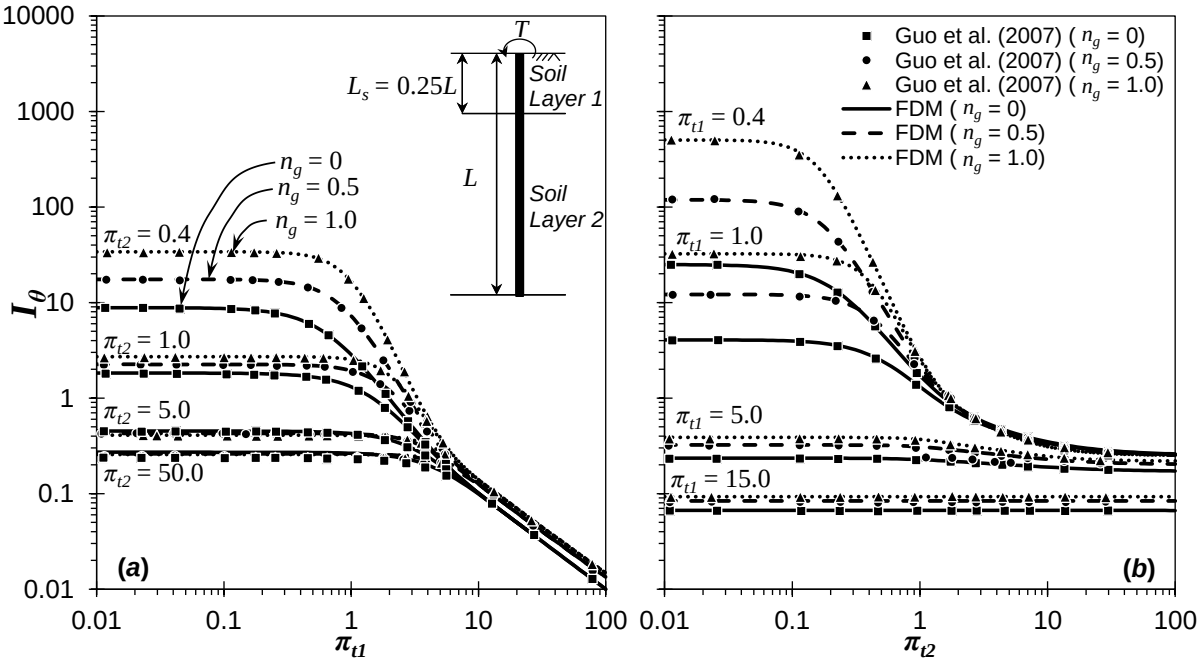

Figure 5.2 Validation of the FDM by comparing the elastic responses of deep foundations in a two-layer soil with the analytical solutions from Guo et al. (2007) for the relationship between (a) I_ϕ and π_{t1} and (b) I_ϕ and π_{t2}.

Linear elastic-perfectly plastic solutions for torsionally loaded deep foundations found with the FDM were also compared with analytical solutions from Poulos (1975) and Guo and Randolph (1996). The relationships between the plastic correction factor, F_θ, and the ratio of the torque at the head of the deep foundation, T_h, and the ultimate torsional resistance, T_u, with various π_t are shown in figure 5.3 for deep foundations in soil with constant and linearly varying stiffness. Again, no toe resistance was considered here to facilitate the comparison; the results from the FDM reproduced those of the previous analytical studies.

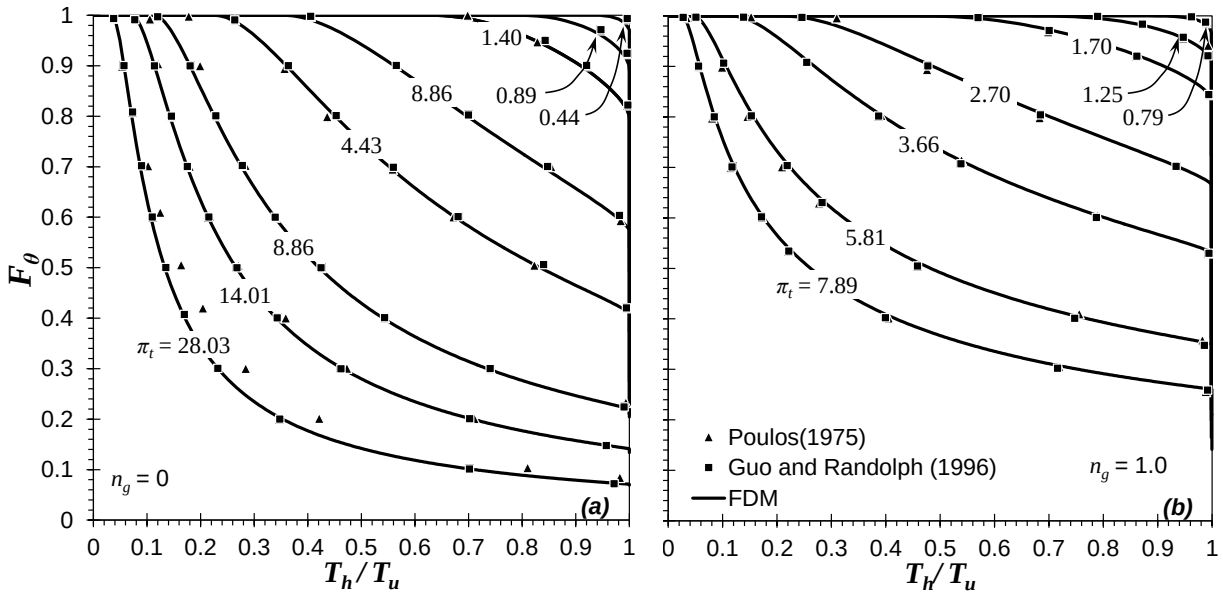

Figure 5.3 Validation of the FDM by comparing the linear elastic-perfectly plastic solutions with previous analytical solutions for deep foundations in (a) soil with constant stiffness, and (b soil with linearly varying stiffness.

5.2 Validation of the FDM using Centrifuge Tests

Centrifuge tests by Zhang and Kong (2006) were conducted to study torsional load transfer using aluminum tubes 300 mm in length, 15.7 mm in outside diameter, and 0.9 mm in wall thickness under 40*g* acceleration. For 40*g* acceleration, the prototype length was 12 m, outside diameter was 628 mm, and wall thickness was 36 mm. The prototype values of the dimension and the test results are reported below. The toe of the pile was conically shaped with a 60° apex angle and 0.6-m length. The pile was jacked into the sand bed following cessation of ground settlement while spinning at 40*g*. The embedded length of the prototype pile was 10.8 m. Six torsional tests were performed with various loading rates (i.e., 0.025, 0.075, and 0.200 deg/s) for each of two relative densities (i.e., 32 percent and 75 percent), for a total of 12 tests. Zhang and Kong (2006) found that the loading rate had little effect on torsional resistance. Detailed load transfer data were only reported for the tests with the lowest loading rate, which are shown in

figures 5.4 and 5.5 for the loose and dense sand beds, respectively. Softening responses were observed at depths above 6.0 m for both loose and dense sand, whereas hardening responses were observed at depths below 6.0 m. The proposed displacement-hardening and -softening models were used to model the respective volumetric responses to construct the τ_s-Δ_s curves. Because the pile jacking densified the sand around the pile and altered the distribution of radial stress around the piles in these tests, particularly in the loose sand, the maximum shear modulus, G_{max}, and the horizontal effective stress , σ'_h, around these experimental piles could not be evaluated accurately (Klotz and Coop 2001, and Kong 2006). Therefore, the model parameters for constructing τ_s-Δ_s curves were back-calculated from the measured load-transfer data (table 5.1). In the FDM, the soil was divided into eight layers on the basis of the locations of the instruments along the test pile. The overall pile was divided into 90 elements; and the cone shape toe was divided into five elements to account for the change of diameter, as shown in figures 5.4b and 5.5b. The τ_s-Δ_s curves using proposed displacement-hardening and -softening models represented the observed response accurately for the loose and dense sand, as shown in figures 5.4a and 5.4b, respectively. The global torque-rotation response at the pile heads, as shown in figures 5.4c and 5.4d, and profiles of torsional load transfer, as shown in figures 5.5a and 5.5b, were also accurately captured by the FDM.

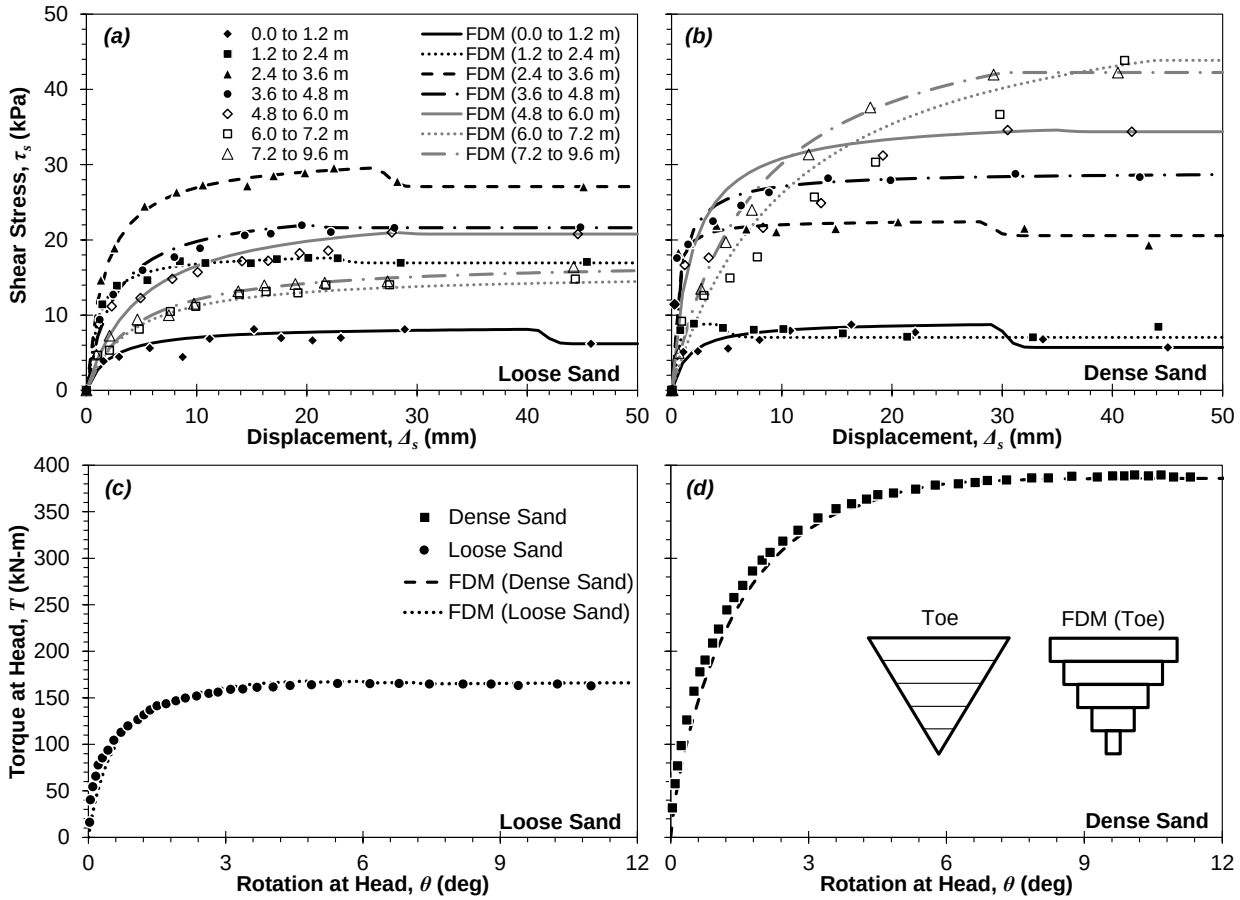

Figure 5.4 Validation of the FDM with the test data from Zhang and Kong (2006) on τ_s-Δ_s curves at each layer for (a) loose and (b) dense sand, and global torque-rotation response at head for (c) loose and (d) dense sand. Inset shows the cone-shaped toe and the model used in the FDM.

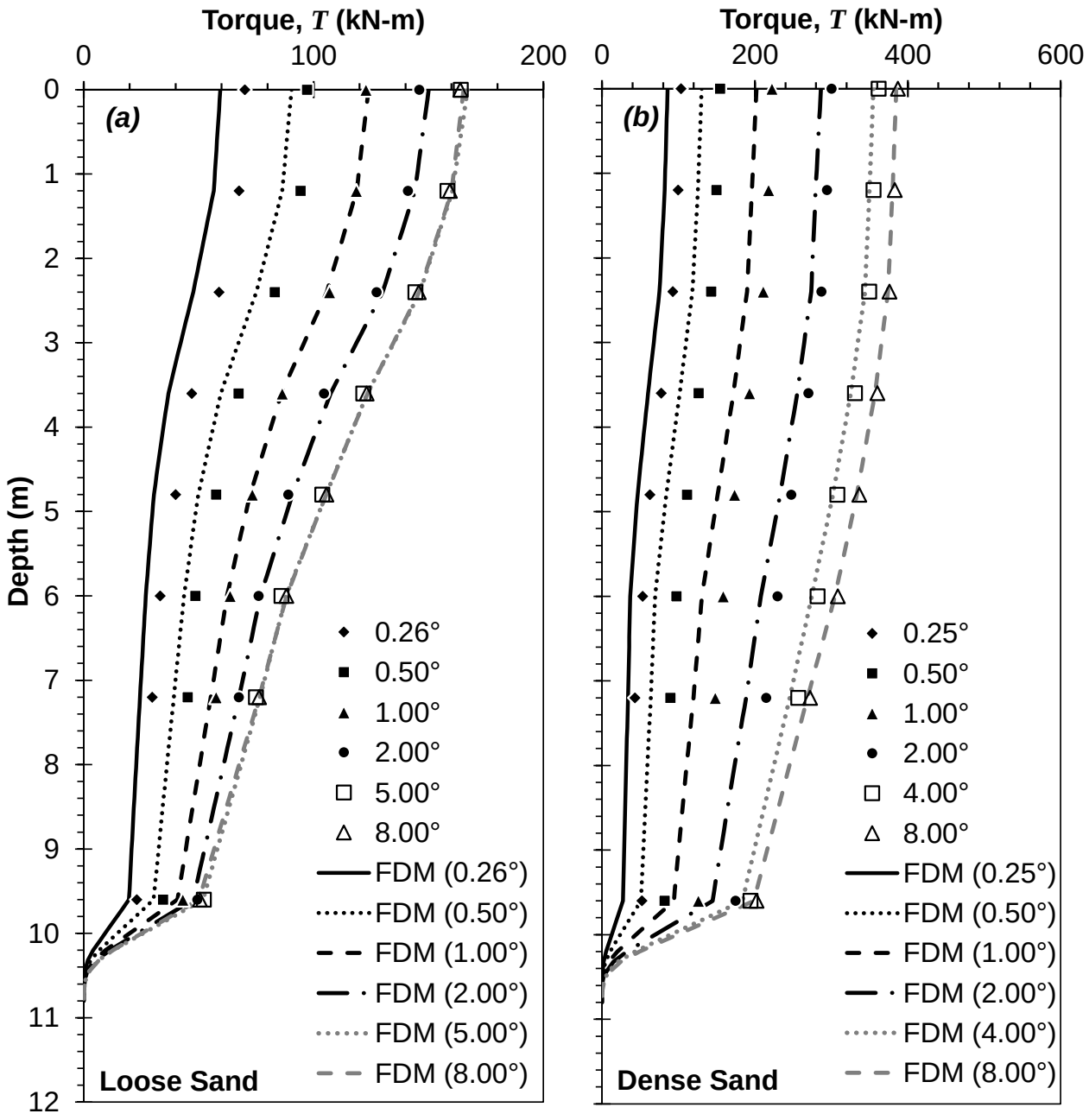

Figure 5.5 Validation of the FDM with the test data from Zhang and Kong (2006) on torque profiles at different head rotations for (a) loose sand, and (b) dense sand.

Table 5.1 Back-calculated model parameters for each instrumented layer in the centrifuge tests conducted by Zhang and Kong (2006).

Depth (m)	K_{si} (kPa/mm)	τ_c (kPa)	τ_p (kPa)	τ_r (kPa)	R_f
Loose					
0.0 to 1.2	4	8.5	8.1	6.2	0.95
1.2 to 2.4	20	18.3	17.6	17.0	0.96
2.4 to 3.6	19	31.5	29.6	27.1	0.94
3.6 to 4.8	10	24.7	22.0	21.6	0.89
4.8 to 6.0	5	24.7	21.0	20.8	0.85
6.0 to 7.2	4	15.6	14.8	14.8	0.95
7.2 to 9.6	4	17.3	16.4	16.4	0.95
9.6 to 10.8	75	99.2	95.2	90.3	0.96
Dense					
0.0 to 1.2	6	9.4	8.8	5.7	0.93
1.2 to 2.4	60	9.3	8.9	7.1	0.96
2.4 to 3.6	80	22.6	22.4	20.6	0.99
3.6 to 4.8	40	29.1	28.8	28.4	0.99
4.8 to 6.0	20	36.4	34.6	34.4	0.95
6.0 to 7.2	5	54.8	43.9	43.9	0.80
7.2 to 9.6	7	52.8	42.2	42.2	0.80
9.6 to 10.8	112	409.7	360.6	360.6	0.88

5.3 Validation and Evaluation of the FDM with Full-Scale Tests

The full-scale loading tests on instrumented drilled shafts TDS and TDSFB reported by Li et al. (2017) were used to validate the FDM and evaluate the accuracy of the proposed load transfer models. First, the FDM was validated against the observed response of the TDSFB by using the measured τ_m to construct the hyperbolic τ_s-Δ_s curves (fig. 5.6a). The torsional resistance was assumed to be zero at the base of TDSFB owing to the intentional use of hydrated bentonite

at that elevation (Li et al. 2017). The comparison of the FDM-computed and observed global torque-rotation response at the head of TDSFB is shown in figure 5.6c, and it produced excellent agreement, indicating the validity of the FDM formulation. The profiles of torsional load transfer from the FDM were compared with the observed responses in figure 5.7a for rotations to 1.75 degrees, also indicating that the FDM can reproduce the observed full-scale response.

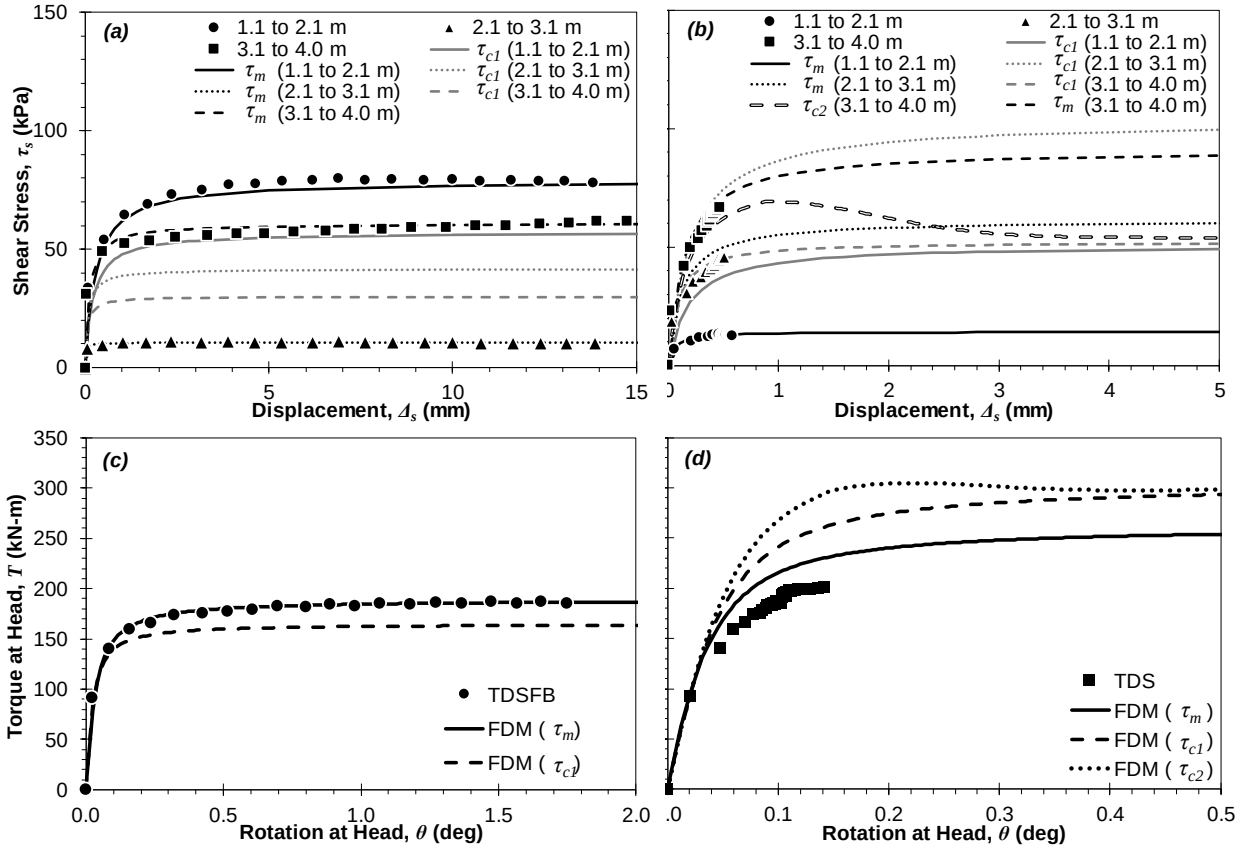

Figure 5.6 Validation and evaluation of the FDM with the test data from Li et al. (2017) on (a) and (b) τ_s-Δ_s curves at each layer for (a) TDSFB and (b) TDS, and global torque-rotation response at the head for (c) TDSFB and (d) TDS. Note: τ_m = extrapolated ultimate unit torsional shaft resistance based on the measured data, τ_{c1} and τ_{c2} = calculated resistance using O'Neill and Reese (1999) and Brown et al. (2010) method, respectively.

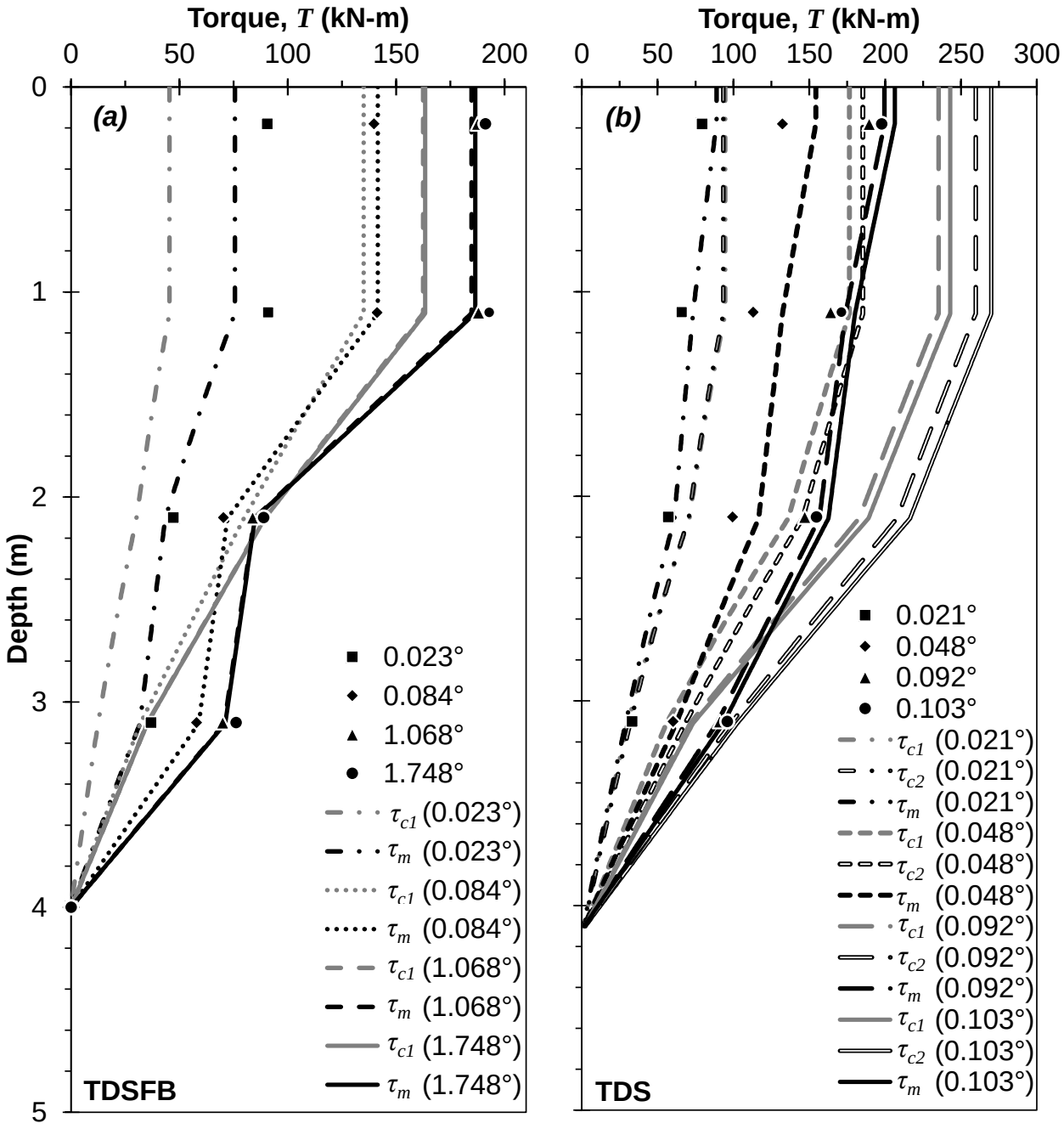

Figure 5.7 Validation and evaluation of the FDM with the test data from Li et al. (2017) on torque profiles at different head rotations for (a) TDSFB and (b) TDS.

The accuracy of the proposed τ_s-Δ_s curve methodology was evaluated by using τ_c calculated through equation 4.11 as summarized in table 4.3. The difference between τ_c calculated with the α method and τ_m may be partially attributed to the use of s_u estimates from a

site-specific correlation to cone tip resistance (Li et al. 2017). Note that the α method was developed by using unconsolidated-undrained triaxial compression tests. Figure 5.6a compares the observed and calculated load-transfer curves and indicates that the proposed model under-estimated the torsional resistance for depths of 1.1 to 2.1 m and 3.1 to 4.0 m and over-estimated the torsional resistance at depths of 2.1 to 3.1 m. The error in the load transfer curves counteracted one another to produce a reasonable, albeit fortuitous, representation of the global torque-rotation response for the shaft head for rotations smaller than 0.1° (fig 5.6b). The result of the over- and under-estimation of the interface shear response for the instrumented tributary areas is reflected in differences between the observed and computed rate of load transfer, as shown in figure 5.7a.

The soil profile for shaft TDS was similar to that of the TDSFB, except for a lens of silty sand with gravel encountered from depths of 2.8 to 3.8 m (fig. 4.4). The base of the TDS rested on the silty clay to clayey silt layer (table 5.2). The unit torsional shaft resistance for each tributary area was not fully mobilized during the test; however, the ultimate unit torsional shaft resistance could be extrapolated by using the measurements at each tributary area (Li et al. 2017). To be consistent, τ_m was used to designate the validation case that was conducted by using the extrapolated ultimate unit torsional shaft resistance to represent "measured data"; and τ_c was used to designate the calculated resistance by using equations 4.6 and 4.11 for the granular and plastic fine-grained soils, respectively. For the granular soil, both of the O'Neill and Reese (1999) and Brown et al. (2010) methods were used to estimate the shaft resistance coefficient, β. The Brown et al. (2010) method was used to evaluate the peak and residual unit torsional shaft resistance on the basis of a peak friction angle of 40° (Li et al. 2017) and critical state friction angle of 33° (Bolton 1986), respectively. Then, the τ_s-Δ_s curves were constructed by using

equation 4.9 with the displacement-softening model. The O'Neill and Reese (1999) method could only be used to evaluate the maximum resistance, so that the displacement-hardening model (equation 4.3) was used to construct the τ_s-Δ_s curves for the granular soils. The torsional resistance for the plastic, fine-grained soils from ground surface to 1.1 m was neglected, similar to the TDSFB. The initial interface stiffness, K_{si}, for each layer was evaluated by using equation 4.8 with G_{max} calculated from the measured V_s, as shown in figure 4.4. The soil and drilled shaft properties and the load transfer model parameters for TDS are summarized in table 5.2. The displacement-hardening and -softening τ_s-Δ_s curves are shown in figure 5.6b and were implemented into the FDM to illustrate their performance. Since τ_m was estimated by using an extrapolation of the hyperbolic displacement-hardening model, the τ_s-Δ_s curves agreed well with each other. However, the τ_s-Δ_s curves generated with the calculated τ_c over-estimated the unit torsional resistance for the depths of 1.1 to 3.1 m. The τ_s-Δ_s curve at the depths of 3.1 to 4.1 m generated by the displacement-hardening model, which used the calculated τ_{c1} with the O'Neill and Reese (1999) method, under-estimated the unit torsional resistance. The displacement-softening model-generated τ_s-Δ_s curve, using the calculated τ_{c2} with the Brown et al. (2010) method, agreed well with the measured data but was smaller than the extrapolated curve.

The comparisons of the FDM-computed results and the measurements on global torque-rotation response at the head and the torque profiles at different head rotations are shown in figures 5.6d and 5.7b, respectively. The good agreement between the FDM using the extrapolated τ_m and the observed full-scale performance on the global response and the torque profiles at different head rotations indicated the validity of the FDM formulation. The FDM with calculated load transfer curves produced higher global resistance with a given head rotation. Softening behavior was computed for the global torque-rotation response for the FDM, reflecting

the softening response of the sandy layer using the displacement-softening model. The differences between the FDM and the observed torque profiles were due to the over- and under-estimation of the interface shear response for the instrumented tributary areas.

Table 5.2 Soil and drilled shaft properties and hyperbolic parameters for the TDS from the torsional loading tests conducted by Li et al. (2017).

Depth (m)	Shaft	Soil						
	r (m)	ρ (kg/m^3)	s_u (kPa) or ϕ'_p/ϕ'_{cv} (°)	V_s (m/s)	G_{max} (MPa)	τ_c/τ_{cv} (kPa)	τ_m (kPa)	K_{si} (kPa/mm)
0.2 to 1.1	0.470	1837	274	156	44	0	25	285
1.1 to 2.1	0.464	1837	93	189	66	51	13	285
2.1 to 3.1	0.480	1837	207	267	131	103	45	564
3.1 to 4.1	0.506	2041	40/29	268	147	52[1] 69[2]/54[2]	91	530
Base	0.506	1837	34	268	132	18.7	-	564

[1]Evaluated using the O'Neill and Reese (1999) method
[2]Evaluated using the Brown et al. (2010) method

The proposed FDM methodology was validated by using several approaches and was shown to reproduce expected and observed behavior. Clearly, the accuracy of foundation rotations for the serviceability and ultimate limit states in forward modeling will depend on the accuracy of the proposed interface shear model parameters, as well as the accuracy of methods used to calibrate interface model parameters (e.g., α-method, β-method, etc.).

Chapter 6 Illustrative Parametric Studies

Parametric studies were conducted to study the responses of deep foundations under pure torsion to evaluate the effects of nonlinear soil response, including hardening and softening of the interface, and the nonlinear structural response. Two types of deep foundation were considered, including the foundation with linear structural response (i.e., constant *GJ*) and nonlinear structural response (i.e., *GJ* decreases with increasing internal rotation). In light of the low contribution to torsional resistance in soils and to facilitate comparison to previous work (e.g., Poulos 1975 and Guo et al 2007), no toe resistance was considered for either case.

The parametric studies were conducted assuming that the deep foundation was embedded in dry, normally consolidated Ottawa sand, with its characterization established by Hardin and Richart (1963), Salgado et al. (2000), and Lee et al. (2004). The properties of Ottawa sand are summarized in table 6.1. According to Hardin and Richart (1963) and Hardin (1978), the maximum soil shear modulus at depth *z*, $G_{max}(z)$, is related with the void ratio, *e*, and the mean effective stress, $\sigma'_m(z)$, and can be estimated by:

$$G_{\max}(z) = C_g \cdot P_a^{1-m_g} \frac{(e_g - e)^2}{1+e} \sigma'_m(z)^{m_g} \tag{6.1}$$

where C_g, e_g, m_g = regression constants depending solely on the type of soil, as summarized in table 6.1. The mean effective stress at depth *z* can be obtained by:

$$\sigma'_m(z) = \frac{\sigma'_{v0} + 2\sigma'_{h0}}{3} = \frac{1+2K_0(z)}{3} \gamma' \cdot z \tag{6.2}$$

where σ'_{h0} = horizontal effective stress, γ' = effective unit weight of the soil, and $K_0(z)$ = coefficient of later earth pressure at rest at depth *z* and can be computed by (Jaky 1944):

$$K_0(z) = 1 - \sin\phi'_p(z) \tag{6.3}$$

where ϕ'_p = effective peak friction angle and can be estimated by (Bolton 1986):

$$\phi'_p(z) = \phi'_{cv} + 3I_R(z) \tag{6.4}$$

which is valid for $0 \leq I_R(z) \leq 4$ and where ϕ'_{cv} = effective critical state friction angle and $I_R(z)$ = dilatancy index:

$$I_R(z) = I_D\left[Q + \ln\frac{P_a}{100\sigma'_m(z)}\right] - R \tag{6.5}$$

where I_D = relative density expressed as a number between 0 and 1, and the empirical constant R and Q for the soil are listed in table 6.1 based on the triaxial tests conducted by Salgado et al. (2000) and Lee et al. (2004). For each deep foundation element at depth z, the selection of the τ_s-Δ_s model parameters depends on the initial computed $I_R(z)$ from equation 6.5. If $I_R(z)$ is negative, then the soil is contractive so that the peak friction angle is equal to the critical state friction angle. Assuming the interface is rough, the interface response may be modeled by using the displacement-hardening model with interface friction angle equal to the internal friction angle of the granular soil. The asymptotic interface shear stress, τ_{ult}, at the depth z is estimated by:

$$\tau_{ult}(z) = \sigma'_{h0}(z) \cdot \tan(\phi'_{cv}) \tag{6.6}$$

Otherwise, if the initial value of $I_R(z)$ is positive, then the interface is dilatant and modeled by using the displacement-softening model. The peak and residual or ultimate interface shear stress, t_p and $t_{res,ult}$, respectively, may be estimated as:

$$\tau_p(z) = \sigma'_{h0}(z) \cdot \tan(\phi'_p) \tag{6.7}$$

$$\tau_{res,ult}(z) = \sigma'_{h0}(z) \cdot \tan(\phi'_{cv}) \tag{6.8}$$

Figure 6.1a shows how the state-dependent τ_s-Δ_s curves varied along the shaft with depth for the selected Ottawa sand with D_r = 10 percent and 90 percent. It indicates softening near the ground surface and transitioning to a hardening response at deeper depth for D_r = 10%, whereas for D_r = 90 percent, softening responses were observed along the entire shaft.

Table 6.1 The intrinsic soil properties for Ottawa sand (Salgado et al. 2000; Lee et al. 2004).

G_s	C_u	d_{50} (mm)	e_{min}	e_{max}	C_g	e_g	m_g	ϕ'_{cv}	Q	R
2.65	1.48	0.39	0.48	0.78	611	2.17	0.44	29.5	9.9	0.86

Note: G_s = specific gravity, C_u = coefficient of uniformity, e_{min} and e_{max} = minimum and maximum void ratio.

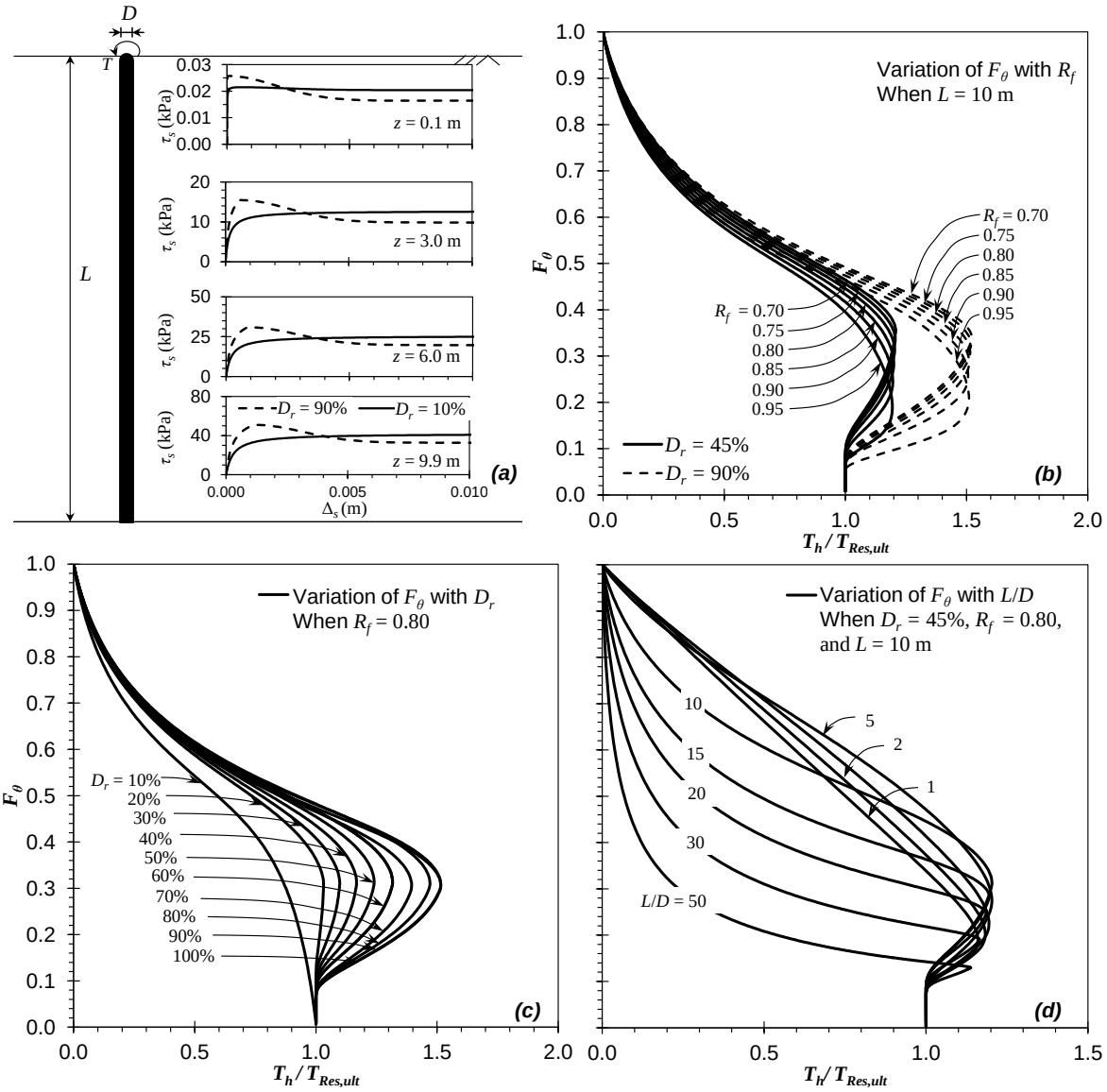

Figure 6.1 Parametric study of (a) a torsionally loaded deep foundation in Ottawa sand with typical τ_s-Δ_s curves along the shaft, and the variation of correction factor, F_θ, with (b) failure ratio, R_f, (c) relative density, D_r, and (d) slenderness ratio, L/D.

6.1 Linear Structural Response of Deep Foundation

First, it was assumed that the selected deep foundation would behave linearly elastic under torsion with G_p = 12 GPa and L = 10 m. To evaluate the effects of relative density, D_r, on torsional foundation response, simulations were performed with D_r ranging from 10 percent to 100 percent within a uniform granular soil deposit. The effects of failure ratio, R_f, were also

evaluated by varying it from 0.70 to 0.95. Figure 6.1b shows the variation of F_θ with R_f when D_r = 45 percent and 90 percent. As expected, the change in R_f did not affect the ratio of peak torque and the residual or ultimate torque at head, $T_{h,max}/ T_{res,ult}$. However, F_θ decreased with increasing R_f for a given ratio of $T_h/T_{res,ult}$, indicating that the relative torsional stiffness decreased with increasing R_f . The variation of F_θ with D_r when R_f = 0.80 is shown in figure 6.1c. It appears that $T_{h,max}/ T_{res,ult}$ increased with increasing D_r because of the increase in ϕ'_p with increasing D_r. Since the governing soil properties (i.e., G_{max}, ϕ'_p, ϕ'_{cv}) vary with depth, the effects of slenderness ratio L/D may be studied by varying D with a constant L = 10 m, as shown in figure 6.1d, when D_r = 45 percent and R_f = 0.80. It shows that the shape of the curve before the torque at head reached the peak value transited from a concave-up shape to linear shape because of the transition from flexible to rigid deep foundation behavior.

6.2 Nonlinear Structural Response of Deep Foundation

Shear cracks may develop within a drilled shaft foundation undergoing large torsional loads if insufficient transverse reinforcement is specified (Li et al. 2017). For a column in torsion, the torque-rotation response becomes nonlinear after cracking, as observed by Hsu and Wang (2000), and the torsional rigidity, defined as the ratio of T and θ/L, may decrease at large rotations (Mondal and Prakash 2015). The FDM proposed here may be used to evaluate the influence of nonlinear torsional rigidity on the torsional response of deep foundations. For this investigation, the measured torque (T)-internal twist/length (θ/L) relationship for a structural column reported by Mondal and Prakash (2015) was used as the prototype; the column was constructed with a diameter of 0.61 m and 1.32 percent transverse steel ratio, as shown in figure 6.2a. The torsional rigidity exhibited distinct nonlinearity with small rotations, as well as softening following the peak torque of 327.5 kN-m.

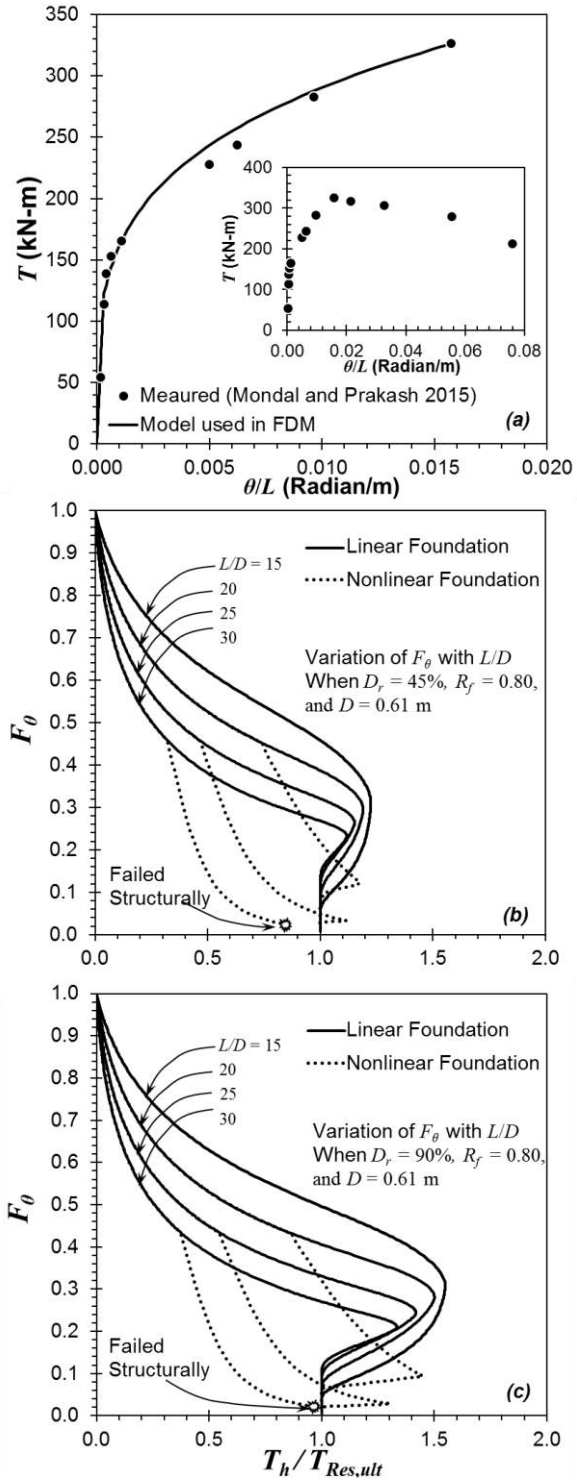

Figure 6.2 Parametric study of a torsionally loaded deep foundation in Ottawa sand with nonlinear structural response using (a) a measured torque (T)-internal twist/length (θ/L) response from Mondal and Prakash (2015); and a comparison between the linear and nonlinear foundations with different slenderness ratio, L/D for relative density (b) D_r = 45 percent and (c) 90 percent.

When unembedded columns soften and form a plastic hinge, no additional torsional resistance can be mobilized within the soil; rather, the supported structure will simply undergo continued rotation. Therefore, for the purposes of the parametric investigation of the effect of nonlinear torsional rigidity on the soil-structure interaction of deep foundations, only the pre-peak or hardening portion of the reported torsional response was evaluated. The investigation assumed a linear response for $T \leq 125$ kN-m with a constant torsional rigidity $(GJ)_{max} = 4\times10^5$ kN-m^2; thereafter a power law of the form:

$$T = c_1 \cdot \left(\frac{\theta}{L}\right)^{c_2} \tag{6.9}$$

It was used to replicate the experimental data, where c_1 and c_2 = 940 and 0.255, respectively, determined by using the least squares method.

It was assumed that the deep foundation was embedded in the same Ottawa sand (table 6.1) with D_r = 45 percent and 90 percent. For comparison purposes, a deep foundation with linear response ($GJ = (GJ)_{max}$) was also considered. For the nonlinear deep foundation, the initial $(GJ)_{max}$ was used to calculate F_θ, since GJ varied along the deep foundation because of the variation of internal rotation. Figures 6.2b and 6.2c show the comparison of the torsional response between the deep foundations with linear and nonlinear structural response with D_r = 45 percent and 90 percent, respectively. The linear and nonlinear foundations had the same response for L/D = 15 and D_r = 45 percent and 90 percent because the maximum internal torque remained smaller than the elastic limit of 125 kN-m. However, for larger L/D ratios, the response of the linear and nonlinear foundations diverged for $F_\theta > 0.44$ as the maximum internal torque exceeded 125 kN-m, and where the linear elastic foundation remained stiffer than the nonlinear

foundation. For L/D = 30 the nonlinear foundation did not mobilize its maximum soil resistance before structural failure when the torque at the head was equal to 327.5 kN-m. Accordingly, structural nonlinearity reduces the foundations' global torsional stiffness, and the estimation of the global torsional capacity of a deep foundation may be unconservative if capacity is estimated without due consideration of nonlinear structural response.

Chapter 7 Summary and Conclusions

This report presents a torsional load transfer method to facilitate the serviceability design of torsionally loaded deep foundations, which may consist of a driven pile, drilled shaft, or other deep foundation alternative. The finite difference model (FDM) framework was selected to solve the governing differential equations that describe the performance of a geometrically variable deep foundation constructed in multi-layered state-dependent soils. In this approach, the deep foundation is treated as a beam, and the complicated SSI is simplified as a beam interacting with discrete nonlinear torsional springs along the shaft and toe elements. Two simplified spring models relating the unit torsional resistance to the magnitude of relative displacement, including a hyperbolic displacement-hardening model for both granular and plastic fine-grained soils with contractive response and a displacement-softening model for granular soils with dilatant response, were developed by using available interface shear tests in the literature. The tendency for dilation can be determined on the basis of the interface roughness, normal effective stress, and the granular soil properties (i.e., relative density and grain type).

The displacement-hardening and -softening load transfer models were validated against experimental interface shear data and load transfer data from Li et al. (2017). The proposed FDM methodology was validated by comparing the torsional responses from the FDM with previous analytical solutions reported by Poulos (1975), Hache and Valsangkar (1988), Guo and Randolph 1996, Guo et al. (2007), and Zhang (2010), and with torsional loading tests, including centrifuge tests by Zhang and Kong (2006) and full-scale tests by Li et al. (2017). On the basis of the evaluation of the proposed τ_s-Δ_s curves using the calculated torsional resistance by equations 4.6 and 4.11, it appears that the accuracy of foundation rotations for the serviceability and ultimate limit states in forward modeling depends on the accuracy of the proposed interface shear model

parameters, as well as the accuracy of methods used to calibrate interface model parameters. Parametric studies illustrate the significant effects of nonlinear hardening and softening soil responses and nonlinear structural response on the torsional behavior of deep foundations. The consideration of structural nonlinearity results in a smaller global torsional stiffness and capacity than that expected, assuming a linear elastic structural section.

References

American Petroleum Institute (API). 1993. *Recommended practice for planning, design, and constructing fixed offshore platforms*, API RP 2A–WSD, 20th Ed., API, Washington, D.C.

Ashour. M., Pilling, P., Norris, G., and Perez, H. 1996. "Development of strain wedge model program for pile group interference and pile cap contribution effects." *CCEER Rep. No. 96-4*, Civil Engrg. Dept., University of Nevada, Reno, Nev

Bizaliele, M. M. 1992. "Torsional cyclic loading response of a single pile in sand." Dissertation, Schriftenreihe des Instituts fur Grundbau, Ruhr-Univ., Bochum, Germany.

Bolton, M. D. 1986. "The strength and dilatancy of sands." *Geotechnique*, 36(1), 65–78.

Boulanger, R. 2003. "Relating Kα to Relative State Parameter Index." *J. Geotech. Geoenviron. Eng.*, 129(8), 770-773.

Broms, B. B. Silberman, J. O. 1964. "Skin Friction Resistance for Piles in Cohesionless soils." *Sols-soils*, pp.10-23.

Brown, D. A., Turner, J. P., and Castelli, R. J. 2010. "Drilled shafts: Construction procedures and LRFD design methods." *Report No. FHWA-NHI-10-016.* US Department of Transportation, Federal Highway Administration, Washington, D.C.

Cao, W., Chen, Y., and Wolfe, W. E. 2014. "New load transfer hyperbolic model for pile-soil interface and negative skin friction on single piles embedded in soft soils." *Int. J. Geomech.*, 14(1), 92–100

Chin, F. K. 1970. "Estimation of the pile Ultimate Load of Piles Not Carried to Failure." *Proceedings of the 2nd Southern Asian Conference on Soil Engineering*, Singapore, 81-90.

Chin, F. K. 1971. "Discussion of 'Pile test, Arkansas River project.". *Soil Mech. and Found. Div*., 97(6), 930-932.

Chow, Y. K. 1985. "Torsional response of piles in nonhomogeneous soil." *J. Geotech. Engrg*., 111(7), 942–947.

Clemence, S. P. 1973. "The development of instrumentation and model testing for the load distribution in a drilled pier." *Ph.D. Dissertation*, Georgia Institute of Technology, Atlanta, GA.

Clemence, S. P., and Brumund, W. F. 1975. "Large-scale model test of drilled pier in sand." *J. Geotech. Engrg. Div*., 101(6), 537–550.

Clough, G. W., and Duncan, J. M. 1971. "Finite element analyses of retaining wall behavior." *J. Soil Mech. Found. Div.,* ASCE, 97(12), 1657–1673.

Cox, W.R., Reese, L.C., Grubbs B.R. 1974. “Field testing of laterally loaded piles in sand.” *Proc. 6th Offshore Technology Conf.,* OTC , Houston, TX, 459-472.

Coyle, H. M., and Reese, L. C. 1966. “Load Transfer for Axially Loaded Piles In Clay.” *J. of Soil Mech. and Found. Engrg. Div.* 92(2), 1-26.

Coyle, H. M., and Sulaiman, I. 1967. ‘‘Skin friction for steel piles in sand.’’ *J. Soil Mech. Found. Div*., 93(6), 261–270.

DeJong, J. T., Frost, J. D. 2002. “A Multisleeve Friction Attachment For The Cone Penetrometer,*” Geotech. Test. J.,* 25(2), 111–127.

Desai, C. S., and Zaman, M. 2014. *Advanced geotechnical engineering soil–structure interaction using computer and material models* , CRC Press, Taylor & Francis Group, Boca Baton, FL.

Dove, J. E. and Frost, J. D. 1999. “Peak Friction Behavior of Smooth Geomembrane-Particle Interfaces,” *Journal of Geotechnical and Geoenvironmental Engineering*, ASCE, 125 (7), 544–555.

Dove, J. E., and Jarrett, J. B. 2002. “Behavior of dilative sand interfaces in a geotribology framework.” *J. Geotech. Geoenviron. Eng*., 128(1), 25–37.

Duncan, J. M., and Chang, C.-Y. 1970. “Nonlinear analysis of stress and strain of soil.” *J. Soil Mech. and Found*. Div., 96(5), 1629–1653.

Dutt, R. N. 1976. “Torsional response of piles in sand.” *Ph.D. thesis,* Univ. of Houston, Houston, Texas.

Dutt, R. N., and O’Neill, M. W. 1983. “Torsional behavior of model piles in sand.” *Geotechnical Practice in Offshore Engineering,* ASCE, New York, 315-334.

Frost, J. D., DeJong, J. T., Recalde, M. 2002. “Shear failure behavior of granular-continuum interfaces”, *Engineering Fracture Mechanics*, 69(17), 2029-2048.

Georgiadis, M. 1987. “Interaction between torsional and axial pile response.” *Int. J. Numer. Analyt. Meth. Geomech.*, 11, 645–650.

Georgiadis, M., and Saflekou, S. 1990. “Piles under axial and torsional loads.” *Comput. Geotech*., 9, 291–305.

Gere, J.M., and Timoshenko, S.P. 1997. *Mechanics of Materials,* PWS Pub.Co., Boston.

Gómez, J. E., Filz, G. M., and Ebeling, R. M. 2000. ‘‘Development of an improved numerical model for concrete-to-soil interfaces in soil-structure interaction analyses.’’ *Technical Rep. ITL-99-1*, U.S. Army Engineer Research and Development Center, Vicksburg, Miss.

Gómez, J. E., Filz, G. M., and Ebeling, R. M. 2000b. ‘‘Extended load/unload/reload hyperbolic model for interfaces: Parameter values and model performance for the contact between concrete and coarse sand.’’ *ERDC/ITL TR-00-7*, U.S. Army Engineer Research and Development Center, Vicksburg, Miss.

Gómez, J., Filz, G., and Ebeling, R. 2003. “Extended Hyperbolic Model for Sand-to-Concrete Interfaces.” *J. Geotech. Geoenviron. Eng.*, 129:(11), 993-1000.

Guo, W. D., Chow, Y. K., and Randolph, M. F. 2007. “Torsional pile in two-layered nonhomogeneous soil.” *Int. J. Geomech.*, 7(6), 410–422.

Guo, W. D., and Randolph, M. F. 1996. “Torsional piles in nonhomogeneous media.” *Comput. Struct.*, 19(4), 265–287.

Hache, R. A. G., and Valsangkar, A. J. 1988. “Torsional resistance of single pile in layered soil.” *J. Geotech. Engrg.*, 114(2), 216–220.

Hardin, B. O. 1978. ‘‘The nature of stress-strain behavior of soils.’’ *Proc., ASCE Geotech. Engrg. Div.., Spec. Conf.*, Vol. 1, ASCE, New York, 3–90.

Hardin, B. O., and Richart, F. E., Jr. 1963. ‘‘Elastic wave velocities in granular soils.’’ *J. Soil Mech. Found. Div.*, ASCE, 89(1), 33–65.

Holloway, D. M., Clough, G. W., and Vesic, A. S. 1975. “Mechanics of pile-soil interaction in cohesionless soil.” *Contract Report S-75-5, U. S. Army Wtrways. Exper. Sta*., Vicksburg, Miss.

Hsu, H. L., and Wang, C. L. 2000. “Flexural-torsional behavior of steel reinforced concrete members subjected to repeated loading.” *Earthquake Eng. Struct. Dyn*., 29(5), 667–682.

Hu, Z. (2003). “Determining the optimum depth of drilled shafts subject to combined torsion and lateral loads in saturated sand from centrifuge testing.” Master’s dissertation, University of Florida, Gainesville, FL.

Huffman, J.C., Strahler, A.W., and Stuedlein, A.W. 2015. “Reliability-based serviceability limit state design for immediate settlement of spread footings on clay,” *Soils and Foundations*, 55(4), 798-812.

Iscimen, M. 2004. “Shearing Behavior of Curved Interfaces.” Master’s thesis, Georgia Institute of Technology, Atlanta, GA.

Jaky, J. (1944). “The coefficient of earth pressure at-rest.” *J. Soc. Hung. Archit. Eng*., 78(22), 355–358.

Kim, S., Jeong, S., Cho, S., and Park, I. 1999. “Shear load transfer characteristics of drilled shafts in weathered rocks.” *J. Geotech. Geoenviron. Eng*., 125(11), 999–1010.

Klotz, E.U., and Coop, M.R. 2001. “An investigation of the effect of soil state on the capacity of driven piles in sand.” *Geotechnique*, 51(9): 733–751.

Kondner, R. L. 1963. “Hyperbolic stress–strain response: Cohesive soils.” *J. Soil Mech. Found. Div.* , 89 (1), 115–143.93q

Kong, L. G. 2006. “Behavior of pile groups subjected to torsion.” Ph.D. thesis, Hong Kong Univ. of Science and Technology, Hong Kong.

Kulhawy, F. H., Peterson, M. S. 1979. “Behavior of Sand-Concrete Interfaces”, Proceedings, *Sixth Pan American Conference On Soil Mechanics And Foundation Engineering*, Vol. 2, Lima, Peru, 225-236.

Laue, J., and Sonntag, T. 1998. “Pile subjected to torsion.” Proc., Centrifuge ’98, Balkema, Rotterdam, the Netherlands, 187–192.

Lee, P. A., Kane, W. F., Drumm, E. C., and Bennett, R. M. 1989. “Investigation and modeling of soil-structure interface properties.” *Foundation engineering: Current principles and practice*, ASCE Geotechnical Special Publication 22, New York, 580–587.

Lee, J., Salgado, R., and Carraro, J. A. H. 2004. “Stiffness degradation and shear strength of silty sands.” *Can. Geotech. J.*, 41(5), 831–843.

Li, Q., and Yang, Z. 2017. “*P–y* approach for laterally loaded piles in frozen silt.” *J. Geotech. Geoenviron. Eng.*, http://dx.doi.org/10.1061/(ASCE)GT.1943-606.0001556

Li, Q., Stuedlein, A. W., Barbosa, A. R. 2017. “Torsional load transfer of drilled shaft foundations.” *J. Geotech. Geoenviron. Eng.*, 10.1061/(ASCE)GT.1943-5606.0001701

Lings, M. L., and Dietz, M. S. 2005. “The peak strength of sand-steel interfaces and the role of dilation.” *Soils Found*., 45(6), 1–14.

Matlock, H. 1970. “Correlations for Design of Laterally Loaded Piles in Soft Clay.” *Proc., 2nd Annual Offshore Technology Conf.,* OTC 1204, Houston, TX, 577-594.

McVay, M.C., F.C. Townsend, D.G. Bloomquist, M.O. O'Brien, and J.A. Caliendo. 1989. "Numerical analysis of vertically loaded pile groups." *Proceedings, Foundation Engineering Congress: Current Principles and Practices*, Evanston, IL, pp. 675-690.

McVay, M. C., Herrera, R., and Hu, Z. 2003. “Determine optimum depths of drilled shafts subject to combined torsion and lateral loads using centrifuge testing.” *Report Contract No. BC-354, RPWO #9*. Florida Department of Transportation, Tallahassee, FL.

McVay, M. C., Bloomquist, D., and Thiyyakkandi, S. 2014. “Field testing of jet-grouted piles and drilled shafts.” *Report BDK75-977-41, 91977.* Florida Department of Transportation, Tallahassee, FL.

Mondal, T. G., and Prakash, S. S. 2015. “Nonlinear finite-element analysis of RC bridge columns under torsion with and without axial compression.” *J. Bridge Eng.*, 10.1061/(ASCE)BE.1943-5592.0000798, 04015037.

Norris, G. M. 1986. “Theoretically based BEF laterally loaded pile analysis.” *Proc., Third Int. Conf. on Numerical Methods in Offshore Piling*, Editions Technip, Paris. France, 361-386.

Nusairat, J., Liang, R., Engel, R., Hanneman, D., AbuHejleh, N., and Yang, K. 2004. “Drilled shaft design for sound barrier walls, signs, and signals.” *Report No. CDOT-DTD-R-2004-8*, Colorado Department of Transportation, Denver, CO.

O’Neill, M. W. 1964. “Determination of the pile-head torque-twist relationship for a circular pile embedded in a clay soil.” Master’s thesis, The Univ. of Texas at Austin, TX.

O’Neill, M. W., and Reese, L. C. 1999. “Drilled shafts: Construction procedures and design methods.” *Publ. No. FHWA-IF-99-025*, Federal Highway Administration, Office of Implementation, McLean, VA

Paikowsky, S. G., Player, C. M., and Connors, P. J. 1995. “A dual interface apparatus for testing unrestricted friction of a soil along solid surfaces.” *Geotech. Test. J.*, 18(2), 168–193.

Peterson, M. S. 1976. “Stress deformation behavior of soil concrete interfaces.” Master’s thesis, Syracuse University, Syracuse, NY.

Poulos, H. G. 1975. “Torsional response of piles.” *J. Geotech. Engrg. Div*.,101(10), 1019–1035.

Randolph, M. F. 1981. “Piles subjected to torsion.” *J. Geotech. Engrg. Div.*, 107(8), 1095–1111.

Randolph, M. F. 1983. “Design consideration for offshore piles.” *Geotechnical Practice in Offshore Engineering*, ASCE, New York, 422–439.

Reese, L. C., Cox, W. R., and Koop, F. D. 1975. “Field testing and analysis of laterally loaded piles in stiff clay.” *Proc., 7th Offshore Technology Conf.*, SPE, Richardson, TX, 671-690.

Reese, L., Welch, R. 1975. “Lateral loading of deep foundations in stiff clay.” *Journal of Geotechnical Engineering Div*., ASCE, 101(GT7), 633-649.

Salgado, R., Bandini, P., and Karim, K. 2000. “Shear strength and stiffness of silty sand.” *J. Geotech. Geoenviron. Eng*., 126(5), 451–462.

Stuedlein, A. W. and Reddy, S. C. 2014. “Factors affecting the reliability of augered cast-in-place piles in granular soils at the serviceability limit state,” *J. of the Deep Foundations Institute*, 7(2), 46-57.

Stoll, U. W. 1972. “Torque shear test of cylindrical friction piles.” *Civil Engineering*, 42(4), 63-65.

Subba Rao, K. S., Allam, M. M., and Robinson, R. G. 1998. “Interfacial friction between sands and solid surfaces.” *Geotech. Eng.*, 131, 75–82.

Tawfiq, K. 2000. “Drilled shafts under torsional loading conditions.” Report Contract No. B-9191, Florida Department of Transportation, Tallahassee, FL.

Teachavorasinskun, S., Shibuya, S., and Tatsuoka, F. 1991. “Stiffness of sands in monotonic and cyclic torsional simple shear.” *In Proceedings of Geotechnical Engineering Congress*, Boulder, Colo., 10–12 June 1991. *Edited by* F.G. McLean, D.A. Campbell, and D.W. Harris. ASCE Geotechnical Special Publication 27, Vol. 1, pp. 863–878.

Tucker, R. L. 1960. *An Investigation of a Rigid Cylinder Subjected to Rotational and Axial Loadings in a Clay Medium*, Master's Thesis, The University of Texas at Austin, Austin, Texas

Uesugi, M., and Kishida, H. 1986. “Frictional resistance at yield between dry sand and mild steel.” *Soils Found*., 26(4), 139–149.

Vijayvergiya, V. N. 1977. “Load-movement characteristics of piles.” *Proc., Ports '77: 4th Annual Symposium of the Waterway, Port, Coastal, and Ocean Division., ASCE*, New York, 269-284

Ward, H. C. 1982. *Profile characterization, chapter 4, in rough surfaces*, Thomas, T. R. (ed.), Longman, London, UK.

Wong, K. S., and Teh, C. I. 1995. “Negative skin friction on piles in layered deposits.” *J. Geotech. Engrg.*, 121(6), 457–465.

Yang, Z., Li, Q., Horazdovsky, J., Hulsey, J. L., and Marx, E. E. (2017). “Performance and design of laterally loaded piles in frozen ground.” *Journal of Geotechnical and Geoenvironmental Engineering*, 143 (5),http://dx.doi.org/10.1061/(ASCE)GT.1943-5606.0001642, 06016031.

Zhang, L. 2010. “Nonlinear analysis of torsionally loaded piles in a two layer soil profile.” *Int. J. Geomech.*, 10(2), 65–73.

Zhang, L.M., and Kong, L.G. 2006. “Centrifuge modeling of torsional response of piles in sand.” *Canadian Geotechnical Journal*, 43(5), 500-515.